Decoding protein phosphorylation during oocyte meiotic divisions using phosphoproteomics

Leonid Peshkin[1#✉], Enrico Maria Daldello[2#], Elizabeth Van Itallie[1], Matthew Sonnett[1], Johannes Kreuzer[1], Wilhelm Haas[1], Marc W Kirschner[1] and Catherine Jessus[2]

[1] Systems Biology Department, Harvard Medical School, Boston, MA, 02115, USA

[2] Sorbonne Université, CNRS, Laboratoire de Biologie du Développement - Institut de Biologie Paris Seine, LBD - IBPS, F-75005 Paris, France

[#] Equal contribution

✉ Corresponding author: Leonid_Peshkin@hms.harvard.edu

Running title: Protein phosphorylation during oocyte meiotic divisions

ABSTRACT

Oocyte meiotic divisions represent a critical process in sexual reproduction, as a diploid non-dividing oocyte is transformed into a haploid fertilizable egg, as a prelude for the subsequent embryonic divisions and differentiation. Although cell differentiation and proliferation are governed by transcription, oocyte maturation and early embryonic divisions depend entirely on changes in protein abundance and post-translational modifications. Here, we analyze the abundance and phosphorylation of proteins during *Xenopus* oocyte meiotic maturation. We reveal significant shifts in protein stability, related to spindle assembly, DNA replication and RNA-binding. Our analysis pinpoints broad changes in phosphorylation correlating with key cytological meiotic milestones, noteworthy changes in membrane trafficking, nuclear envelope disassembly and modifications in microtubule dynamics. Additionally, specific phosphorylation events target regulators of protein translation, Cdk1 and the Mos/MAPK pathway, thereby providing insight into the dynamics of Cdk1 activity, as related to the meiotic cell cycle. This study sheds light on the orchestration of protein dynamics and phosphorylation events during oocyte meiotic divisions, providing a rich resource for understanding the molecular pathways orchestrating meiotic progression in the frog, and most likely applicable to other vertebrate species.

Key Words: Meiotic divisions/Protein phosphorylation/Phosphoproteome/*Xenopus* oocyte

INTRODUCTION

In mature females, the oocyte undergoes a long period of growth, during which meiosis is arrested at prophase I. In the *Xenopus* oocyte, transcription is switched off when the oocyte reaches the end of its growth phase (Dumont, 1972). The full-grown oocyte is transcriptionally silent and equipped with a stock of mRNAs and proteins that will support without transcription three critical embryonic processes: first, two meiotic divisions that transform the oocyte into a fertilizable haploid egg; second, the process of fertilization; and third, 13 embryonic divisions, after which transcription is initiated.

The transformation of a fully-grown oocyte arrested in prophase into a fertilizable cell, arrested in metaphase of the second meiotic division is a process called meiotic maturation. Meiotic maturation is triggered by progesterone, secreted by the follicle cells surrounding the oocyte. The secretion of progesterone is stimulated by Luteinizing Hormone produced by the pituitary. Progesterone initiates a molecular signaling cascade that lasts 3 to 4 hours and occurs with little change in oocyte morphology. Notably, this cascade leads to the activation of the Cdk1-Cyclin B kinase, the universal inducer of cell division in eukaryotes. Cdk1 phosphorylates many substrates that promote meiotic nuclear events: nuclear envelope breakdown (NEBD), the formation of the first meiotic spindle (MI), the completion of the first meiotic division with expulsion of a polar body, and formation of the second meiotic spindle (MII) (Figure 1). As in all vertebrates, the frog oocyte arrests a second time in metaphase II, until fertilization stimulates the completion of the second meiotic division. The entire process of oocyte maturation occurs in the absence of transcription. The regulation of the two meiotic divisions and the 13 embryonic divisions that follow are thought to be largely regulated by changes in protein abundance and phosphorylation/dephosphorylation.

The prophase-arrested oocyte contains a store of Cdk1-Cyclin B complexes that are kept inhibited by Cdk1 phosphorylation at Y15 and T14, which are substrates of the kinase, Myt1 (Mueller *et al*, 1995). In all vertebrates, the prophase arrest is maintained by high levels of cAMP and PKA (cAMP-activated protein kinase) activity (Figure 1). The release of this prophase block is triggered by a drop in the levels of cAMP and the consequent inhibition of PKA, which occurs within 60 min after progesterone stimulation. The identity of the critical PKA substrates whose dephosphorylation is thought to induce the pathway leading to Cdk1 activation is still unknown, with the exception of Arpp19 whose mechanism of action is not completely understood (Dupré *et al*, 2014; Santoni *et al*, 2024). Nevertheless, a drop in PKA activity leads to the synthesis of new proteins from cytoplasmic stockpiles of mRNAs as well as increases in protein level through regulation of the ubiquitination machinery (Santoni *et al*, 2024). Among the accumulated proteins are Cyclin B1, the best-known activator of Cdk1 in mitotic cells, and Mos, a kinase specific to the

oocytes (Figure 1). The newly synthesized B1-Cyclins bind to monomeric Cdk1 to form a small pool of active complexes that evade the inhibition of Myt1 (Hochegger *et al*, 2001; Gaffré *et al*, 2011). Subsequently, this small amount of active Cdk1 initiates a complex network of feedback loops, involving many kinases and phosphatases, thereby creating an auto-amplification loop (Jessus, 2010) (Figure 1). Within this loop, the activation of the Cdc25 phosphatase that dephosphorylates Cdk1 and the inhibition of the PP2A phosphatase that counteracts Cdk1, lead to a rapid and full activation of Cdk1-Cyclin B (Jessus, 2010; Lemonnier *et al*, 2020). Another important player in this positive feedback loop is Mos, whose translation is induced by progesterone and which accumulates at the time of Cdk1 activation (Sagata *et al*, 1988, 1989a; Frank-Vaillant *et al*, 1999). Mos activates Erk1/2 (also known as MAPK) indirectly, which modulates the core regulators of Cdk1 (Haccard & Jessus, 2006) (Figure 1). Cdk1 and the kinases activated under its control (Mos/MAPK, Aurora-A, Plk1, etc.) trigger a second wave of protein translation and accumulation, as well as mediating the structural changes of cell division: NEBD, chromosome condensation and formation of the Meiosis I spindle (Jessus, 2010; Santoni *et al*, 2024). They also activate the anaphase-promoting complex (APC), an E3 ubiquitin ligase, leading to the degradation of both Cyclin B and securin, thus enabling entry into anaphase I, chromosome separation and the expulsion of the 1st polar body (Figure 1). The decrease in Cdk1 activity is rapidly followed by the inhibition of APC, which then allows the accumulation of B-Cyclins and increase of Cdk1 activity (Figure 1). These events trigger the entry into metaphase II and the formation of the MII spindle. In all vertebrates, oocytes arrest in the middle of the meiotic division as a result of the stabilization of cyclin B, resulting from APC inhibition by the Emi2/Erp1 (Jessus, 2010) (Figure 1).

The burst of phosphorylation, which occurs at NEBD when Cdk1 is activated, targets proteins belonging to three categories (Maller *et al*, 1977): first, regulators of translation and/or degradation of proteins that are essential for the progression of meiotic divisions; second, proteins directly involved in the intracellular reorganization of the oocyte, such as the components of meiotic spindles, the nuclear envelope or other cytoskeletal elements; third, proteins that do not have a role in meiotic divisions but regulate fertilization and early embryonic development. Notably, the sperm does not contribute any proteins or RNA except for its genome and its two centrioles. With fertilization there is extrusion of the 2nd polar body, the fusion of the male and female pronuclei. Within a few minutes after fertilization, the first S-phase starts, followed by the first 13 embryonic division cycles, all occurring in the absence of transcription. Thus, these events depend exclusively on maternal proteins and mRNA. Phosphoregulation is a central and conserved mechanism that enables remodeling of the oocyte proteome and supports cell division. It prepares the oocyte to transform into the egg and undertake development. In the absence transcription our knowledge

of the dynamic patterns of phosphorylation of thousands of oocyte phosphosites represents an essential tool for study of oogenesis, embryogenesis, especially the unique meiotic and mitotic processes. Interestingly, three recent studies based on phosphoproteomics have revealed new insights into how phosphorylation dynamics regulate meiotic divisions in yeast (Celebic *et al*, 2024; Koch *et al*, 2024) and mouse(Sun et al., 2024). We now extend this analysis to the physiological process of oogenesis specific to non-mammalian metazoans. The study of mitotic processes in somatic cells, which are short in duration, requires exquisite synchronization, which is difficult. Although previous studies of protein phosphorylation during mitosis have revealed the identity of numerous players of cell division, especially those controlling the structural reorganization of the dividing cell and its checkpoints, they have not been able to fully elucidate the epistatic relationships between kinases and phosphatases, which are nonetheless crucial to understanding the temporal sequences regulating the various events of mitosis. This weakness is due to the fact that cell proliferation is a continuous phenomenon, without physiological arrest. Its duration varies from one cell to another within the same population. The necessity of using synchronizing agents induces non-physiological arrests, which activate checkpoints, leading to the resumption of the cell cycle not comparable to that of untreated cells. Moreover, these studies often use transformed cell lines with accumulation of mutations that makes it hard to compare with cells in a physiological cellular context. The exceptional features of oocyte maturation for experimental studies of mitosis and meiosis are: 1) the synchronicity of the process in the oocyte, initiated by a physiological signal, progesterone, 2) the natural oocyte arrests in oocyte maturation at either prophase I (equivalent to a late G2-arrest) or at MII (M-phase arrest), 3) and the large size of the oocyte (1.2 mm in diameter) and its high protein content (30 mg soluble proteins per cell), offering the rare opportunity of single-cell proteomics of events at the single cell level. In addition, the *Xenopus* model offers great assets. From a technical perspective, in the mouse, the small number of oocytes and their low protein content limit proteomic approaches (30,000 oocytes isolated from 950 mice were required for the phosphoproteomic profiling by (Sun et al., 2024)). Furthermore, the resumption of meiotic divisions in mouse obeys a particular regulation: unlike other mammalian models (including the human species) and other vertebrates whose entry into meiosis I depends strictly on protein translation, it does not require the synthesis of new proteins, making it a somewhat marginal model (Meneau *et al*, 2020). For these reasons, we performed time-resolved proteomics and phosphoproteomics in *Xenopus* oocytes from prophase I through the MII arrest of the unfertilized egg.

In this study, we have analyzed the changes in the phosphorylation in relation to three categories of events: specific periods of meiotic maturation, activities of the master regulators of meiosis and

peculiar cellular features of meiosis. Our analysis confirms the high quality of our phosphoproteome by the detection of multiple phosphorylation events with previously-documented functional effects on meiotic divisions or early development. Through the detection of many new regulated phosphosites, it provides a rich pool of candidate proteins for multiple avenues of investigation of previously uncharacterized important players of the oocyte to embryo transition.

RESULTS

The temporal resolution of the events of meiotic divisions

Prophase-arrested oocytes (PRO) and oocytes resuming meiosis were collected at regular intervals after progesterone exposure. To correlate the time-points of this experiment with the cytological events known to occur during meiosis resumption, a set of proteins whose accumulation had been extensively studied during *Xenopus* oocyte meiosis progression were used as markers (Figure 2A-video supplement 1). One of the first events following progesterone stimulation is the accumulation of Cyclin B1 that begins before and independently of Cdk1 activation (Santoni *et al*, 2024; Frank-Vaillant *et al*, 1999). In our experiments, Cyclin B1 accumulation starts at about 2 hours and increases linearly until MII arrest at 6.5 hours (Figure 2A). It has been reported that Mos translation is stimulated by progesterone concomitant with the accumulation of Cyclin B1; however, the Mos protein does not accumulate before NEBD because it turns over rapidly (Santoni *et al*, 2024; Frank-Vaillant *et al*, 1999). Another critical well documented event that occurs downstream to Cdk1 activation is the degradation of CPEB1 (Santoni *et al*, 2024; Mendez *et al*, 2002), an RNA-binding protein whose degradation activates protein translation in MI. Hence, Mos accumulation and the degradation of CPEB1 are well established markers for the timing of NEBD. After NEBD, activation of the anaphase-promoting complex (APC) leads to the ubiquitination and degradation of Cyclin B2, which marks the entry into anaphase I. During the MI-MII transition, multiple additional events take place: Cyclin B3 is degraded (Bouftas *et al*, 2022), Cdc6 (Lemaître *et al*, 2002; Whitmire *et al*, 2002; Daldello *et al*, 2015), Wee2 (Nakajo *et al*, 2000) and Cyclin E (Rempel *et al*, 1995) accumulate, reaching their maximal levels in MII. These four events mark the entry into MII. Based on these markers, the timing of cytological events in our experiment is as follows (Figure 2A): NEBD and MI occur between 3 and 4 hours, the MI-MII transition takes place between 5 and 6 hours, and entry and arrest in MII are at 7 hours. This time course is in agreement with the cytological previously described events (Huchon *et al*, 1981; Gard, 1992). A physiological measure of MII arrest can be ascertained by the ability of the oocytes to be activated by an electric shock, a property that is acquired only in MII (Figure 2-video supplement 2).

Validation of the quantitative proteomic data

The quality of oocytes resuming meiosis is also confirmed by the dynamics of protein accumulation and degradation that occur during meiotic progression (Figure 2B). A set of 34 proteins, whose changes in concentration have been previously studied during meiotic divisions was used to validate the quality of our quantitative proteomics data (Figure 2B-figure supplement 3A). Our proteome correctly classifies 15 out of 18 proteins accumulating during *Xenopus* meiosis resumption (FC(MII/PRO) > 1.5), 11 out of 12

proteins whose concentration is constant (0.75 < FC(MII/PRO) < 1.5), and 4 out of 4 proteins whose accumulation was reported to decrease (FC(MII/PRO) < 0.75) (Figure 2B-figure supplement 3A). The concordance between our dataset (30/34 proteins) with the changes in the protein levels reported in the literature is substantially higher than in a previously published system-wide proteomic dataset from *Xenopus* oocytes where only 7 out of these 34 proteins were correctly measured (Peuchen *et al*, 2017) (Figure 2-figure supplement 3A-B). This also may explain why changes in protein concentration reported in that study poorly correlate with the one measured in our proteomic study (Figure 2-figure supplement 3B). The high quality of the new proteomic data is also confirmed by the strong correlation of the translational pattern of *Xenopus* allo-alleles (Figure 2-figure supplement 3C-D), which were derived by genome endoduplication (Session *et al*, 2016).

Protein homeostasis during meiotic divisions

Absolute concentrations of proteins during meiotic maturation

The absolute concentration of 7974 proteins identified in our proteome dataset was calculated (See Appendix 1). We then performed a qualitative comparison of average oocyte abundance of proteins belonging to distinct functional groups (see Appendix 2). As expected, the less abundant subgroups include signaling molecules and transcription factors. Perhaps of more surprise, E3 enzymes and kinases are not abundant. At the other end of the spectrum are glycolytic and tricarboxylic acid cycle enzymes, as well as proteasome and ribosome components. These observations are expected because the oocyte has a stock of nutrient molecules and all the enzymes linked to their metabolism, which are used in viviparous animals throughout embryonic and larval development. For instance, the glycolytic enzyme GAPDH that catalyzes an important energy-yielding step in carbohydrate metabolism, is a very abundant protein in the oocyte (average concentration of between 8.88 μM and 17.83 μM). The ribogenesis program, which takes place during the oocyte growth from stage III to stage VI, before meiosis resumption, allows the accumulation of very large quantities of ribosomal RNAs and proteins that are used during embryonic development, until the swimming tadpole stage (Woodland, 1974). Similarly, the components of the DNA replication machinery are quite abundant, probably in anticipation of the post-fertilization cell cycles. All these data are therefore consistent with biological understanding of their roles during embryonic development after post-fertilization (Peshkin *et al*, 2015).

Temporal profiles of protein levels

We clustered the relative data for protein abundance across subsequent hourly timepoints post-progesterone stimulation (see Methods). As illustrated in Appendix 3A, the majority of the 60 expression

profiles are flat, demonstrating that most (over 80%) proteins are stable during meiotic maturation. Our proteomic dataset allowed to identify 12% of proteins affected by changes in concentration during meiotic progression by applying the same fold change threshold: 413 proteins that accumulate and 562 proteins whose concentration decreases (Figure 2B-figure supplement 3E; see Appendix 4). Although these changes only concern a minority of proteins, they are critical for the meiotic process. Since transcription is silent during this period, these documented changes must result from the regulation of translation or/and degradation (Meneau *et al*, 2020).

Protein accumulation: the machinery of cell division and DNA replication. Gene ontology analysis was used to characterize the functional significance of the 413 proteins whose level increases during meiosis. Proteins involved in spindle assembly and mitotic division were significantly enriched (Figure 2C). Among these important regulators are the Targeting-protein-for-Xklp2 (Tpx2) and Protein-regulator-of-cytokinesis 1 (Prc1) that also accumulate during meiotic maturation in mouse oocytes (Brunet *et al*, 2008; Li *et al*, 2021). We also find that the centrosomal maturation factor, SSX2IP, and two plus-end motors, the kinesins Kifc1 and Kif11 (Eg5) (Houliston *et al*, 1994), also accumulate significantly during meiotic maturation. Three of these proteins, Tpx2 and the two kinesins, play an important role in the assembly of both acentrosomal meiotic spindles and centrosomal mitotic spindles (Gruss, 2018; Kufer *et al*, 2002; Ems-McClung *et al*, 2020; Miller *et al*, 2019). Interestingly, the prophase oocyte is equipped with most of the proteins essential for the formation of division spindles. Hence these new results suggest that increases in the relative level of some components is required to support the meiotic and first rapid embryonic divisions.

Another protein category found to increase is the machinery of DNA replication initiation (Figure 2C). Indeed, oocytes accumulate the components of the DNA replication machinery during meiosis resumption to support the 13 rapid rounds of cell cycles occurring during early embryogenesis, all of which occur in the absence of transcription. In *Xenopus*, it was shown that Cdc6 is the only missing factor of the pre-replicative (pre-RC) complex in the prophase-arrested oocyte and that its accumulation occurs during the MI-MII transition (Lemaître *et al*, 2002; Whitmire *et al*, 2002; Daldello *et al*, 2015) (Figure 1). Translational and then post-translational mechanisms targeting Cdc6 prevent the pre-RC from functioning between the two meiotic divisions, thus ensuring the production of a haploid gamete. Our proteomic analysis shows that, even though the other pre-RC proteins, as ORC1, ORC2 and ORC6, are already expressed in prophase oocytes, they accumulate further during meiotic maturation, revealing a strong co-regulation of the components of the pre-RC.

Another process controlled by highly enriched proteins is vesicle tethering, which includes the family of exocyst proteins (Figure 2C). Interestingly, exocyst proteins are involved in the completion of cell division during the secretory-vesicle-mediated abscission (Gromley *et al*, 2005). The accumulation of these proteins during meiotic maturation could be important to support the extrusion of the polar bodies, as already suggested in *C. elegans* (Kumar *et al*, 2019) and the rapid cell divisions sustaining early embryogenesis.

Protein degradation: RNA-binding proteins (RBPs). Gene ontology analysis of the 562 proteins whose concentration decreases during meiosis reveals that 116 (21 %) are annotated to bind RNA. Among them, a large portion are RNA helicases (Figure 2D). Among these RBPs, another important group are proteins that are involved in ribosome biogenesis. The ribogenesis program takes place during the oocyte growth, allowing the accumulation of ribosomal RNAs and proteins that are used during embryonic development (Woodland, 1974). This process is downregulated during meiotic maturation (Hyman & Wormington, 1988; Chen *et al*, 2011). The decrease in the concentration of proteins involved in rRNA synthesis and processing does not result in a general decrease of ribosomal proteins that are stable during meiotic divisions (Figure 2-figure supplement 4A). Halting ribogenesis may allow the oocyte to re-allocate its energy resources to the production of other cellular components required for meiotic divisions and embryogenesis. Intriguingly, Rpl26 (Ribosomal protein L26) is the only ribosomal protein detected to decrease during meiotic divisions (Figure 2-figure supplement 4A). Since this protein is known to be dispensable for ribosome formation in yeast (Babiano *et al*, 2012; Warner & McIntosh, 2009; Takagi *et al*, 2005), the distinct regulation of Rpl26 as compared to the other Rpls suggests that Rpl26 might have extra-ribosomal functions. This hypothesis is reinforced by its specific modification by the ubiquitin-like UFMylation modification (Walczak *et al*, 2019) and its role in the regulation of protein stability (Zhang *et al*, 2016). Another subgroup of RBPs that decrease during meiotic divisions is involved in the repression of translation during prophase arrest, such as CPEB1 (Mendez *et al*, 2002; Reverte *et al*, 2001; Piqué *et al*, 2008), PATL2 (Nakamura *et al*, 2010; Cao *et al*, 2021; Christou-Kent *et al*, 2018) and Zar1l (Zar2) (Charlesworth *et al*, 2012; Yamamoto *et al*, 2013; Rong *et al*, 2019). Remodeling the repertoire of RBPs in the oocyte could be a general mechanism to regulate translation during meiotic divisions. Among these RBPs is Serbp1, which in mouse is involved in the stabilization of mRNA involved in meiosis resumption (Chew *et al*, 2013), as well as Caprin2, whose degradation is also observed during meiotic maturation of human oocytes (Virant-Klun *et al*, 2016). Caprin2 is an RBP with unknown function and highly enriched in the oocyte Balbiani body (Boke *et al*, 2016), a non-membrane compartment specific to the early diplotene oocytes, which contains mitochondria, RNAs and endoplasmic reticulum. The functions of this organelle

are not clear, although it is strongly correlated in *Xenopus* to the establishment of oocyte polarity and to the localization of maternal determinants (Jamieson-Lucy & Mullins, 2019). In *Xenopus*, it disperses at the onset of vitellogenesis, leaving a wedge-shaped cytoplasmic region rich in mitochondria (Wilk *et al*, 2005) and promotes the formation of RNP condensates in the vegetal cortex of the oocyte (Yang *et al*, 2022). Interestingly, Rbpms2, another regulator of the Balbiani body (Kaufman *et al*, 2018), is strongly degraded during meiotic maturation, highlighting how dynamic during meiosis is the composition of this transient compartment specific to the oocyte.

Interestingly, distinct E3 ubiquitin ligases, mainly APC and SCF (Skp, Cullin, F-box containing complex) have been shown to be active at different time periods of meiosis resumption in *Xenopus* oocytes (Kinterová *et al*, 2022). 186 proteins (37%) identified as decreasing in our proteome include in their sequences one of the APC degrons (Figure 2-figure supplement 4B). This group of proteins includes two known APC targets, Cyclin B2 (Glotzer *et al*, 1991) and Securin (Cohen-Fix *et al*, 1996). Additionally, 30 proteins (6%) whose concentration decreases in the oocytes have one SCF degron in their sequence (Figure 2-figure supplement 4B), including CPEB1 (Reverte *et al*, 2001) and Cdc6 (Daldello *et al*, 2015), two characterized SCF-targets. Interestingly, 253 proteins (57%) of proteins that decrease during meiotic divisions do not bear in their sequence any of the degrons for the ubiquitination systems identified in *Xenopus* oocytes (Figure 2-figure supplement 4B). Further research is therefore required to identify the sequences and the E3 enzymes and deubiquitinating enzymes that control the turnover of this important protein class.

The highly dynamic landscape of phosphorylation during meiotic maturation

We performed phosphoproteomic mass spectrometry analysis in order to measure the overall dynamics of protein phosphorylation taking place during meiotic divisions and to identify which specific proteins and which sites are phosphorylated during this process. We identified 6783 different phosphopeptides and quantified the dynamics of relative change across all time points (see Appendix 5). These peptides came from 2308 distinct proteins. When respective protein and un-phosphorylated peptide were also measured, we were able to compute the stoichiometry (see Methods). A list of all 415 phospho-sites for which it was possible to calculate the phospho-occupancy is provided as (see Appendix 6).

We identified the human homologous counterparts of 5901 (87%) among the 6783 sites found to be phosphorylated during meiotic divisions. Interestingly, only 177 (3%) out of 5901 conserved sites were already known to be phosphorylated on phosphosite.org database. Thus, our phosphosite dataset identifies a very large number of novel phosphosites, never previously identified and characterized. Such

308 a small number of previously reported phosphorylations among those detected by our phosphoproteome
309 might suggest that a large portion of these phosphorylation events are related to cell division. Dividing
310 cells generally account for a small fraction of tissue mass. This leads to a high dilution of the
311 phosphorylation signature of cell division, as compared to the highly synchronous meiotic divisions of
312 oocyte maturation. Interestingly, 60% of the phosphosites detected in oocytes are dynamically regulated
313 during meiotic maturation, highlighting the importance of this post-translational regulation in controlling
314 this last step of oogenesis and meiosis. Unbiased clustering reveals that changes in protein
315 phosphorylation are pervasive and far more dynamic than changes in protein abundance (see Appendix
316 3), which was also noted during yeast meiosis (Koch *et al*, 2024). Comparing the three stages of meiotic
317 division (PRO, MI and MII) and based on the main cellular events of these stages, we can group
318 phosphopeptide stoichiometry into 5 classes (Figure 3A; see Appendix 5). Class I includes proteins bearing
319 a phosphosite whose occupancy decreases during the first 2 hours following progesterone stimulation.
320 This class includes only 136 phosphopeptides (2%) which might be involved in the early signaling pathway
321 induced by progesterone and PKA downregulation. This small number was expected since there is a low
322 level of phosphorylation detectable in prophase-arrested oocytes (Maller *et al*, 1977). This makes sense
323 since there are presumably only a few substrates of PKA sufficient to initiate meiosis resumption. Class II
324 is larger (39% of the phosphopeptides) and includes proteins whose phosphorylation increases between
325 NEBD and MI and which remain highly phosphorylated in both MI and MII. The massive amount of Class
326 II phosphosites presumably reflects the catalytic power of Cdk1 as well as its downstream kinases, to
327 generate the thousands of substrates essential for cell division. Our measurements that most of the sites,
328 which are phosphorylated in MI, remain stably phosphorylated during MI to MII transition is consistent
329 with the observations made in yeast showing that most of Cdk1 motifs remain phosphorylated at the end
330 of meiosis I (Celebic *et al*, 2024). Class III (5%) consists of proteins whose phosphorylation peaks in MI
331 then decreases while oocytes progress throughout meiotic maturation. This is the most predominant class
332 of phosphosites present during meiotic maturation in starfish (Swartz *et al*, 2021) and follow the peculiar
333 pattern of Cdk1 activity peaking at MI in these oocytes (Okano-Uchida *et al*, 1998; Kishimoto, 2003). Class
334 IV (9%) is composed of proteins whose phosphorylation progressively increases from MI to MII, hence
335 potentially implicated in MII entry. Finally, Class V (5%) comprises proteins whose phosphorylation
336 increases from MII and which could play a role in establishing the MII arrest. The phosphosites that are
337 specific for either MI (Class III) or MII (Classes IV and V) are much less abundant (5%, 9% and 5%
338 respectively, Figure 3A) and might distinguish the biochemical state of the two meiotic divisions.
339

340 **The release of the prophase arrest: receptors and membrane trafficking**

341 ***Receptors.*** Since meiotic maturation signaling begins with the interaction of progesterone with
342 membrane receptors, we first focused our analysis on these proteins (Josefsberg Ben-Yehoshua *et al*,
343 2007; Sadler & Maller, 1985). Progesterone signals through activation of a seven-pass-transmembrane
344 progesterone receptor (mPRβ or PAQR8) that belongs to the progestin and adiponectin receptor family
345 (Josefsberg Ben-Yehoshua *et al*, 2007; Nader *et al*, 2018, 2020) (Figure 1). The release of the prophase
346 block also involves the inactivation of an orphan constitutively active GPCR, GPR185, responsible for
347 maintaining oocyte prophase arrest by ensuring high cAMP levels and PKA activity (Ríos-Cardona *et al*,
348 2008; Deng *et al*, 2008). Progesterone decreases GPR185 signaling either through its cleavage by a
349 metalloproteinase (Deng *et al*, 2008) or through its endocytosis (Nader *et al*, 2014). One limitation of our
350 dataset lies in the loss of some membrane proteins during the fractionation protocol, explaining why our
351 proteomic workflow did not detect mPRβ and GPR185 or its close relative GPR12. Nevertheless, it does
352 detect some proteins that interact with mPR, *i.e.* PGRMC1, VLDLR and APPL1. PGRMC1 is known to form
353 a receptor complex with mPRα and is necessary for mediating progesterone signaling in zebrafish oocytes
354 (Wu *et al*, 2018). Interestingly, our phosphorylation data reveals that PGRMC1 and its close relative
355 PGRMC2 are phosphorylated on two homologous threonine residues during meiotic maturation,
356 suggesting that these proteins may contribute to mPRβ activity in *Xenopus* oocytes. In the prophase-
357 arrested oocyte, VLDLR regulates mPR trafficking from the endoplasmic reticulum through the Golgi to
358 the plasma membrane, preparing the oocyte to be responsive to progesterone (Nader *et al*, 2018). In
359 contrast, progesterone induces clathrin-dependent endocytosis of mPRβ into signaling endosomes, where
360 mPR interacts transiently with APPL1 and Akt2 to induce meiosis (Nader *et al*, 2020). The
361 phosphoproteomic data reveal that both APPL1 and Akt are phosphorylated in response to progesterone
362 at the time of Cdk1 activation, suggesting that phosphorylation events regulate the traffic and activity of
363 this receptor.

364 ***Membrane traffic.*** Vesicular trafficking at the cell membrane appears to be crucial for the
365 maintenance and the release the prophase meiotic arrest, and may also function through early
366 embryogenesis (Figure 1). In the prophase-arrested oocyte, the accumulation of the GPR185 receptor at
367 the plasma membrane maintains high cAMP levels (Nader *et al*, 2014) while the plasma membrane
368 targeting of mPRβ renders the oocyte competent to respond to progesterone (Nader *et al*, 2018).

369 Exocytosis is also crucial for the formation of the fluid-filled blastocoele cavity during
370 embryogenesis (Müller, 2001). Indeed, the apical membrane of the epithelium surrounding the blastula,
371 where the polarized activities of ion channels and transporters generate the blastocoele fluid, is formed

372 from the oocyte cell membrane (Müller, 2001). This requires further remodeling. Progesterone rapidly
373 blocks this exocytosis pathway (Colman *et al*, 1985; Leaf *et al*, 1990), leading to a decrease in membrane
374 surface area, which is revealed by the disappearance of microvilli that are enriched in oocytes but almost
375 absent in eggs (Dumont, 1972; Kado *et al*, 1981; Larabell & Chandler, 1989; Bluemink *et al*, 1983).
376 Importantly, blocking exocytosis induces meiotic maturation, in the absence of hormonal stimulation
377 (Mulner-Lorillon *et al*, 1995; El-Jouni *et al*, 2007). Furthermore, progesterone stimulates endocytosis of
378 membrane proteins, such as GPR185, whose activity is suppressed by its internalization, and mPRβ, whose
379 internalization is required to transduce its effects (Nader *et al*, 2018, 2020, 2014). The stimulation of
380 endocytosis also converts plasma membrane into intracellular vesicles that can provide membrane
381 reserves, necessary to support the rapid cell divisions, and hence the requirement for greater total
382 membrane surface area, during embryogenesis (Angres *et al*, 1991; Gawantka *et al*, 1992). However, it is
383 unknown whether PKA is responsible for the active secretory transport during the prophase arrest and
384 how progesterone blocks exocytosis and stimulates endocytosis (Figure 1).

385 To improve our understanding of vesicular trafficking and membrane organization, we analyzed
386 the proteins involved in these processes whose phosphosites belong to Class I (Figure 3B). Among these
387 proteins, PI4KB deserves special attention. This protein is critical for the maintenance of the Golgi and
388 trans-Golgi phosphatidylinositol-4-phosphate (PI4) pools. PI4KB regulates Golgi
389 disintegration/reorganization during mitosis and is involved in Golgi-to-plasma membrane trafficking (De
390 Matteis *et al*, 2013). The phosphoproteome reveals that PI4KB is dephosphorylated within 2 hours after
391 progesterone stimulation, on a PKA consensus phosphorylation site conserved in vertebrates. The
392 phosphorylation of this site by PKA is known to control the interaction of PI4KB with Armadillo-like helical
393 domain-containing protein 3 (ARMH3), an interaction important for the Golgi membrane integrity
394 (McPhail *et al*, 2020; Isobe *et al*, 2017; Blomen *et al*, 2015). PI4KB is also regulated by its interaction with
395 ACBD3, an AKAP-like scaffold platform in Golgi, which directly binds the R regulatory subunit of PKA and
396 regulates the traffic between Golgi and endoplasmic reticulum in a PKA-depending manner (Jia *et al*, 2023;
397 Klima *et al*, 2016; Sasaki *et al*, 2012). The phosphoproteome reveals that ACBD3 is phosphorylated during
398 meiotic maturation at the time of NEBD (Class II). PI4KB is therefore at the crossroad between PKA and
399 intra-membrane endoplasmic reticulum-Golgi-plasma membrane trafficking. Since these are key events
400 involved in meiosis resumption, PI4KB is a particularly attractive candidate as a PKA substrate for future
401 functional studies of membrane relocalization.

402 Proteins involved in the actin cytoskeleton are also represented in Class I phosphosites (Figure
403 3B). Their early post-translational modifications could regulate the reorganization of the actin

404 cytoskeleton that is known to accompany the modification of the secretory/endocytosis pathways (Gard,
405 1999). Among them, ITPRID2/KRAP tethers IP_3 receptors, which are located in the membrane of the
406 endoplasmic reticulum, to the actin under the plasma membrane, to mediate Ca^{2+} signalling (Thillaiappan
407 *et al*, 2021). During meiotic maturation, the endoplasmic reticulum, which is the major Ca^{2+} store, is
408 enriched in the cortex of the oocyte (Campanella *et al*, 1984; Charbonneau & Grey, 1984; Terasaki *et al*,
409 2001). This remodeling brings the Ca^{2+} source close to its primary targets at fertilization, when Ca^{2+} release
410 from endoplasmic reticulum activates the oocyte and blocks polyspermy. The proteins highlighted above
411 (Figure 3B) could participate to this critical reorganization of the endoplasmic reticulum.
412
413 **Protein translation and accumulation orchestrate meiotic divisions**
414 Two waves of translation take place in the oocytes: the first depends on PKA inactivation. It occurs
415 upstream and independently of Cdk1 activity and is required for Cdk1 activation. The second translation
416 wave takes place downstream Cdk1 activation (Santoni *et al*, 2024). Hence, in contrast to mitosis, a period
417 when protein synthesis is repressed (Ross, 1997), translation is activated during meiotic maturation,
418 indicating the existence of meiosis-specific controls of the process. However, the regulation of the two
419 waves of protein translation and the identity of the newly translated proteins had not been unraveled.
420 Interestingly, protein translation components are extensively regulated at the level of phosphorylation as
421 demonstrated by the enrichment of the proteins regulating these processes among 3 of the 5
422 phosphopeptide classes (Figure 4A).
423 ***RBPs and translational control.*** Interestingly, several proteins implicated in the control of
424 translation bear phosphosites belonging to Class I, as eIF4ENIF1/4E-T, PATL1 and TACC3/Maskin (Figs. 3B
425 and 4B). eIF4ENIF1/4E-T is required for eIF4e1b localization to P-bodies where mRNAs are stored in a
426 dormant state in zebrafish oocytes (Lorenzo-Orts *et al*, 2023). Both 4E-T and eIF4e1b are extensively
427 phosphorylated on multiple residues during meiotic divisions, suggesting a highly dynamic regulation of
428 P-bodies during this process (Figure 4B). Many RBPs known to control translation in oocytes are also
429 regulated at the phosphorylation level, including Pum proteins (Nakahata *et al*, 2003; Ota *et al*, 2011;
430 Padmanabhan, 2006), Zar proteins (Charlesworth *et al*, 2012; Yamamoto *et al*, 2013; Rong *et al*, 2019;
431 Heim *et al*, 2022) and PATL proteins (Christou-Kent *et al*, 2018; Zhang *et al*, 2023; Marnef *et al*, 2010).
432 PATL1 is a RNA-binding protein required for cytoplasmic mRNA P-body assembly in oocytes (Marnef *et al*,
433 2010). PATL1 and PATL2 have mutually exclusive expression patterns in *Xenopus* oocytes: PATL2 is
434 degraded while PATL1 accumulates during meiotic maturation (Marnef *et al*, 2010), as confirmed by our
435 proteomic data (Figure 2B,D-figure supplement 3). Although the role of PATL2 and the regulation of its

436 stability by phosphorylation have been well documented in the oocyte (Christou-Kent *et al*, 2018; Zhang
437 *et al*, 2023), little is known about the role of PATL1 during meiosis. Both PATL1 and 2 inhibit translation
438 when tethered to mRNA and assemble a complex that includes CPEB1, Xp54/DDX6, Rap55B/LSM14b
439 (Marnef *et al*, 2010) (Figure 4B). The early dephosphorylation of PATL1 detected in the phosphoproteome
440 could modulate this inhibitory complex during early events of meiotic maturation, while the extensive
441 phosphorylation of the other components of the complex could control its activity later during meiotic
442 divisions (Figure 4B). Another component of the repressive complex that interacts with CPEB1 is
443 TACC3/Maskin, which is found widely regulated during meiotic divisions in the phosphoproteome (Figure
444 4B). TACC3/Maskin plays a dual function, regulating the centrosome-mediated microtubule nucleation
445 through γ-TuRC (Peset *et al*, 2005) but also translation (Barnard *et al*, 2005; Groisman *et al*, 2002). Eight
446 residues in TACC3/Maskin, of which only two are conserved in human Maskin (214/228 and 298/317 in
447 human/*Xenopus*), exhibit a complex profile of phosphorylation (Figure 4B). Two sites identified in the
448 phosphoproteome, S266 and S298, were previously found to be phosphorylated in egg extracts, regulating
449 the function of TACC3/Maskin in the control of translation (Barnard *et al*, 2005). S626 was also reported
450 to be phosphorylated in prophase oocytes and during oocyte meiotic maturation, although there is some
451 controversy about the kinase (either PKA or Aurora-A) and the role of this phosphorylation in either the
452 control of translation or centrosome attachment (Barnard *et al*, 2005; Pascreau *et al*, 2005). Interestingly,
453 in our studies S240 is phosphorylated in the prophase oocyte and dephosphorylated early in response to
454 progesterone (Class I) (Figure 4B). Since the sequence surrounding S240 does not correspond to a PKA
455 consensus motif, it is hard to establish the biological significance; nevertheless, such an early
456 dephosphorylation deserves further attention.

457 ***The control of translation initiation.*** Translation regulation might not only depend on the
458 expression and post-translational regulation of the RBPs but could also involve the regulation of the core
459 translation initiation machinery, since we find that many of its components are phosphorylated (Figure
460 4C). Indeed, eIF4b, an activator of the eIF4a helicase that facilitates ribosome scanning (Jackson *et al*,
461 2010), eIF2b/eIF2s2, a component of the molecular machinery recruitment on the met-tRNA (Jackson *et*
462 *al*, 2010), and eIF4g, involved in the recognition of the mRNA 5'Cap (Jackson *et al*, 2010), are among the
463 proteins bearing sites whose phosphorylation peaks in MII (Figure 4-figure supplement 1). These
464 phosphorylation patterns correlate with the second wave of activation of translation that begins under
465 the control of Cdk1 activity in MI and continues progressively through MII (Meneau *et al*, 2020; Santoni
466 *et al*, 2024).

467 ***The control of ubiquitin ligases***. The levels of specific proteins are also regulated by proteolysis
468 at each step of meiotic maturation. Targeted regulation allows for the accumulation of key proteins
469 independently of any general increase in their translation, such as for Cyclin B1 (Santoni *et al*, 2024), or
470 the well-studied degradation of proteins, such as Cyclin B2, securin or CPEB1 (Taieb *et al*, 2001;
471 Wassmann, 2022; Setoyama *et al*, 2007). Interestingly, proteins controlling polyubiquitination display
472 phosphopeptides enriched in Class II, strengthening the view that a major regulation of protein turnover
473 takes place at NEBD in order to orchestrate meiotic divisions (Figures 3 and 5A). APC is the key E3 ubiquitin
474 ligase that promotes metaphase-anaphase transition. Although the phosphorylation status of some
475 substrates determines their recognition by APC and influences the precise timing of their degradation,
476 APC activity is also regulated by the phosphorylation of its core subunits (Bansal & Tiwari, 2019) (Figure
477 5B).

478 Another important ubiquitination system that regulates stability of proteins during mitosis and
479 meiosis is the SCF complex (Kinterová *et al*, 2022). SCF is composed of three main components: Cul1, a
480 scaffold protein; Skp1, which interacts with specific F-box proteins that are involved in the substrate
481 recognition; and Rbx1, which interacts with the E2-ubiquitin ligases (Kinterová *et al*, 2022) (Figure 5C). SCF
482 ligases play important roles during oocyte meiotic maturation, especially the $SCF^{\beta TrCP}$ complex. $SCF^{\beta TrCP}$-
483 mediated degradation of Emi1, Emi2/Erp1, CPEB1 and BTG4 is essential for progression through MI and
484 MII of mouse and *Xenopus* oocytes (Kinterová *et al*, 2022). This is very similar to the role of Emi1 in mitosis
485 and is thought to set the time between binding of cyclin B and its destruction (Reimann *et al*, 2001).

486 Many F-Box proteins are also expressed in *Xenopus* oocytes, but they do not display high
487 phosphorylation dynamics. An exception is Lmo7/Fbxo20, which is degraded during meiosis, and is
488 dynamically phosphorylated (Figure 5C). Interestingly, Lmo7 overexpression causes defects at the spindle
489 assembly checkpoint, affecting the progression through mitotic divisions (Tzeng *et al*, 2018).

490 Additionally, many E2 enzymes were identified in our datasets as highly regulated at the
491 translational/accumulation and post-translational levels during meiotic maturation (Figure 5C). This layer
492 of regulation of protein ubiquitination remains understudied. Interestingly, an E2/E3 hybrid ubiquitin-
493 protein ligase, UBE2O, UBE4B (also known as UBOX3 or E4) and FAF2 (or Ubxn3B/UBXD8) display
494 phosphorylation sites belonging to Class I (Figures 3B and 5C). FAF2 is involved in stress granule clearance
495 (Gwon *et al*, 2021). UBE2O is also known to be involved in the drastic proteome remodeling during
496 erythroid differentiation (Nguyen *et al*, 2017), as well as quality control factor for orphans of multiprotein
497 complexes (Yanagitani *et al*, 2017). Ribosomal proteins are known substrates of UBE2O which leads to
498 their degradation (Nguyen *et al*, 2017). Whether UBE2O is involved in the downregulation of ribosome

499 biogenesis that occurs during meiotic maturation (Hyman & Wormington, 1988), and in the decrease of
500 Rpl26 (Figure 2-figure supplement 4A), is an interesting question. The dephosphorylation of UBE2O,
501 UBE4B and FAF2 could also be involved in the accumulation of Cyclin B1, which was recently shown to
502 occur independently of any increase in translation but to result from protein stabilization (Santoni *et al*,
503 2024).

504 Another important regulator of the SCF system, DCUN1D5, is found regulated in our
505 phosphoproteome. DCUN1D5 catalyzes the neddylation of all cullins, which is necessary for the activation
506 of cullin-RING E3 ubiquitin ligases (Keuss *et al*, 2016). DCUN1D5 is dephosphorylated at S9, a PKA
507 consensus site, and phosphorylated starting NEBD at S10 and S12 (Figure 5C). These phosphorylations
508 could control DCUN1D5 ability to activate SCF, especially since the inhibition of neddylation causes a
509 meiotic arrest in MI in mouse oocytes (Yang *et al*, 2019). Altogether, our dataset provides attractive
510 candidates to be involved in the regulation of both translation and protein stability that occur during
511 meiotic maturation.

512

513 **Activation of Cdk1 occurs through an intricate network of phosphorylation of Cdk1 regulators**

514 The activation of Cdk1 during oocyte maturation relies on an intricate network of feedforward and
515 feedback phosphorylation pathways mediated by kinases and phosphatases (Figure 1). Indeed,
516 components of the cell division machinery are highly enriched among Class II, III, IV and V (Figure 6A).
517 Some of the phosphorylation sites implicated in cell division control have been identified previously
518 through detailed studies using site-specific mutagenesis and phospho-specific antibodies. Our
519 phosphoproteomic analysis of oocyte maturation provides new regulatory elements (Figure 6B). An
520 important regulator of the Cdk1 auto-amplification loop is the kinase Plk1 that contributes to the
521 phosphorylation of the two direct Cdk1 regulators, Cdc25 and Myt1 (Myt1, a membrane-bound protein,
522 was not detected in our proteome). Plk1 is activated by Aurora-A, a kinase itself under the indirect control
523 of Cdk1 in *Xenopus* oocyte (Maton *et al*, 2003), through the phosphorylation of T210 (T201 in
524 *Xenopus*)(Macůrek *et al*, 2008), a residue localized in the activation T-loop of the kinase domain. We show
525 here that Plk1 phosphorylation at T210 increases in MI and is then constant throughout meiotic
526 maturation (Class II) (Figure 6B-figure supplement 1A). This is consistent with the function of Plk1, which
527 phosphorylates multiple proteins required for the mechanics of division, and which must logically be kept
528 active throughout both meiotic divisions (Hansen *et al*, 2006; Solc *et al*, 2015). Interestingly, the
529 phosphoproteome also detects additional phosphorylation sites of Plk1, S326 (S335 in human) and S340
530 (not conserved in human), which were previously found to be upregulated in response to okadaic acid

531 (Wind *et al*, 2002), an inhibitor of PP2A that strongly induces M-phase. These two residues are located
532 between the two functional domains of Plk1, the kinase domain and the Polo-box domain (Cheng, 2003).
533 This suggests that the phosphorylation of other critical residues than T210 of Plk1 could be essential for
534 its catalytic activation. Aurora-A kinase is activated during meiotic maturation downstream Cdk1 (Maton
535 *et al*, 2003; Castro *et al*, 2003; Maton *et al*, 2005). While our phosphoproteome does not detect Aurora-
536 A autophosphorylation at T288 (T295 in *Xenopus*), it registers the extensive phosphorylation of Bora, an
537 activator of Aurora-A involved in Plk1 activation (Thomas *et al*, 2016) (Figure 6B-figure supplement 1B).
538 Several phosphorylation sites of Bora have been reported to be important for its function as an Aurora-A
539 activator: S41/38, S112/110, S137/135 and S252/S252 (human/*Xenopus*) (Thomas *et al*, 2016; Vigneron
540 *et al*, 2018; Tavernier *et al*, 2015, 2021). Among these sites, S110 phosphorylation of Bora by Cdk1-Cyclin
541 A is critical for mitotic entry in *Xenopus* egg extracts (Vigneron *et al*, 2018; Tavernier *et al*, 2015, 2021).
542 Our phosphoproteome reveals that Bora belongs to Class II, being phosphorylated starting NEBD, but
543 surprisingly on distinct sites that were never reported in the literature: S191/189, T294/287, S552/549, S-
544 /521, T12/9 and T15/12 (human/*Xenopus*), with the exception of S278/285. In contrast to the situation in
545 mitosis, Cyclin A is very weakly expressed in the prophase oocyte and accumulates during meiotic
546 maturation (Kobayashi *et al*, 1991). Our proteome dataset reveals that Cyclin A accumulates after MI.
547 Hence, the phosphorylation of Bora at MI cannot be catalyzed by Cdk1-Cyclin A in the *Xenopus* oocyte.
548 Cdk1-Cyclin B is probably involved in these phosphorylations that take place concomitantly with its activity
549 and at Cdk1 phosphorylation consensus sites for 5 of the 7 phosphosites (Figure 6B-figure supplement
550 1B). Thus, this analysis reveals that Bora activation correlates with its phosphorylation at residues not
551 previously identified in earlier studies of the oocyte. We also detect additional phosphorylation events on
552 other players of the Cdk1 amplification loop, as Cdc25 and Gwl/MASTL (Figure 6B-figure supplement 1C-
553 D), whose extensive phosphorylation during M-phase is usually detected by a large electrophoretic shift
554 (Dupré *et al*, 2014).
555
556 **Phosphoregulation of the bimodal activity of Cdk1 during MI-MII transition**
557 In *Xenopus* oocytes, Cdk1 is not fully inactivated at anaphase I and during extrusion of the 1st polar body.
558 Indeed, the low Cdk1 activity that persists during the MI-MII transition is essential to avoid the
559 reformation of a nucleus, chromosome decondensation and DNA replication (Huchon *et al*, 1993; Thibier
560 *et al*, 1997). This short period is followed by a further increase of Cdk1 activity, due to a sustained synthesis
561 of B-cyclins; the increased Cdk1 activity allows the formation of the MII spindle (Gerhart *et al*, 1984)
562 (Figure 1). Although this bimodal subtle regulation of Cdk1 activity is essential for the success of meiosis,

563 *i.e*. linking two successive divisions without intervening DNA replication, it has never been quantified
564 precisely. Cdk1 activity can be measured by looking at the phosphorylation of one of its direct substrates,
565 Cdc27, a core APC component, at S428 (S426 in human)(Patra & Dunphy, 1998). Our precise quantification
566 of the phospho-occupancy of this site shows that its phosphorylation is virtually absent in prophase,
567 increases by 40% in MI, decreases during the MI-MII transition to 20%, then increases again in MII by 60%
568 (Figure 6-figure supplement 1E). Three other residues of Cdc27, T205/207, S435/437 and S438/440
569 (human/*Xenopus*), also known to be phosphorylated at M-phase (Kraft, 2003), follow the same bimodal
570 pattern than S428. The subsequent increase in Cdk1 activity essential for MII entry requires that the kinase
571 escapes inhibitory phosphorylations by Myt1 and Wee2. Both Myt1 and Wee2 are reported to be inhibited
572 by phosphorylations, although the sites responsible for this inhibition are not precisely defined. Myt1, a
573 membrane protein, was not detected in our proteome. In *Xenopus*, Wee2 is not expressed in prophase
574 oocytes and accumulates after NEBD (Nakajo *et al*, 2000; Charlesworth *et al*, 2012) (Figure 1). Our analysis
575 reveals that newly synthesized Wee2 is immediately phosphorylated at 4 sites (Classes II and IV), one of
576 them being not conserved in human, and none of them corresponding to the proposed inhibitory S53 and
577 S123 sites (Figure 6A-B-figure supplement 1F). Hence, these data provide exciting new avenues of
578 research to discover unexpected new regulations of old players in Cdk1 activation.
579
580 **The Mos/MAPK pathway activation**
581 Mos plays a well-known role at the origin of a critical pathway controlling meiotic maturation (Yew *et al*,
582 1992; Furuno *et al*, 1994). It phosphorylates Mek1/2, which in turn phosphorylates Erk1/2 (also known as
583 MAPK) which leads to Rsk1/2 activation (Figure 6B). These play multiple essential roles, such as preventing
584 the reformation of a replicating nucleus between MI and MII (Dupre *et al*, 2002), enabling arrest in MII
585 (Sagata *et al*, 1989b), but also participating in Cdk1 activation (Sagata *et al*, 1989a) and the functioning of
586 meiotic spindles (Araki *et al*, 1996; Choi *et al*, 1996; Bodart *et al*, 2005). The phosphoproteome detects
587 the activation of the Mos-MAPK module, with the phosphorylation of Erk2 on T185 and Y187 (T188 and
588 Y190 in *Xenopus*) by MEK1/2 (Payne *et al*, 1991), an event that begins in MI (Figure 6B-figure supplement
589 2A). Interestingly, additional phosphorylation sites are identified in MEK1 and Rsk1/2, the latter being
590 hyperphosphorylated during meiosis as detected by a large electrophoretic shift (Bhatt & Ferrell, 2000)
591 (Figure 6B-figure supplement 2B-E). Rsk1 auto-phosphorylation at S381 (S380 in human) is required for
592 its activity (Vik & Ryder, 1997). Our phosphoproteome measures a highly-confident phospho-occupancy
593 for this site demonstrating the switch-like activation of the MAPK pathway at NEBD, followed by the
594 maintenance of a constant level of its activity (Figure 6B-figure supplement 2F). The timing of activation

595 of the Mos-MAPK cascade has been controversial, one hypothesis being that it is activated before Cdk1
596 and participates in the activation of this kinase (Sagata *et al*, 1988; Gavin *et al*, 1999), while another is that
597 it is under the control of the starter Cdk1 activity and is only involved in the autoamplification loop
598 (Santoni *et al*, 2024; Dupre *et al*, 2002; Fisher *et al*, 1999). The phosphoproteomic data clearly support the
599 latter.
600
601 **Phosphorylation of key components of the nuclear envelope during breakdown**
602 As a result of the massive activation of kinase activities under the control of Cdk1, hundreds of proteins
603 are phosphorylated and orchestrate the structural events choreographing the mechanics of meiotic
604 divisions. The first of these is the massive vesiculation of the nuclear envelope surrounding the enormous
605 oocyte nucleus. During mitosis, nuclear pore proteins are extensively phosphorylated by Cdk1-Cyclin B,
606 Plk1 and Nek6/7 to promote the breakdown of the nuclear envelope (Kutay *et al*, 2021). The *Xenopus*
607 oocyte has the unusual feature of having an enormous nucleus (475 μm in diameter), and therefore a
608 considerable surface area of the nuclear envelope (0.96 mm^2), as well as large stocks of annulate lamellae
609 in the cytoplasm. Annulate lamellae are cytoplasmic stack cisternae of nuclear envelope perforated with
610 nuclear pores, 10 times more abundant than in the nucleus in the *Xenopus* oocyte, but devoid of lamins
611 (Bement & Capco, 1990; Miller & Forbes, 2000; Cordes *et al*, 1995). Their surface area also far exceeds
612 that of the nuclear envelope surrounding the nucleus (Cordes *et al*, 1995). This correlates with the high
613 protein concentrations of the nuclear pore proteins (0.1 to 0.7 μM) that we have measured (Figure 7A).
614 Annulate lamellae play a critical role as a reservoir for the formation of the 4000 of nuclei that form during
615 the embryonic cell divisions leading up to the mid-blastula transition and the onset of transcription (Kessel
616 *et al*, 1986; De Magistris & Antonin, 2018; Feldherr, 1974). During meiotic maturation, NEBD and
617 vesiculation of annulate lamellae occur at the same time, in a progressive spatial manner, starting from
618 the vegetal pole. Importantly, the nucleus and annulate lamellae do not re-form between the two meiotic
619 divisions, reducing the risk that an S-phase can take place between MI and MII (Bement & Capco, 1990).
620 A gene ontology analysis of our phosphoproteome highlights that the phosphorylation of nuclear pore
621 components is enriched in Classes II, III and IV, displaying the highest level of enrichment in Class III, hence
622 characteristic of MI (Figure 7B). The nucleoporin Nup53 (also called Nup35) is a component of the soluble
623 core region of the nuclear pore complex that is extensively phosphorylated in mitosis by Cdk1 and Plk1
624 (Linder *et al*, 2017). Phosphomimetic mutations of all Cdk1 and Plk1 sites in Nup53 slow down the
625 reformation of nuclear pores in interphase and mutation to phospho-null amino acids impairs the nuclear
626 breakdown during meiosis (Linder *et al*, 2017). Our phosphoproteome reveals that Nup53

627 phosphorylation is more dynamic than previously believed (Figure 7C). Indeed, 6 phosphopeptides are
628 found to peak in MI (Class III), 9 phosphopeptides are phosphorylated both in MI and MII (Class II), and 2
629 phosphopeptides continuously increase in phosphorylation during meiotic maturation (Class IV) (Figure
630 7C). We were able to calculate the phospho-occupancy of the S59 (S66 in human), showing that it
631 increases from 30% in prophase to 90% in MI oocytes and stays constant until MII (Class II) (Figure 7D).
632 Several other transmembrane nucleoporins, notably NDC1 and POM121C, undergo dramatic increase of
633 phosphorylation at transition to MI. Altogether, these observations indicate that dissociation of the
634 nuclear envelope and the annulate lamellae occurring in MI might require either a specific set of
635 phosphorylations and/or a general level of phosphorylation that is higher than the level of
636 phosphorylation required to maintain the nucleus and the annulate lamellae dissociated during the MI-
637 MII transition through MII.
638
639 **The regulation of centrosomal proteins during oocyte maturation**
640 An intriguing feature of oocytes in most, if not all, metazoan species is the elimination of their centrioles.
641 This allows the sperm to contribute its centriole and thereby initiates the division cycle and the cell cycle.
642 There is longstanding literature that proves that the oocyte or egg has retained its ability to generate
643 centrioles. However, in nature, the female centrioles are lost and the sperm centriole is the main
644 contributor. In *Xenopus*, oocytes entering prophase I contain a typical centrosome, including a pair of
645 centrioles and pericentriolar material (PCM) containing γ-tubulin and pericentrin. Centrioles disappear at
646 the end of the pachytene stage of prophase I and PCM disperses in multiple foci in the cytoplasm that are
647 no longer functional as microtubule nucleation sites (Gard *et al*, 1995). At fertilization, the male gamete
648 delivers two centrioles but does not provide the PCM (Delattre & Gönczy, 2004). Therefore, in most
649 species (with the exception of rodents), the complete centrosome of the one-cell stage embryo is a bi-
650 parental inheritance, reconstituted from paternal centrioles and maternal PCM (Delattre & Gönczy, 2004).
651 In *Xenopus*, oocytes store enough quiescent centrosomal building blocks for duplicating and assembling
652 1000 to 2000 centrosomes (Gard *et al*, 1990). This implies that oocytes should comprise an enormous
653 reserve of centrosomal proteins, *i.e.* centriolar and PCM proteins, that sustain the reconstitution of a
654 functional centrosome at fertilization and its subsequent rounds of duplication in the early embryo.
655 ***Centriolar proteins.*** The centriole is formed by a polarized cylinder of microtubule triplets,
656 decorated along the proximal to distal axis with several appendages that define the three main regions of
657 the organelle: the proximal part, the central core, and the distal region (LeGuennec *et al*, 2021). In
658 agreement with a published RNA-seq and proteome of *Xenopus* eggs (Session *et al*, 2016; Wühr *et al*,

659 2014), our proteome reveals that most of the centriolar proteins are expressed in the oocyte (Table 1).
660 The components of the proximal part, as SAS-6 and CPAP/CENPJ, and of the central core, as POC1B, POC5
661 and Centrin 1, are either constant or accumulate during meiotic maturation (Table 1). In contrast, proteins
662 of distal and subdistal appendages are present at lower concentration, either constant or decreasing
663 during meiotic maturation (Table 1). Indeed, the appendages are critical for the docking of mature
664 centrioles at the plasma membrane and ciliogenesis (Tanos *et al*, 2013), a process that is not functional in
665 the oocyte and during the early embryonic divisions (Drysdale & Elinson, 1992).

666 Besides the basic building blocks forming the centriole, the oocyte is expected to provide the
667 machinery for its duplication, the first cycle occurring immediately after fertilization. The key regulators
668 of centriole duplication, including Plk4, SAS-6 and STIL, are generally expressed at very low levels (Bauer
669 *et al*, 2016). While Plk4 is expressed at the mRNA level in oocytes but escaped our proteomic detection,
670 SAS-6 and STIL are expressed at a constant level during meiotic maturation (Table 1). The estimated
671 concentrations of both proteins are in agreement with the previous predictions, that cartwheels comprise
672 one molecule of STIL for every SAS-6 dimer (Bauer *et al*, 2016). Other important regulators of centriole
673 duplication, such as CEP192, CEP152, CEP63, RTTN, CEP110/CCP110, CEP97 and CEP76 were also
674 detected, and are either constant or accumulate during meiotic divisions (Table 1). Interestingly, our
675 phosphoproteome reveals that several of these proteins are phosphorylated during meiotic maturation.
676 STIL is phosphorylated at S554, which is located in a Cdk1 phosphorylation consensus (Table 1-table
677 supplement 1A), an interesting observation since phosphorylation of STIL by Cdk1-Cyclin reduces the
678 efficiency of daughter centriole assembly. This phosphorylation provides an explanation why centrioles
679 cannot duplicate during M-phase (Zitouni *et al*, 2016; Steinacker *et al*, 2022). A massive CEP97
680 phosphorylation occurs at MI at 8 distinct sites, only 3 of them lying within a Cdk1 consensus motif (Table
681 1-table supplement 1B). Remarkably, one of the phosphosites of CEP97, S633, has been recently shown
682 to be phosphorylated by the kinase Dyrk1a in multiciliated cells of *Xenopus* embryos (Lee *et al*, 2022); it
683 is required for centriole duplication. Therefore, although centrioles are not assembled, all centriolar
684 proteins are expressed in the full-grown oocyte and these components serve as a stock for the biogenesis
685 of the centrioles of the embryo. Our results suggest that specific phosphorylations of proteins regulating
686 centriole assembly could prevent the *de novo* establishment of centrioles in the oocyte.

687 ***PCM proteins.*** The core element of the PCM is the γ-tubulin ring complex (γ-TuRC) which is the
688 basic element for nucleation of microtubules from microtubule-organizing centers (MTOCs) (Oakley &
689 Oakley, 1989). It includes γ-tubulin that is combined with other proteins known as GCP2/tubgcp2 to
690 GCP6/tubgcp6. Some PCM proteins or regulators of PCM assembly have been described in functional

691 studies to be present in the oocyte and then recruited to the zygotic centrosome as maternal components.
692 These include γ-tubulin (Stearns & Kirschner, 1994; Gard, 1994; Félix *et al*, 1994), pericentrin (Dictenberg
693 *et al*, 1998), Nek2B (Fry *et al*, 2000; Uto, 2000), SSX2IP (Bärenz *et al*, 2013),TPX2, PRC1, Kif4A, Eg5/Kif11,
694 CLASP1/Xorbit and Kif22/Xkid, CEP152 (Hatch *et al*, 2010), NEDD1 (Liu & Wiese, 2008), Maskin/TACC3
695 (Stebbins-Boaz *et al*, 1999; Peset *et al*, 2005), XMAP215/CKAP5 (Popov *et al*, 2002; Kinoshita *et al*, 2002)
696 and Nercc1/NEK9 (Roig *et al*, 2005).

697 Most of the PCM proteins were detected in our proteomic dataset and either accumulate or stay
698 constant during meiotic divisions (Table 1). Our dataset highlights that γ-tubulin accumulates during
699 meiotic divisions at the time the oocytes enter MII (Table 1-table supplement 1C). GCP2 and 4 are
700 expressed at a lower level than γ-tubulin (Table 1), in agreement with the expected stoichiometry of GCPs-
701 γ-tubulin in the γ-TuRC (Sulimenko *et al*, 2022). The phosphorylation of γ-TuRC components is known to
702 affect the stability and the activation of the complex (Sulimenko *et al*, 2022). We detected the
703 phosphorylation of GCP3 at S814 (Class IV) and GCP6 at S1173 (Class III) (Table 1-table supplement 1D).
704 This second phosphosite is well conserved in the human protein and targeted by Plk4, which regulates
705 centriole duplication (Bahtz *et al*, 2012). These results indicate that the oocyte, despite the absence of
706 centrioles, prepares a functional centrosomal machinery by accumulating and/or phosphorylating some
707 of the PCM proteins. Apart of the γ-TuRC complex, we found that 10 other PCM proteins are
708 phosphorylated during meiotic maturation (CEP192, SSX2IP, CEP41, TACC3/Maskin, Nucleophosmin,
709 Katanin, Kif11, Kif15/Eg5, Numa and Dynein). CEP192 is a coiled-coil scaffolding protein that recruits γ-
710 TuRC, Aurora-A and Plk1 to the centrosome for its maturation. Our phosphoproteome reveals that
711 CEP192, a Class II protein, is phosphorylated at 7 sites between prophase and MI, 5 of them corresponding
712 to Cdk1 phosphorylation sites (Table 1-table supplement 1E). Plk1 is recruited to its many different
713 locations in the cell through its Polo-Box-Domain (PBD), which binds to phosphorylated S-S/T(p) motifs
714 (Elia *et al*, 2003a, 2003b; Lee *et al*, 1998; Reynolds & Ohkura, 2003). Two of the CEP192 sites identified in
715 our phosphoproteome, S991 and S1227, correspond to such motifs. Therefore, by attracting Plk1, CEP192
716 phosphorylation could prepare the reconstitution of a functional centrosome at fertilization.
717

718 **Assembly of microtubule spindles and microtubule dynamics**

719 *Xenopus* prophase oocytes are inefficient in their ability to support microtubule polymerization (Jessus *et*
720 *al*, 1984; Gard & Kirschner, 1987; Heidemann & Kirschner, 1975), although microtubules are formed at
721 the cortical and nuclear envelope level, where γ-tubulin foci are also localized (Gard, 1994; Jessus *et al*,
722 1988). The ability to assemble microtubule asters is acquired at the time of NEBD, when a giant disk-

723 shaped MTOC generates a large microtubular monoaster at the basal region of the disintegrating nucleus
724 (Huchon *et al*, 1981; Gard, 1994). Therefore, MTOC and microtubule-associated proteins (MAPs) must be
725 finely regulated by post-translational modifications at time of NEBD. The transient microtubule monoaster
726 transports the meiotic chromosomes to the animal cortex, where the first meiotic spindle is assembled
727 (Huchon *et al*, 1981; Gard, 1992). Due to the absence of centrioles, meiotic spindles are barrel-shaped
728 and are formed by centrosome-independent microtubule nucleation originating from the chromosomes
729 and involving chromatin and the Ran GTPase (Gruss & Vernos, 2004), much like spindles of vascular plant
730 cells. Moreover, the two successive spindles are differentially regulated. The MI spindle is a transient and
731 dynamic structure while the MII spindle is stable for hours, anchored to the plasma membrane until
732 fertilization (Gard, 1992). Therefore, it is possible that MAPs are specifically and differentially regulated
733 at MI and MII (Classes III and V). Finally, a major change in microtubule assembly occurs during the
734 transition from meiosis to embryonic mitosis. The assembly of the first embryonic spindle integrates the
735 meiotic chromosome-dependent pathway with the newly formed centrosomes (Cavazza *et al*, 2016).
736 Thereafter, subsequent embryonic spindles depend solely on the microtubule nucleating activity of the
737 centrosomes (Kirschner, 1986). All these critical transitions in the way of assembling a microtubular
738 spindle depend on the proteins stored in the oocyte.

739 At least 5 microtubule regulatory proteins undergo specific patterns of phosphorylation that
740 deserve attention (Figure 8). Katanin (KATNB1), which is responsible for the majority of M-phase severing
741 activity in *Xenopus* eggs and is activated by Cdk1 (McNally & Thomas, 1998), displays a bi-modal pattern
742 of phosphorylation, increasing at the time of formation of the monoaster-MTOC and MI spindle,
743 decreasing during MI-MII transition and increasing again at MII (Figure 8). Kif11/Eg5 phosphorylation
744 occurs at T936 and T937 starting NEBD (Figure 8). Both phosphosites were reported in a broad range of
745 models, and the second site was shown to be phosphorylated by Cdk1 (Blangy *et al*, 1995; Cahu *et al*,
746 2008; Giet *et al*, 1999) (Figure 8). Kif11/Eg5 controls the relative stability of bipolar versus monopolar
747 organization of spindles in *Xenopus* egg extracts (Mitchison *et al*, 2005) but also centrosome disjunction
748 and/or separation. Hence, Kif11 is a good candidate to be an important player regulating the original
749 changes in microtubule dynamics and organization of the two successive spindles. Kif15, also known as
750 XKlp2, a plus end-directed kinesin protein required for centrosome separation and maintenance of spindle
751 bipolarity in *Xenopus* egg extracts (Boleti *et al*, 1996), is phosphorylated at S681 and S692 during meiotic
752 maturation. S681 is rather phosphorylated at MI while S692 is specific of MII (Figure 8), suggesting a
753 potential distinct regulation of Kif15 on microtubule dynamics at MI and MII. Dyneins are a family of motor
754 proteins that move to microtubules in an opposed direction to kinesins. Among this family, the two

755 paralog genes dynein light intermediate chain (DynC1LI1 and DynC1LI2) play important roles in mitosis,
756 including positioning the spindle and focusing the MTs into poles. Our phosphoproteome reveals multiple
757 phosphorylations of these proteins, starting in MI and remaining constant or progressively increasing until
758 MII, as for S197 of DynC1LI1 (S207 in human) (Figure 8). This agrees with previous data showing that S197
759 is phosphorylated by Cdk1 (Dell *et al*, 2000; Addinall *et al*, 2001) and that DynC1LI becomes
760 hyperphosphorylated at the time of NEBD and remains hyperphosphorylated throughout the rest of
761 meiosis (Huang *et al*, 1999). Additionally, our phosphoproteome reveals that 3 sites (495, 498 and 501)
762 are phosphorylated around NEBD and get dephosphorylated after MI (Class III), hence being correlated
763 with the 1st meiotic division and not the 2nd one, while 6 other sites (197,396, 409,446, 452, and 467) are
764 phosphorylated both in MI and MII (Class II) (Figure 8). Dynein is required for organization of the original
765 microtubule/MTOC array that is organized at NEBD, together with XMAP215, XKCM1 and Numa (Becker
766 *et al*, 2003). The formation of this oocyte original monoaster/MTOC could involve the dynein
767 phosphorylations that transiently take place precisely at this period.
768 Strikingly, MI and MII spindles segregate chromosomes and chromatids in a very different way. In
769 MI, the homologous chromosomes are segregated, whereas in MII the sister chromatids are displaced in
770 the daughter cells, due to a specific organization of kinetochores and regulation of cohesins. In MI, arm
771 cohesins are phosphorylated and degraded whereas centromeric cohesins are protected from cleavage
772 by Sugoshin (Sgo1)-PP2A. This allows the separation of chromosomes, but chromatids are still attached
773 together. In MII, centromeric cohesins are fully degraded, allowing the segregation of sister chromatids,
774 as during mitosis (Wassmann, 2022). How a fraction of cohesins is protected from cleavage in MI but not
775 in MII is still not entirely clear since the phosphorylation of cohesins and their partners, which are not very
776 abundant proteins, is difficult to be detected with conventional shotgun phosphoproteomics. Notably,
777 our phosphoproteomic studies highlight new sites differentially phosphorylated between MI and MII
778 within these proteins. Sgo1 and two components of the cohesin complex, Pds5b and Wapl, are
779 increasingly phosphorylated during meiotic divisions (Class IV) (Figure 8-figure supplement 1).
780 Noteworthy, S1069 of Wapl is a putative Plk1 site (Grosstessner-Hain *et al*, 2011; Kettenbach *et al*, 2011).
781 By highlighting new sites differentially phosphorylated between MI and MII, our phosphoproteomic
782 studies provide clues to elucidate the still unknown mechanisms of the meiotic mechanism of cohesion
783 protection-deprotection.
784

785 **DISCUSSION**

786 The amphibian oocyte and egg have long been a source of inspiration and a source of
787 experimental opportunity for important areas of biology, such as nuclear organization, spindle formation,
788 cell polarity, fertilization, mitosis and meiosis, endocrine signaling and intracellular signal transduction. As
789 experimental embryology gave way to genetic approaches in the late 20th century to study embryonic
790 development, the attractiveness of amphibian oocytes declined.

791 The original advantages of the amphibian oocyte are now becoming more obvious, as it becomes
792 important to link complex cellular processes, like cell division, to signal transduction. These processes are
793 difficult to study because they occur at a single cell or even at subcellular level. Indeed, many important
794 cell-division related processes involve transient changes occurring in specific compartments of the cell,
795 like the endoplasmic reticulum, the mitotic apparatus, the nuclear and plasma membranes, or the
796 cytoskeleton. Additionally, meiotic and mitotic divisions occupy a very short fraction of the life span of
797 germ and somatic cells, making it hard to study them in cultured cells. Frog oocytes and eggs show
798 exquisite synchrony of cell division, allowing to have large cohort of cells at the same stage of the cell
799 cycle. Therefore, we and others have returned to the awesome power of the amphibian oocyte and egg
800 to study the signal transduction, intracellular posttranslational changes surrounding the onset of meiotic
801 and mitotic divisions and fertilization at a single cell level.

802 Importantly, the ingenious and sensitive tools developed to study the transcriptional regulation
803 are of little use in the study of a cell type that does not transcribe RNA and of events that are regulated
804 post-translationally, as meiotic and early embryonic divisions. For a long time, we lacked general tools for
805 identification and measurement of the activity of the regulators of these processes, impairing our ability
806 to connect the morphological changes previously described by histology to the respective molecular
807 events. One manner to investigate these pathways is using pharmacological inhibitors, but their non-
808 specificity and the complexity of pathways pose serious limitations. For years, phosphorylation events
809 have been extensively studied using candidate-based approaches, as site-specific mutagenesis and
810 phosphospecific antibodies. These targeted-approaches have several caveats. The selection of the
811 putative sites of phosphorylation is based on *in silico* evidence, limiting the analysis to proteins bearing
812 canonical consensus sequences and hence our knowledge of novel phosphorylation motifs. When
813 multiple putative phosphorylation sites are present in the same protein, mutagenesis of individual sites
814 or combinations of sites becomes too complex, impairing identification of the phosphorylation sites used
815 *in vivo* and their interdependency or redundancy. Moreover, the time-consuming production of phospho-
816 specific antibodies is not scalable to high throughput applications. Mass spectrometry has the potential

of shedding light on these intricated networks. However, the current tools are unable to accurately quantify the level of proteins and phosphorylated proteins at the single cell level -except for the frog oocytes and eggs, thanks to their exceptional size and high protein content.

Oocyte meiotic maturation is a key biological process. First, it transforms the oocyte into a fertilizable cell at the origin of life of any animal. Second, since meiosis derives from mitosis, thanks to cellular adaptations that were necessary to produce a haploid gamete (preventing an S-phase between the two divisions, modifying the functioning of the spindle during meiosis I, establishing division arrests needed for the oocyte to grow or to wait for sperm, performing asymmetrical divisions to save nutrient reserves, etc.), its study provides the opportunity to understand how cell division can adapt and diversify in living systems, depending on specific cellular organization and specialized functions.

In this paper, we have applied the current state of the art of quantitative mass spectrometry to oocyte maturation and meiotic divisions using quantitative proteomics and quantitative phosphoproteomics. We have temporally correlated events with oocyte maturation induced naturally by progesterone to *Xenopus* full-grown oocytes and watched the progression through meiosis I to the natural arrest at the second meiotic metaphase. We have been able to correlate the proteomic measurements with the physiological changes as the oocyte, as it goes from an early prophase I state through to a second meiotic metaphase state. We find dramatic changes in the oocyte nucleus and the meiotic spindles and drastic modifications to the standard cell cycle. These dramatic changes are choreographed principally by signaling pathways employing kinases and phosphatases. In all animals, meiotic maturation relies on the dynamics of phosphorylation events, either during the signaling pathway that leads to Cdk1 activation or during the Cdk1 downstream period that orchestrates the structural events of the two meiotic divisions. The candidate-based approaches have provided a global scheme of this process based on the knowledge of a few kinases that have been extensively studied for years. However, this scheme still does not provide a very comprehensive picture of the meiotic process, since it does not take into account hundreds of unknown critical kinases, substrates and phosphosites. Our quantitative proteomics and phosphoproteomics approach allowed to obtain a much deeper and comprehensive dynamic picture of the phosphorylated sites during meiotic maturation. This has enabled us to describe and support with biochemical precision the various processes in the oocyte, determine the relative timing of various site phosphorylations and molecular processes, thereby challenging or suggesting the epistatic sequences of specific molecular pathways. Furthermore, we confirmed the importance of certain previously known phosphosites, identified the likely kinases or in some cases the kinase families responsible for substrate

848 phosphorylation, and established connections between phosphorylation events and intracellular
849 remodeling, as well as regulatory mechanisms such as translation and protein degradation.
850 In addition to explaining the order of diverse events of chromatin remodeling, nuclear
851 organization, plasma membrane transformations, cytoskeletal changes of meiosis, our proteomic and
852 phospho-proteomic datasets should provide a large number of experimental avenues for exploring similar
853 events in both mitotic and meiotic stages of diverse organisms. This molecular data will enable us to better
854 understand regulatory pathways involving chromosome behavior, spindle formation, nuclear and plasma
855 membrane regulation, and signal transduction and derive insights far beyond the scope of meiosis and
856 oocyte maturation. One such insight might come from a closer analysis of the quality control mechanisms
857 in the oocyte. Both nucleopore remodeling (King *et al*, 2019) and E2/E3 ubiquitin ligases are involved in
858 housekeeping and quality control, specifically in the removal of aggregated and orphan complex proteins,
859 as the germ cell of an organism prepares to become the next generation
860

861 **METHODS**

862 **Oocytes collection and *in vitro* maturation**

863 The research with *Xenopus laevis* was performed under the oversight of the Harvard Medical Area
864 Institutional Animal Care and Use Committee. Mature *Xenopus laevis* females were used after priming
865 with pregnant mare serum gonadotropin (PMSG, 50 IU per frog). A sample of ovary tissue was surgically
866 removed, rinsed in 1× Marc's modified Ringer's (MMR) and placed in OR2 buffer (83 mM NaCl, 2.5 mM
867 KCl, 1 mM $CaCl_2$, 1 mM $MgCl_2$, 1 mM Na_2HPO_4, 5 mM HEPES, pH 7.8) and oocytes were manually
868 defolliculated. Stage VI oocytes were selected and kept in dishes with agar beds to avoid sticking to the
869 dish. Maturation was induced by incubation at 18 °C with 10 μg/mL progesterone in OR2 buffer.
870 Eggs were flash frozen with liquid nitrogen in bunches of ten or fifty for protein and phospho-proteomics
871 measurements respectively. All samples were taken in triplicates, each biological replicate was performed
872 with different frogs. The first sample was taken from untreated oocytes at the time of progesterone
873 treatment, the second timepoint 2 hours after progesterone treatment, with hourly timepoints past that,
874 up to 9 hours post treatment.
875

876 **Embryo lysis and digestion into peptides**

877 For each condition the embryos were lysed at a ratio of 6 μL buffer/embryo in the same buffer as (Presler
878 *et al*, 2017) (0.25 M sucrose, 1% replacement NP-40, 10 mM EDTA, 25 mM HEPES, 1 mM TCEP, 10 μM
879 Combretastatin, 10 μM Cytochalasin D, Roche Protease Inhibitor Mini EDTA free, and Phosstop inhibitor
880 (Roche) at pH 7.2). The yolk was removed by spinning the samples at 4,000 g for 4 minutes at 4°C. Both
881 the supernatant and all lipids were transferred for a new tube. The concentration of HEPES was raised to
882 0.1 M and SDS was added to 20%. After addition of DTT to 5 mM, the samples were denatured in a 60°C
883 water bath for 20 minutes. After the samples temperatures return to room temperature, N-
884 Ethylmaleimide (NEM) was added to 15 mM, tubes were mixed thoroughly, and the reaction proceeded
885 for 1 hour. Then additional DTT was added to 5 mM to quench the excess NEM. The samples were flash
886 frozen and stored at -80°C until the methanol chloroform precipitation (Wessel & Flügge, 1984). Protein
887 was precipitated by methanol-chloroform precipitation. Due to the large volume of lysate (~ 1 mL), the
888 precipitation was performed in glass 15 mL Corex tubes (No. 8441). The tubes were cleaned for a two-
889 hour chromic acid incubation and rinsed extensively in filtered water. Then they were autoclaved and
890 before use for the precipitation, they were rinsed with HPLC H_20. The centrifugations were done in a JA
891 50 30 Ti rotor in a Beckman Avanti J-30I centrifuge at 21,000 g for either 6 minutes or 15 minutes. After
892 the last supernatant was removed, the pellets were air dried for 15 minutes and resuspended in 0.6 mL

of 6 M guanidine, 50 M EPPS pH 8.5 and transferred to a 2 mL eppendorf tube. The samples were incubated for 5 minutes at 65°C and the protein amount was determined by a BCA Assay. The solution was diluted to 2 M guanidine with 10 mM EPPS pH 8.5. Lysyl endopeptidase (FUJIFILM WAKO (129-02541) resuspended with HPLC H_20 to ~2 mg/mL) was added to a concentration of 20 ng/mL and the initial digestion proceeded for 12 hours at room temperature with gentle shaking. The samples were further diluted to 0.5 M guanidine with 10 mM EPPS pH 8.5 and Trypsin protease (Sequencing Grade Modified Trypsin, Promega) was added to a final concentration of 10 ng/mL along with an additional 20 ng/mL of LysC. The samples were incubated in a 37°C room for 8 hours on a nutator.

Phospho-peptide enrichment

To carry out the phosphoproteomic analysis, we made the conventional steps of digesting the proteins from each time sample with trypsin and specifically labeling them with isobaric tags (TMT-10 reagents). Tagged samples and the phosphopeptides were enriched on an IMAC column. Importantly, we chose to multiplex peptides before the phosphopeptide enrichment to improve data quality. There is a tradeoff of decreased yield and therefore depth, as it is not economical to label more than a few milligrams of material. We used 2.5-4 mgs of TMT-labeled peptides per replicate, enriched with 5 µm Titanium Dioxide microspheres (GL Sciences 5020-75000) and fractioned as previously described (Presler *et al*, 2017). A typical yield of 50-80 µg of peptides eluted from the column, with a median phosphopeptide enrichment of ~80%.

Phosphatase treatment of *Xenopus* samples prepared for parallel phospho-enrichment

We adapted the method that we used to phosphatase-treat digested peptides (Presler *et al*, 2017) for the larger samples used here for the parallel phospho-enrichment. We chose to phosphatase treat when proteases were present in the samples (but after the protease digestion sequence described above) to enable the de-phosphorylated peptides to have the cleavage pattern expected if they were present initially in the de-phosphorylated state. We used the heat-labile Alkaline Shrimp Phosphatase (Affymetrix Inc, USA). We used a 3k Amicon Centrifugal Filter to exchange the enzyme storage buffer to 10 mM EPPS pH 8.5 instead of Tris-HCl pH 7.5. We also concentrated the phosphatase to between 3-4 U/µL (confirmed by p-nitrophenyl phosphate assay). We added an estimated 833 units of phosphatase to two of the samples built to contain representative mixture of peptides (TMT 131N, channel 10: 100 oocytes collected at the latest timepoint, and TMT 131C, channel 11: 50 oocytes collected at the first timepoint combined with 50 oocytes collected at the last timepoint). To samples that were not phosphatase-treated, we added

925 the same volume of blank phosphatase buffer: 5 mM EPPS pH 8, 50% glycerol. To all samples, we added
926 $MgCl_2$ to 10 mM and EDTA to 0.1 mM (to chelate metals that might compete with the magnesium
927 necessary for enzymatic activity). All the samples were incubated with gentle shaking at room
928 temperature for 12 hours. The phosphatase was then inactivated by incubation with gentle shaking in an
929 air-incubator at 65°C for 15 minutes. Peptide fractionation and TMT-MS3 LC/MS were carried out as done
930 previously (Presler *et al*, 2017).
931
932 **Computing phospho-occupancy systematically**
933 We grouped phospho-peptides by unique phospho-site identifiers. In order to rigorously reflect the
934 measurement accuracy and to take advantage of many measurements of the same phospho-site
935 (including on peptides with different missed-cleavages or oxidized methionines), we used BACIQ (Peshkin
936 *et al*, 2019) to compute the estimated trend with confidence intervals. Then, we created phospho-site
937 sets to connect phospho-sites on residues that could be on the same peptide. We made these assignments
938 based on whether the individual phospho-sites were ever measured with another phospho-site as a
939 composite phospho-site. In order to determine occupancy, we needed to measure the phospho-site as a
940 different form (usually not-phosphorylated). To do this, we identified non-phosphorylated peptides
941 measured from the same experimental conditions that include the residue(s) of the phospho-site. Again,
942 multiple non-phosphorylated peptides can include the residues of interest and the same peptide
943 sequences can be measured multiple times. Therefore, we again use BACIQ (Peshkin *et al*, 2019) to
944 aggregate these measurements in a trend with confidence intervals. The MATLAB implementation is freely
945 available at https://github.com/elizabeth-van-itallie/phospho_occupancy_matlab.
946
947 **Mass spectrometry data mapping and analysis**
948 Peptide-Spectra matches were performed as previously described (Sonnett *et al*, 2018). Assignment of
949 MS2 spectra was performed using the SEQUEST (Eng *et al*, 1994) algorithm by searching the data against
950 the appropriate proteome reference set acquired from Xenbase (*Xenopus laevis* assembly 9.1) along with
951 common contaminants: human keratins and trypsin. The target-decoy strategy was used to construct a
952 second database of reversed sequences that were used to estimate the false discovery rate on the peptide
953 level. SEQUEST searches were performed using a 20 ppm precursor ion tolerance with the requirement
954 that both N- and C-terminal peptide ends are consistent with the protease specificities of LysC and Trypsin.
955 TMT (+229.162932 Da) was set as a static modification on N-termini and lysines peptides, and N-ethyl
956 maleimide (+125.047679 Da) was set as a static modification on cysteine residues. Oxidation of

957 methionine (+15.99492 Da) was set as a variable modification. A peptide level MS2 spectral assignment
958 false discovery rate of 1% was obtained by applying the target-decoy strategy with linear discriminant
959 analysis. Peptides of 7 amino acids length or longer were ranked by linear discriminant analysis score and
960 were filtered to a ratio of 1% reverses/forwards + reverses. Peptides were assigned to proteins and a
961 second filtering step to obtain a 1% FDR on the protein level was applied. Peptides that matched multiple
962 proteins were assigned to the proteins with the most unique peptides. We only used Isolation Specificity
963 > 0.75 spectra.
964
965 **Estimation of the absolute abundance of proteins**
966 The absolute protein concentration was estimated according previously published methods (Wühr *et al*,
967 2014; Peshkin *et al*, 2015), based here on ion current prorated to the isobarically labeled fractions. The
968 respective sample fractions were estimated using our previously published Bayesian approach (Peshkin
969 *et al*, 2019), which integrates peptide signal and peptide-level measurement agreement into a maximum
970 likelihood estimate of the true protein ratio and the associated confidence interval (Peshkin *et al*, 2019).
971 See Appendix 1.
972
973 **Data availability**
974 The mass spectrometry proteomics raw data and reference set of sequences have been deposited to the
975 ProteomeXchange consortium via the PRIDE partner repository with the dataset identifier MassIVE
976 MSV000094498. In addition, we developed a multi-functional Web portal to release the data and enable
977 interactive interrogation (https://xenopus.hms.harvard.edu/index_oocyte.html). All of the aspects from
978 overall protein trends to individual clusters to specific phosphosites and stoichiometry information are
979 easily available. The portal provides per-protein link to external information about each human protein
980 by symbol from GeneCards (https://www.genecards.org/) and respective *Xenopus* protein at Xenbase
981 (https://www.xenbase.org/xenbase/).
982
983

ACKNOWLEDGMENTS

This work was supported by the National Center for Scientific Research (CNRS) and Sorbonne University, the National Research Agency (ANR) grants 18-CE13-0013-01 (CJ) and ANR-23-CE12-0045-01 (EMD), Sorbonne University Emergence grant (EMD), the ARC foundation grant ARCPJA2023080006901 (EMD), Amaranth Foundation (LP) and the NIH OD award R24 OD031956 (LP and MWK).

AUTHOR CONTRIBUTIONS

Leonid Peshkin: Conceptualization; Methodology; Experiments; Software; Formal Analysis; Data Curation; Writing; Supervision. **Enrico M Daldello**: Formal Analysis; Writing. **Elizabeth Van Itallie**: Software; Formal Analysis; Data Curation; Writing. **Matthew Sonnett**: Methodology; Formal Analysis. **Johannes Kreuzer**: Formal Analysis; Data Curation. **Wilhelm Haas**: Methodology; Formal Analysis. **Marc W Kirschner**: Conceptualization; Methodology; Experiments; Writing; Supervision. **Catherine Jessus**: Writing; Formal Analysis; Supervision. **Marc W Kirschner** and **Catherine Jessus** contributed equally to this work.

DISCLOSURE AND COMPETING INTERESTS STATEMENT

The authors declare no competing interests.

1003 **REFERENCES**
1004

1005 Addinall SG, Mayr PS, Doyle S, Sheehan JK, Woodman PG & Allan VJ (2001) Phosphorylation by cdc2-
1006 CyclinB1 Kinase Releases Cytoplasmic Dynein from Membranes. *Journal of Biological Chemistry*
1007 276: 15939–15944

1008 Angres B, Müller AHJ, Kellermann J & Hausen P (1991) Differential expression of two cadherins in
1009 *Xenopus laevis*. *Development* 111: 829–844

1010 Araki K, Naito K, Haraguchi S, Suzuki R, Yokoyama M, Inoue M, Aizawa S, Toyoda Y & Sato E (1996)
1011 Meiotic Abnormalities of c-mos Knockout Mouse Oocytes: Activation after First Meiosis or
1012 Entrance into Third Meiotic Metaphase1. *Biol Reprod* 55: 1315–1324

1013 Babiano R, Gamalinda M, Woolford JL & de la Cruz J (2012) Saccharomyces cerevisiae ribosomal protein
1014 L26 is not essential for ribosome assembly and function. *Mol Cell Biol* 32: 3228–3241

1015 Bahtz R, Seidler J, Arnold M, Haselmann-Weiss U, Antony C, Lehmann WD & Hoffmann I (2012) GCP6 is a
1016 substrate of Plk4 and required for centriole duplication. *Journal of Cell Science* 125: 486–496

1017 Bansal S & Tiwari S (2019) Mechanisms for the temporal regulation of substrate ubiquitination by the
1018 anaphase-promoting complex/cyclosome. *Cell Div* 14: 14

1019 Bärenz F, Inoue D, Yokoyama H, Tegha-Dunghu J, Freiss S, Draeger S, Mayilo D, Cado I, Merker S, Klinger
1020 M, *et al* (2013) The centriolar satellite protein SSX2IP promotes centrosome maturation. *Journal*
1021 *of Cell Biology* 202: 81–95

1022 Barnard DC, Cao Q & Richter JD (2005) Differential Phosphorylation Controls Maskin Association with
1023 Eukaryotic Translation Initiation Factor 4E and Localization on the Mitotic Apparatus. *Molecular*
1024 *and Cellular Biology* 25: 7605–7615

1025 Bauer M, Cubizolles F, Schmidt A & Nigg EA (2016) Quantitative analysis of human centrosome
1026 architecture by targeted proteomics and fluorescence imaging. *The EMBO Journal* 35: 2152–
1027 2166

1028 Becker BE, Romney SJ & Gard DL (2003) XMAP215, XKCM1, NuMA, and cytoplasmic dynein are required
1029 for the assembly and organization of the transient microtubule array during the maturation of
1030 Xenopus oocytes. *Developmental Biology* 261: 488–505

1031 Bement WM & Capco DG (1990) Transformation of the amphibian oocyte into the egg: Structural and
1032 biochemical events. *J Elec Microsc Tech* 16: 202–234

1033 Bhatt RR & Ferrell JE (2000) Cloning and Characterization of Xenopus Rsk2, the Predominant p90 Rsk
1034 Isozyme in Oocytes and Eggs. *Journal of Biological Chemistry* 275: 32983–32990

1035 Blangy A, Lane HA, d'Hérin P, Harper M, Kress M & Niggt EA (1995) Phosphorylation by p34cdc2
1036 regulates spindle association of human Eg5, a kinesin-related motor essential for bipolar spindle
1037 formation in vivo. *Cell* 83: 1159–1169

1038 Blomen VA, Májek P, Jae LT, Bigenzahn JW, Nieuwenhuis J, Staring J, Sacco R, Van Diemen FR, Olk N,
1039 Stukalov A, *et al* (2015) Gene essentiality and synthetic lethality in haploid human cells. *Science*
1040 350: 1092–1096

1041 Bluemink JG, Hage WJ, van den Hoef MH & Dictus WJ (1983) Freeze-fracture electron microscopy of
1042 membrane changes in progesterone-induced maturing oocytes and eggs of Xenopus laevis. *Eur J*
1043 *Cell Biol* 31: 85–93

1044 Bodart J-FL, Baert FY, Sellier C, Duesbery NS, Flament S & Vilain J-P (2005) Differential roles of p39Mos–
1045 Xp42Mpk1 cascade proteins on Raf1 phosphorylation and spindle morphogenesis in Xenopus
1046 oocytes. *Developmental Biology* 283: 373–383

1047 Boke E, Ruer M, Wühr M, Coughlin M, Lemaitre R, Gygi SP, Alberti S, Drechsel D, Hyman AA & Mitchison
1048 TJ (2016) Amyloid-like Self-Assembly of a Cellular Compartment. *Cell* 166: 637–650

1049 Boleti H, Karsenti E & Vernos I (1996) Xklp2, a Novel Xenopus Centrosomal Kinesin-like Protein Required
1050 for Centrosome Separation during Mitosis. *Cell* 84: 49–59

1051 Bouftas N, Schneider L, Halder M, Demmig R, Baack M, Cladière D, Walter M, Al Abdallah H, Kleinhempel
1052 C, Messaritaki R, *et al* (2022) Cyclin B3 implements timely vertebrate oocyte arrest for
1053 fertilization. *Developmental Cell* 57: 2305-2320.e6

1054 Brunet S, Dumont J, Lee KW, Kinoshita K, Hikal P, Gruss OJ, Maro B & Verlhac M-H (2008) Meiotic
1055 Regulation of TPX2 Protein Levels Governs Cell Cycle Progression in Mouse Oocytes. *PLoS ONE* 3:
1056 e3338

1057 Cahu J, Olichon A, Hentrich C, Schek H, Drinjakovic J, Zhang C, Doherty-Kirby A, Lajoie G & Surrey T
1058 (2008) Phosphorylation by Cdk1 Increases the Binding of Eg5 to Microtubules In Vitro and in
1059 Xenopus Egg Extract Spindles. *PLoS ONE* 3: e3936

1060 Campanella C, Andreuccetti P, Taddei C & Talevi R (1984) The modifications of cortical endoplasmic
1061 reticulum during in vitro maturation of *Xenopus laevis* oocytes and its involvement in cortical
1062 granule exocytosis. *J Exp Zool* 229: 283–293

1063 Cao Q, Zhao C, Wang C, Cai L, Xia M, Zhang X, Han J, Xu Y, Zhang J, Ling X, *et al* (2021) The Recurrent
1064 Mutation in PATL2 Inhibits Its Degradation Thus Causing Female Infertility Characterized by
1065 Oocyte Maturation Defect Through Regulation of the Mos-MAPK Pathway. *Front Cell Dev Biol* 9:
1066 628649

1067 Castro A, Mandart E, Lorca T & Galas S (2003) Involvement of Aurora A Kinase during Meiosis I-II
1068 Transition in Xenopus Oocytes. *J Biol Chem* 278: 2236–2241

1069 Cavazza T, Peset I & Vernos I (2016) From meiosis to mitosis: the sperm centrosome defines the kinetics
1070 of spindle assembly after fertilization. *Journal of Cell Science*: jcs.183624

1071 Celebic D, Polat I, Legros V, Chevreux G, Wassmann K & Touati SA (2024) Qualitative rather than
1072 quantitative phosphoregulation shapes the end of meiosis I in budding yeast. *EMBO J*

1073 Charbonneau M & Grey RD (1984) The onset of activation responsiveness during maturation coincides
1074 with the formation of the cortical endoplasmic reticulum in oocytes of Xenopus laevis.
1075 *Developmental Biology* 102: 90–97

1076 Charlesworth A, Yamamoto TM, Cook JM, Silva KD, Kotter CV, Carter GS, Holt JW, Lavender HF, MacNicol
1077 AM, Ying Wang Y, *et al* (2012) Xenopus laevis zygote arrest 2 (zar2) encodes a zinc finger RNA-
1078 binding protein that binds to the translational control sequence in the maternal Wee1 mRNA
1079 and regulates translation. *Dev Biol* 369: 177–190

1080 Chen J, Melton C, Suh N, Oh JS, Horner K, Xie F, Sette C, Blelloch R & Conti M (2011) Genome-wide
1081 analysis of translation reveals a critical role for deleted in azoospermia-like (Dazl) at the oocyte-
1082 to-zygote transition. *Genes Dev* 25: 755–766

1083 Cheng K-Y (2003) The crystal structure of the human polo-like kinase-1 polo box domain and its
1084 phospho-peptide complex. *The EMBO Journal* 22: 5757–5768

1085 Chew TG, Peaston A, Lim AK, Lorthongpanich C, Knowles BB & Solter D (2013) A Tudor Domain Protein
1086 SPINDLIN1 Interacts with the mRNA-Binding Protein SERBP1 and Is Involved in Mouse Oocyte
1087 Meiotic Resumption. *PLoS ONE* 8: e69764

1088 Choi T, Fukasawa K, Zhou R, Tessarollo L, Borror K, Resau J & Vande Woude GF (1996) The Mos/mitogen-
1089 activated protein kinase (MAPK) pathway regulates the size and degradation of the first polar
1090 body in maturing mouse oocytes. *Proc Natl Acad Sci USA* 93: 7032–7035

1091 Christou-Kent M, Kherraf Z, Amiri-Yekta A, Le Blévec E, Karaouzène T, Conne B, Escoffier J, Assou S,
1092 Guttin A, Lambert E, *et al* (2018) PATL 2 is a key actor of oocyte maturation whose invalidation
1093 causes infertility in women and mice. *EMBO Mol Med* 10

1094 Cohen-Fix O, Peters JM, Kirschner MW & Koshland D (1996) Anaphase initiation in Saccharomyces
1095 cerevisiae is controlled by the APC-dependent degradation of the anaphase inhibitor Pds1p.
1096 *Genes Dev* 10: 3081–3093

1097 Colman A, Jones EA & Heasman J (1985) Meiotic maturation in Xenopus oocytes: a link between the
1098 cessation of protein secretion and the polarized disappearance of Golgi apparati. *The Journal of*
1099 *cell biology* 101: 313–318

1100 Cordes VC, Reidenbach S & Franke WW (1995) High content of a nuclear pore complex protein in
1101 cytoplasmic annulate lamellae of Xenopus oocytes. *Eur J Cell Biol* 68: 240–255

1102 Daldello EM, Le T, Poulhe R, Jessus C, Haccard O & Dupré A (2015) Control of Cdc6 accumulation by Cdk1
1103 and MAPK is essential for completion of oocyte meiotic divisions in *Xenopus*. *J Cell Sci* 128:
1104 2482–2496

1105 De Magistris P & Antonin W (2018) The Dynamic Nature of the Nuclear Envelope. *Current Biology* 28:
1106 R487–R497

1107 De Matteis MA, Wilson C & D'Angelo G (2013) Phosphatidylinositol-4-phosphate: The Golgi and beyond.
1108 *BioEssays* 35: 612–622

1109 Delattre M & Gönczy P (2004) The arithmetic of centrosome biogenesis. *Journal of Cell Science* 117:
1110 1619–1630

1111 Dell KR, Turck CW & Vale RD (2000) Mitotic Phosphorylation of the Dynein Light Intermediate Chain is
1112 Mediated by cdc2 Kinase. *Traffic* 1: 38–44

1113 Deng J, Lang S, Wylie C & Hammes SR (2008) The Xenopus laevis Isoform of G Protein-Coupled Receptor
1114 3 (GPR3) Is a Constitutively Active Cell Surface Receptor that Participates in Maintaining Meiotic
1115 Arrest in X. laevis Oocytes. *Molecular Endocrinology* 22: 1853–1865

1116 Dictenberg JB, Zimmerman W, Sparks CA, Young A, Vidair C, Zheng Y, Carrington W, Fay FS & Doxsey SJ
1117 (1998) Pericentrin and γ-Tubulin Form a Protein Complex and Are Organized into a Novel Lattice
1118 at the Centrosome. *The Journal of Cell Biology* 141: 163–174

1119 Drysdale TA & Elinson RP (1992) Cell Migration and Induction in the Development of the Surface
1120 Ectodermal Pattern of the *Xenopus laevis* Tadpole: (*Xenopus* /ciliated cell/hatching
1121 gland/cement gland/ectodermal differentiation). *Dev Growth Differ* 34: 51–59

1122 Dumont JN (1972) Oogenesis inXenopus laevis (Daudin). I. Stages of oocyte development in laboratory
1123 maintained animals. *J Morphol* 136: 153–179

1124 Dupré A, Daldello EM, Nairn AC, Jessus C & Haccard O (2014) Phosphorylation of ARPP19 by protein
1125 kinase A prevents meiosis resumption in Xenopus oocytes. *Nat Commun* 5: 3318

1126 Dupre A, Jessus C, Ozon R & Haccard O (2002) Mos is not required for the initiation of meiotic
1127 maturation in Xenopus oocytes. *EMBO J* 21: 4026–4036

1128 Elia AEH, Cantley LC & Yaffe MB (2003a) Proteomic Screen Finds pSer/pThr-Binding Domain Localizing
1129 Plk1 to Mitotic Substrates. *Science* 299: 1228–1231

1130 Elia AEH, Rellos P, Haire LF, Chao JW, Ivins FJ, Hoepker K, Mohammad D, Cantley LC, Smerdon SJ & Yaffe
1131 MB (2003b) The Molecular Basis for Phosphodependent Substrate Targeting and Regulation of
1132 Plks by the Polo-Box Domain. *Cell* 115: 83–95

1133 El-Jouni W, Haun S, Hodeify R, Hosein Walker A & Machaca K (2007) Vesicular traffic at the cell
1134 membrane regulates oocyte meiotic arrest. *Development* 134: 3307–3315

1135 Ems-McClung SC, Emch M, Zhang S, Mahnoor S, Weaver LN & Walczak CE (2020) RanGTP induces an
1136 effector gradient of XCTK2 and importin α/β for spindle microtubule cross-linking. *Journal of Cell*
1137 *Biology* 219: e201906045

1138 Eng JK, McCormack AL & Yates JR (1994) An approach to correlate tandem mass spectral data of
1139 peptides with amino acid sequences in a protein database. *J Am Soc Mass Spectrom* 5: 976–989

1140 Feldherr CM (1974) The binding characteristics of the nuclear annuli. *Experimental Cell Research* 85:
1141 271–277

1142 Félix M, Antony C, Wright M & Maro B (1994) Centrosome assembly in vitro: role of gamma-tubulin
1143 recruitment in Xenopus sperm aster formation. *The Journal of cell biology* 124: 19–31

1144 Fisher DL, Brassac T, Galas S & Dorée M (1999) Dissociation of MAP kinase activation and MPF activation
1145 in hormone-stimulated maturation of Xenopus oocytes. *Development* 126: 4537–4546

1146 Frank-Vaillant M, Jessus C, Ozon R, Maller JL & Haccard O (1999) Two Distinct Mechanisms Control the
1147 Accumulation of Cyclin B1 and Mos in *Xenopus* Oocytes in Response to Progesterone. *MBoC* 10:
1148 3279–3288

1149 Fry AM, Descombes P, Twomey C, Bacchieri R & Nigg EA (2000) The NIMA-related kinase X-Nek2B is
1150 required for efficient assembly of the zygotic centrosome in Xenopus laevis. *Journal of Cell*
1151 *Science* 113: 1973–1984

1152 Furuno N, Nishizawa M, Okazaki K, Tanaka H, Iwashita J, Nakajo N, Ogawa Y & Sagata N (1994)
1153 Suppression of DNA replication via Mos function during meiotic divisions in Xenopus oocytes.
1154 *EMBO J* 13: 2399–2410

1155 Gaffré M, Martoriati A, Belhachemi N, Chambon J-P, Houliston E, Jessus C & Karaiskou A (2011) A critical
1156 balance between Cyclin B synthesis and Myt1 activity controls meiosis entry in *Xenopus* oocytes.
1157 *Development* 138: 3735–3744

1158 Gard DL (1992) Microtubule organization during maturation of Xenopus oocytes: Assembly and rotation
1159 of the meiotic spindles. *Developmental Biology* 151: 516–530

1160 Gard DL (1994) γ-Tubulin Is Asymmetrically Distributed in the Cortex of Xenopus Oocytes.
1161 *Developmental Biology* 161: 131–140

1162 Gard DL (1999) Confocal microscopy and 3-D reconstruction of the cytoskeleton ofXenopus oocytes.
1163 *Microsc Res Tech* 44: 388–414

1164 Gard DL, Affleck D & Error BM (1995) Microtubule Organization, Acetylation, and Nucleation in Xenopus
1165 laevis Oocytes: II. A Developmental Transition in Microtubule Organization during Early
1166 Diplotene. *Developmental Biology* 168: 189–201

1167 Gard DL, Hafezi S, Zhang T & Doxsey SJ (1990) Centrosome duplication continues in cycloheximide-
1168 treated Xenopus blastulae in the absence of a detectable cell cycle. *The Journal of cell biology*
1169 110: 2033–2042

1170 Gard DL & Kirschner MW (1987) Microtubule assembly in cytoplasmic extracts of Xenopus oocytes and
1171 eggs. *The Journal of cell biology* 105: 2191–2201

1172 Gavin A-C, Ainle AN, Chierici E, Jones M & Nebreda AR (1999) A p90 ^{rsk} Mutant Constitutively Interacting
1173 with MAP Kinase Uncouples MAP Kinase from p34 ^{cdc2} /Cyclin B Activation in *Xenopus* Oocytes.
1174 *MBoC* 10: 2971–2986

1175 Gawantka V, Ellinger-Ziegelbauer H & Hausen P (1992) β-integrin is a maternal protein that is inserted
1176 into all newly formed plasma membranes during early *Xenopus* embryogenesis. *Development*
1177 115: 595–605

1178 Gerhart J, Wu M & Kirschner M (1984) Cell cycle dynamics of an M-phase-specific cytoplasmic factor in
1179 Xenopus laevis oocytes and eggs. *The Journal of cell biology* 98: 1247–1255

1180 Giet R, Uzbekov R, Cubizolles F, Le Guellec K & Prigent C (1999) The Xenopus laevis Aurora-related
1181 Protein Kinase pEg2 Associates with and Phosphorylates the Kinesin-related Protein XlEg5.
1182 *Journal of Biological Chemistry* 274: 15005–15013

1183 Glotzer M, Murray AW & Kirschner MW (1991) Cyclin is degraded by the ubiquitin pathway. *Nature* 349:
1184 132–138

1185 Groisman I, Jung M-Y, Sarkissian M, Cao Q & Richter JD (2002) Translational Control of the Embryonic
1186 Cell Cycle. *Cell* 109: 473–483

1187 Gromley A, Yeaman C, Rosa J, Redick S, Chen C-T, Mirabelle S, Guha M, Sillibourne J & Doxsey SJ (2005)
1188 Centriolin Anchoring of Exocyst and SNARE Complexes at the Midbody Is Required for Secretory-
1189 Vesicle-Mediated Abscission. *Cell* 123: 75–87

1190 Grosstessner-Hain K, Hegemann B, Novatchkova M, Rameseder J, Joughin BA, Hudecz O, Roitinger E,
1191 Pichler P, Kraut N, Yaffe MB, *et al* (2011) Quantitative Phospho-proteomics to Investigate the
1192 Polo-like Kinase 1-Dependent Phospho-proteome. *Molecular & Cellular Proteomics* 10:
1193 M111.008540

1194 Gruss O (2018) Animal Female Meiosis: The Challenges of Eliminating Centrosomes. *Cells* 7: 73

1195 Gruss OJ & Vernos I (2004) The mechanism of spindle assembly. *The Journal of Cell Biology* 166: 949–955

1196 Gwon Y, Maxwell BA, Kolaitis R-M, Zhang P, Kim HJ & Taylor JP (2021) Ubiquitination of G3BP1 mediates
1197 stress granule disassembly in a context-specific manner. *Science* 372: eabf6548

1198 Haccard O & Jessus C (2006) Oocyte Maturation, Mos and Cyclins—A Matter of Synthesis: Two
1199 Functionally Redundant Ways to Induce Meiotic Maturation. *Cell Cycle* 5: 1152–1159

1200 Hansen DV, Tung JJ & Jackson PK (2006) CaMKII and Polo-like kinase 1 sequentially phosphorylate the
1201 cytostatic factor Emi2/XErp1 to trigger its destruction and meiotic exit. *Proceedings of the*
1202 *National Academy of Sciences* 103: 608–613

1203 Hatch EM, Kulukian A, Holland AJ, Cleveland DW & Stearns T (2010) Cep152 interacts with Plk4 and is
1204 required for centriole duplication. *Journal of Cell Biology* 191: 721–729

1205 Heidemann SR & Kirschner MW (1975) Aster formation in eggs of Xenopus laevis. Induction by isolated
1206 basal bodies. *The Journal of cell biology* 67: 105–117

1207 Heim A, Niedermeier ML, Stengel F & Mayer TU (2022) The translation regulator Zar1l controls timing of
1208 meiosis in *Xenopus* oocytes. *Development* 149: dev200900

1209 Hochegger H, Klotzbücher A, Kirk J, Howell M, le Guellec K, Fletcher K, Duncan T, Sohail M & Hunt T
1210 (2001) New B-type cyclin synthesis is required between meiosis I and II during Xenopus oocyte
1211 maturation. *Development* 128: 3795–3807

1212 Houliston E, Le Guellec R, Kress M, Philippe M & Le Guellec K (1994) The kinesin-related protein Eg5
1213 associates with both interphase and spindle microtubules during Xenopus early development.
1214 *Dev Biol* 164: 147–159

1215 Huang C-YF, Chang C-PB, Huang C-L & Ferrell JE (1999) M Phase Phosphorylation of Cytoplasmic Dynein
1216 Intermediate Chain and p150Glued. *Journal of Biological Chemistry* 274: 14262–14269

1217 Huchon D, Crozet N, Cantenot N & Ozon R (1981) Germinal vesicle breakdown in the Xenopus laevis
1218 oocyte : description of a transient microtubular structure. *Reprod Nutr Dévelop* 21: 135–148

1219 Huchon D, Rime H, Jessus C & Ozon R (1993) Control of metaphase I formation in *Xenopus* oocyte:
1220 Effects of an indestructible cyclin B and of protein synthesis. *Biology of the Cell* 77: 133–141

1221 Hyman LE & Wormington WM (1988) Translational inactivation of ribosomal protein mRNAs during
1222 Xenopus oocyte maturation. *Genes Dev* 2: 598–605

1223 Isobe K, Jung HJ, Yang C-R, Claxton J, Sandoval P, Burg MB, Raghuram V & Knepper MA (2017) Systems-
1224 level identification of PKA-dependent signaling in epithelial cells. *Proc Natl Acad Sci USA* 114

1225 Jackson RJ, Hellen CUT & Pestova TV (2010) The mechanism of eukaryotic translation initiation and
1226 principles of its regulation. *Nat Rev Mol Cell Biol* 11: 113–127

1227 Jamieson-Lucy A & Mullins MC (2019) The vertebrate Balbiani body, germ plasm, and oocyte polarity. In
1228 *Current Topics in Developmental Biology* pp 1–34. Elsevier

1229 Jessus C (2010) MPF and the Control of Meiotic Divisions: Old Problems, New Concepts. In *Oogenesis*,
1230 Verlhac M & Villeneuve A (eds) pp 227–265. Wiley

1231 Jessus C, Friederich E, Francon J & Ozon R (1984) In vitro inhibition of tubulin assembly by a
1232 ribonucleoprotein complex associated with the free ribosome fraction isolated from Xenopus
1233 laevis oocytes: effect at the level of microtubule-associated proteins. *Cell Differentiation* 14:
1234 179–187

1235 Jessus C, Thibier C, Huchon D & Ozon R (1988) Taxol reveals cortical sites of microtubule assembly in
1236 Xenopus oocytes. Role of the nucleus. *Cell Differentiation and Development* 25: 57–63

1237 Jia J, Tang S, Yue X, Jing S, Zhu L, Tan C, Gao J, Du Y, Lee I & Qian Y (2023) An A-kinase anchoring protein
1238 (ACBD3) coordinates traffic-induced PKA activation at the Golgi. *Journal of Biological Chemistry*
1239 299: 104696

1240 Josefsberg Ben-Yehoshua L, Lewellyn AL, Thomas P & Maller JL (2007) The Role of Xenopus Membrane
1241 Progesterone Receptor β in Mediating the Effect of Progesterone on Oocyte Maturation.
1242 *Molecular Endocrinology* 21: 664–673

1243 Kado RT, Marcher K & Ozon R (1981) Electrical membrane properties of the Xenopus laevis oocyte
1244 during progesterone-induced meiotic maturation. *Developmental Biology* 84: 471–476

1245 Kaufman OH, Lee K, Martin M, Rothhämel S & Marlow FL (2018) rbpms2 functions in Balbiani body
1246 architecture and ovary fate. *PLoS Genet* 14: e1007489

1247 Kessel RG, Tung HN, Beams HW & Lin JJ-C (1986) Is the nuclear envelope a 'generator' of membrane?:
1248 Developmental sequences in cytomembrane elaboration. *Cell Tissue Res* 245

Kettenbach AN, Schweppe DK, Faherty BK, Pechenick D, Pletnev AA & Gerber SA (2011) Quantitative Phosphoproteomics Identifies Substrates and Functional Modules of Aurora and Polo-Like Kinase Activities in Mitotic Cells. *Sci Signal* 4

Keuss MJ, Thomas Y, Mcarthur R, Wood NT, Knebel A & Kurz T (2016) Characterisation of the mammalian family of DCN-type NEDD8 E3 ligases. *Journal of Cell Science*: jcs.181784

King GA, Goodman JS, Schick JG, Chetlapalli K, Jorgens DM, McDonald KL & Ünal E (2019) Meiotic cellular rejuvenation is coupled to nuclear remodeling in budding yeast. *Elife* 8: e47156

Kinoshita K, Habermann B & Hyman AA (2002) XMAP215: a key component of the dynamic microtubule cytoskeleton. *Trends in Cell Biology* 12: 267–273

Kinterová V, Kaňka J, Bartková A & Toralová T (2022) SCF Ligases and Their Functions in Oogenesis and Embryogenesis—Summary of the Most Important Findings throughout the Animal Kingdom. *Cells* 11: 234

Kirschner M (1986) Beyond self-assembly: From microtubules to morphogenesis. *Cell* 45: 329–342

Kishimoto T (2003) Cell-cycle control during meiotic maturation. *Current Opinion in Cell Biology* 15: 654–663

Klima M, Tóth DJ, Hexnerova R, Baumlova A, Chalupska D, Tykvart J, Rezabkova L, Sengupta N, Man P, Dubankova A, *et al* (2016) Structural insights and in vitro reconstitution of membrane targeting and activation of human PI4KB by the ACBD3 protein. *Sci Rep* 6: 23641

Kobayashi H, Minshull J, Ford C, Golsteyn R, Poon R & Hunt T (1991) On the synthesis and destruction of A- and B-type cyclins during oogenesis and meiotic maturation in Xenopus laevis. *J Cell Biol* 114: 755–765

Koch LB, Spanos C, Kelly V, Ly T & Marston AL (2024) Rewiring of the phosphoproteome executes two meiotic divisions in budding yeast. *EMBO J* 43: 1351–1383

Kraft C (2003) Mitotic regulation of the human anaphase-promoting complex by phosphorylation. *The EMBO Journal* 22: 6598–6609

Kufer TA, Silljé HHW, Körner R, Gruss OJ, Meraldi P & Nigg EA (2002) Human TPX2 is required for targeting Aurora-A kinase to the spindle. *The Journal of Cell Biology* 158: 617–623

Kumar H, Pushpa K, Kumari A, Verma K, Pergu R & Mylavarapu SVS (2019) The exocyst complex and Rab5 are required for abscission by localizing ESCRT III subunits to the cytokinetic bridge. *Journal of Cell Science* 132: jcs226001

Kutay U, Jühlen R & Antonin W (2021) Mitotic disassembly and reassembly of nuclear pore complexes. *Trends in Cell Biology* 31: 1019–1033

Larabell CA & Chandler DE (1989) The coelomic envelope of Xenopus laevis eggs: A quick-freeze, deep-etch analysis. *Developmental Biology* 131: 126–135

Leaf DS, Roberts SJ, Gerhart JC & Moore H-P (1990) The secretory pathway is blocked between the trans-Golgi and the plasma membrane during meiotic maturation in Xenopus oocytes. *Developmental Biology* 141: 1–12

Lee KS, Grenfell TZ, Yarm FR & Erikson RL (1998) Mutation of the polo-box disrupts localization and mitotic functions of the mammalian polo kinase Plk. *Proc Natl Acad Sci USA* 95: 9301–9306

Lee M, Nagashima K, Yoon J, Sun J, Wang Z, Carpenter C, Lee H-K, Hwang Y-S, Westlake CJ & Daar IO (2022) CEP97 phosphorylation by Dyrk1a is critical for centriole separation during multiciliogenesis. *Journal of Cell Biology* 221: e202102110

LeGuennec M, Klena N, Aeschlimann G, Hamel V & Guichard P (2021) Overview of the centriole architecture. *Current Opinion in Structural Biology* 66: 58–65

Lemaître J-M, Bocquet S & Méchali M (2002) Competence to replicate in the unfertilized egg is conferred by Cdc6 during meiotic maturation. *Nature* 419: 718–722

Lemonnier T, Dupré A & Jessus C (2020) The G2-to-M transition from a phosphatase perspective: a new vision of the meiotic division. *Cell Div* 15: 9

Li X, Ju J, Pan Z, Wang H, Wan X, Pan M, Xu Y, Sun M & Sun S (2021) PRC1 is a critical regulator for anaphase spindle midzone assembly and cytokinesis in mouse oocyte meiosis. *FEBS J* 288: 3055–3067

Linder MI, Köhler M, Boersema P, Weberruss M, Wandke C, Marino J, Ashiono C, Picotti P, Antonin W & Kutay U (2017) Mitotic Disassembly of Nuclear Pore Complexes Involves CDK1- and PLK1-Mediated Phosphorylation of Key Interconnecting Nucleoporins. *Developmental Cell* 43: 141-156.e7

Liu L & Wiese C (2008) *Xenopus* NEDD1 is required for microtubule organization in *Xenopus* egg extracts. *Journal of Cell Science* 121: 578–589

Lorenzo-Orts L, Strobl M, Steinmetz B, Leesch F, Pribitzer C, Roehsner J, Schutzbier M, Dürnberger G & Pauli A (2023) eIF4E1b is a non-canonical eIF4E protecting maternal dormant mRNAs. *EMBO Rep*

Macůrek L, Lindqvist A, Lim D, Lampson MA, Klompmaker R, Freire R, Clouin C, Taylor SS, Yaffe MB & Medema RH (2008) Polo-like kinase-1 is activated by aurora A to promote checkpoint recovery. *Nature* 455: 119–123

Maller J, Wu M & Gerhart JC (1977) Changes in protein phosphorylation accompanying maturation of Xenopus laevis oocytes. *Developmental Biology* 58: 295–312

Marnef A, Maldonado M, Bugaut A, Balasubramanian S, Kress M, Weil D & Standart N (2010) Distinct functions of maternal and somatic Pat1 protein paralogs. *RNA* 16: 2094–2107

Maton G, Lorca T, Girault J-A, Ozon R & Jessus C (2005) Differential regulation of Cdc2 and Aurora-A in *Xenopus* oocytes: a crucial role of phosphatase 2A. *Journal of Cell Science* 118: 2485–2494

Maton G, Thibier C, Castro A, Lorca T, Prigent C & Jessus C (2003) Cdc2-Cyclin B Triggers H3 Kinase Activation of Aurora-A in Xenopus Oocytes. *J Biol Chem* 278: 21439–21449

McNally FJ & Thomas S (1998) Katanin Is Responsible for the M-Phase Microtubule-severing Activity in *Xenopus* Eggs. *MBoC* 9: 1847–1861

McPhail JA, Lyoo H, Pemberton JG, Hoffmann RM, Van Elst W, Strating JR, Jenkins ML, Stariha JT, Powell CJ, Boulanger MJ, *et al* (2020) Characterization of the c10orf76-PI4KB complex and its necessity for Golgi PI4P levels and enterovirus replication. *EMBO Reports* 21: e48441

Mendez R, Barnard D & Richter JD (2002) Differential mRNA translation and meiotic progression require Cdc2-mediated CPEB destruction. *EMBO J* 21: 1833–1844

Meneau F, Dupré A, Jessus C & Daldello EM (2020) Translational Control of Xenopus Oocyte Meiosis: Toward the Genomic Era. *Cells* 9: 1502

Miller BR & Forbes DJ (2000) Purification of the Vertebrate Nuclear Pore Complex by Biochemical Criteria. *Traffic* 1: 941–951

Miller KE, Session AM & Heald R (2019) Kif2a Scales Meiotic Spindle Size in Hymenochirus boettgeri. *Current Biology* 29: 3720-3727.e5

Mitchison TJ, Maddox P, Gaetz J, Groen A, Shirasu M, Desai A, Salmon ED & Kapoor TM (2005) Roles of Polymerization Dynamics, Opposed Motors, and a Tensile Element in Governing the Length of *Xenopus* Extract Meiotic Spindles. *MBoC* 16: 3064–3076

Mueller PR, Coleman TR & Dunphy WG (1995) Cell cycle regulation of a Xenopus Wee1-like kinase. *MBoC* 6: 119–134

Müller H -Arno J (2001) Of mice, frogs and flies: Generation of membrane asymmetries in early development. *Dev Growth Differ* 43: 327–342

Mulner-Lorillon O, Bellé R, Cormier P, Drewing S, Minella O, Poulhe R & Schmalzing G (1995) Brefeldin A Provokes Indirect Activation of cdc2 Kinase (MPF) in Xenopus Oocytes, Resulting in Meiotic Cell Division. *Developmental Biology* 170: 223–229

Nader N, Dib M, Courjaret R, Hodeify R, Machaca R, Graumann J & Machaca K (2018) VLDL receptor regulates membrane progesterone receptor trafficking and non-genomic signaling. *Journal of Cell Science*: jcs.212522

Nader N, Dib M, Daalis A, Kulkarni RP & Machaca K (2014) Role for endocytosis of a constitutively active GPCR (GPR185) in releasing vertebrate oocyte meiotic arrest. *Developmental Biology* 395: 355–366

Nader N, Dib M, Hodeify R, Courjaret R, Elmi A, Hammad AS, Dey R, Huang X-Y & Machaca K (2020) Membrane progesterone receptor induces meiosis in Xenopus oocytes through endocytosis into signaling endosomes and interaction with APPL1 and Akt2. *PLoS Biol* 18: e3000901

Nakahata S, Kotani T, Mita K, Kawasaki T, Katsu Y, Nagahama Y & Yamashita M (2003) Involvement of Xenopus Pumilio in the translational regulation that is specific to cyclin B1 mRNA during oocyte maturation. *Mechanisms of Development* 120: 865–880

Nakajo N, Yoshitome S, Iwashita J, Iida M, Uto K, Ueno S, Okamoto K & Sagata N (2000) Absence of Wee1 ensures the meiotic cell cycle in Xenopus oocytes. *Genes Dev* 14: 328–338

Nakamura Y, Tanaka KJ, Miyauchi M, Huang L, Tsujimoto M & Matsumoto K (2010) Translational repression by the oocyte-specific protein P100 in Xenopus. *Dev Biol* 344: 272–283

Nguyen AT, Prado MA, Schmidt PJ, Sendamarai AK, Wilson-Grady JT, Min M, Campagna DR, Tian G, Shi Y, Dederer V, *et al* (2017) UBE2O remodels the proteome during terminal erythroid differentiation. *Science* 357: eaan0218

Oakley CE & Oakley BR (1989) Identification of γ-tubulin, a new member of the tubulin superfamily encoded by mipA gene of Aspergillus nidulans. *Nature* 338: 662–664

Okano-Uchida T, Sekiai T, Lee K, Okumura E, Tachibana K & Kishimoto T (1998) In VivoRegulation of Cyclin A/Cdc2 and Cyclin B/Cdc2 through Meiotic and Early Cleavage Cycles in Starfish. *Developmental Biology* 197: 39–53

Ota R, Kotani T & Yamashita M (2011) Biochemical Characterization of Pumilio1 and Pumilio2 in Xenopus Oocytes. *Journal of Biological Chemistry* 286: 2853–2863

Padmanabhan K (2006) Regulated Pumilio-2 binding controls RINGO/Spy mRNA translation and CPEB activation. *Genes Dev* 20: 199–209

Pascreau G, Delcros J-G, Cremet J-Y, Prigent C & Arlot-Bonnemains Y (2005) Phosphorylation of Maskin by Aurora-A Participates in the Control of Sequential Protein Synthesis during Xenopus laevis Oocyte Maturation. *Journal of Biological Chemistry* 280: 13415–13423

Patra D & Dunphy WG (1998) Xe-p9, a *Xenopus* Suc1/Cks protein, is essential for the Cdc2-dependent phosphorylation of the anaphase- promoting complex at mitosis. *Genes Dev* 12: 2549–2559

Payne DM, Rossomando AJ, Martino P, Erickson AK, Her JH, Shabanowitz J, Hunt DF, Weber MJ & Sturgill TW (1991) Identification of the regulatory phosphorylation sites in pp42/mitogen-activated protein kinase (MAP kinase). *The EMBO Journal* 10: 885–892

Peset I, Seiler J, Sardon T, Bejarano LA, Rybina S & Vernos I (2005) Function and regulation of Maskin, a TACC family protein, in microtubule growth during mitosis. *The Journal of Cell Biology* 170: 1057–1066

Peshkin L, Gupta M, Ryazanova L & Wühr M (2019) Bayesian Confidence Intervals for Multiplexed Proteomics Integrate Ion-statistics with Peptide Quantification Concordance*[S]. *Molecular & Cellular Proteomics* 18: 2108–2120

Peshkin L, Wühr M, Pearl E, Haas W, Freeman RM, Gerhart JC, Klein AM, Horb M, Gygi SP & Kirschner MW (2015) On the Relationship of Protein and mRNA Dynamics in Vertebrate Embryonic Development. *Developmental Cell* 35: 383–394

1387 Peuchen EH, Cox OF, Sun L, Hebert AS, Coon JJ, Champion MM, Dovichi NJ & Huber PW (2017)
1388 Phosphorylation Dynamics Dominate the Regulated Proteome during Early Xenopus
1389 Development. *Sci Rep* 7: 15647

1390 Piqué M, López JM, Foissac S, Guigó R & Méndez R (2008) A Combinatorial Code for CPE-Mediated
1391 Translational Control. *Cell* 132: 434–448

1392 Popov AV, Severin F & Karsenti E (2002) XMAP215 Is Required for the Microtubule-Nucleating Activity of
1393 Centrosomes. *Current Biology* 12: 1326–1330

1394 Presler M, Van Itallie E, Klein AM, Kunz R, Coughlin ML, Peshkin L, Gygi SP, Wühr M & Kirschner MW
1395 (2017) Proteomics of phosphorylation and protein dynamics during fertilization and meiotic exit
1396 in the *Xenopus* egg. *Proc Natl Acad Sci USA* 114: E10838–E10847

1397 Reimann JDR, Freed E, Hsu JY, Kramer ER, Peters J-M & Jackson PK (2001) Emi1 Is a Mitotic Regulator
1398 that Interacts with Cdc20 and Inhibits the Anaphase Promoting Complex. *Cell* 105: 645–655

1399 Rempel RE, Sleight SB & Maller JL (1995) Maternal Xenopus Cdk2-Cyclin E Complexes Function during
1400 Meiotic and Early Embryonic Cell Cycles That Lack a G1 Phase. *Journal of Biological Chemistry*
1401 270: 6843–6855

1402 Reverte CG, Ahearn MD & Hake LE (2001) CPEB Degradation during Xenopus Oocyte Maturation
1403 Requires a PEST Domain and the 26S Proteasome. *Dev Biol* 231: 447–458

1404 Reynolds N & Ohkura H (2003) Polo boxes form a single functional domain that mediates interactions
1405 with multiple proteins in fission yeast polo kinase. *Journal of Cell Science* 116: 1377–1387

1406 Ríos-Cardona D, Ricardo-González RR, Chawla A & Ferrell JE (2008) A role for GPRx, a novel GPR3/6/12-
1407 related G-protein coupled receptor, in the maintenance of meiotic arrest in Xenopus laevis
1408 oocytes. *Dev Biol* 317: 380–388

1409 Roig J, Groen A, Caldwell J & Avruch J (2005) Active Nercc1 Protein Kinase Concentrates at Centrosomes
1410 Early in Mitosis and Is Necessary for Proper Spindle Assembly. *MBoC* 16: 4827–4840

1411 Rong Y, Ji S-Y, Zhu Y-Z, Wu Y-W, Shen L & Fan H-Y (2019) ZAR1 and ZAR2 are required for oocyte meiotic
1412 maturation by regulating the maternal transcriptome and mRNA translational activation. *Nucleic*
1413 *Acids Research* 47: 11387–11402

1414 Ross J (1997) A hypothesis to explain why translation inhibitors stabilize mRNAs in mammalian cells:
1415 mRNA Stability and mitosis. *BioEssays* 19: 527–529

1416 Sadler SE & Maller JL (1985) Inhibition of Xenopus oocyte adenylate cyclase by progesterone: a novel
1417 mechanism of action. *Adv Cyclic Nucleotide Protein Phosphorylation Res* 19: 179–194

1418 Sagata N, Daar I, Oskarsson M, Showalter S & Vande Woude G (1989a) The product of the mos proto-
1419 oncogene as a candidate 'initiator' for oocyte maturation. *Science* 245: 643–646

1420 Sagata N, Oskarsson M, Copeland T, Brumbaugh J & Woude GFV (1988) Function of c-mos proto-
1421 oncogene product in meiotic maturation in Xenopus oocytes. *Nature* 335: 519–525

1422 Sagata N, Watanabe N, Vande Woude GF & Ikawa Y (1989b) The c-mos proto-oncogene product is a
1423 cytostatic factor responsible for meiotic arrest in vertebrate eggs. *Nature* 342: 512–518

1424 Santoni M, Meneau F, Sekhsoukh N, Castella S, Le T, Miot M & Daldello EM (2024) Unraveling the
1425 interplay between PKA inhibition and Cdk1 activation during oocyte meiotic maturation. *Cell*
1426 *Reports* 43: 113782

1427 Sasaki J, Ishikawa K, Arita M & Taniguchi K (2012) ACBD3-mediated recruitment of PI4KB to picornavirus
1428 RNA replication sites: Picornaviral protein/ACBD3/PI4KB complex. *The EMBO Journal* 31: 754–
1429 766

1430 Session AM, Uno Y, Kwon T, Chapman JA, Toyoda A, Takahashi S, Fukui A, Hikosaka A, Suzuki A, Kondo
1431 M, *et al* (2016) Genome evolution in the allotetraploid frog Xenopus laevis. *Nature* 538: 336–343

1432 Setoyama D, Yamashita M & Sagata N (2007) Mechanism of degradation of CPEB during Xenopus oocyte
1433 maturation. *Proc Natl Acad Sci USA* 104: 18001–18006

1434 Solc P, Kitajima TS, Yoshida S, Brzakova A, Kaido M, Baran V, Mayer A, Samalova P, Motlik J & Ellenberg J
1435 (2015) Multiple Requirements of PLK1 during Mouse Oocyte Maturation. *PLoS ONE* 10:
1436 e0116783

1437 Sonnett M, Gupta M, Nguyen T & Wühr M (2018) Quantitative Proteomics for Xenopus Embryos II, Data
1438 Analysis. In *Xenopus*, Vleminckx K (ed) pp 195–215. New York, NY: Springer New York

1439 Stearns T & Kirschner M (1994) In vitro reconstitution of centrosome assembly and function: The central
1440 role of γ-tubulin. *Cell* 76: 623–637

1441 Stebbins-Boaz B, Cao Q, de Moor CH, Mendez R & Richter JD (1999) Maskin Is a CPEB-Associated Factor
1442 that Transiently Interacts with eIF-4E. *Molecular Cell* 4: 1017–1027

1443 Steinacker TL, Wong S-S, Novak ZA, Saurya S, Gartenmann L, Van Houtum EJH, Sayers JR, Lagerholm BC
1444 & Raff JW (2022) Centriole growth is limited by the Cdk/Cyclin-dependent phosphorylation of
1445 Ana2/STIL. *Journal of Cell Biology* 221: e202205058

1446 Sulimenko V, Dráberová E & Dráber P (2022) γ-Tubulin in microtubule nucleation and beyond. *Front Cell*
1447 *Dev Biol* 10: 880761

1448 Swartz SZ, Nguyen HT, McEwan BC, Adamo ME, Cheeseman IM & Kettenbach AN (2021) Selective
1449 dephosphorylation by PP2A-B55 directs the meiosis I-meiosis II transition in oocytes. *eLife* 10:
1450 e70588

1451 Taieb FE, Gross SD, Lewellyn AL & Maller JL (2001) Activation of the anaphase-promoting complex and
1452 degradation of cyclin B is not required for progression from Meiosis I to II in Xenopus oocytes.
1453 *Current Biology* 11: 508–513

1454 Takagi M, Absalon MJ, McLure KG & Kastan MB (2005) Regulation of p53 Translation and Induction after
1455 DNA Damage by Ribosomal Protein L26 and Nucleolin. *Cell* 123: 49–63

1456 Tanos BE, Yang H-J, Soni R, Wang W-J, Macaluso FP, Asara JM & Tsou M-FB (2013) Centriole distal
1457 appendages promote membrane docking, leading to cilia initiation. *Genes Dev* 27: 163–168

1458 Tavernier N, Noatynska A, Panbianco C, Martino L, Van Hove L, Schwager F, Léger T, Gotta M & Pintard L
1459 (2015) Cdk1 phosphorylates SPAT-1/Bora to trigger PLK-1 activation and drive mitotic entry in *C.*
1460 *elegans* embryos. *Journal of Cell Biology* 208: 661–669

1461 Tavernier N, Sicheri F & Pintard L (2021) Aurora A kinase activation: Different means to different ends.
1462 *Journal of Cell Biology* 220: e202106128

1463 Terasaki M, Runft LL & Hand AR (2001) Changes in Organization of the Endoplasmic Reticulum during
1464 *Xenopus* Oocyte Maturation and Activation. *MBoC* 12: 1103–1116

1465 Thibier C, De Smedt V, Poulhe R, Huchon D, Jessus C & Ozon R (1997) In Vivo Regulation of Cytostatic
1466 Activity inXenopusMetaphase II-Arrested Oocytes. *Developmental Biology* 185: 55–66

1467 Thillaiappan NB, Smith HA, Atakpa-Adaji P & Taylor CW (2021) KRAP tethers IP3 receptors to actin and
1468 licenses them to evoke cytosolic Ca2+ signals. *Nat Commun* 12: 4514

1469 Thomas Y, Cirillo L, Panbianco C, Martino L, Tavernier N, Schwager F, Van Hove L, Joly N, Santamaria A,
1470 Pintard L, *et al* (2016) Cdk1 Phosphorylates SPAT-1/Bora to Promote Plk1 Activation in C.
1471 elegans and Human Cells. *Cell Reports* 15: 510–518

1472 Tzeng Y-W, Li D-Y, Chen Y, Yang C-H, Chang C-Y & Juang Y-L (2018) LMO7 exerts an effect on mitosis
1473 progression and the spindle assembly checkpoint. *The International Journal of Biochemistry &*
1474 *Cell Biology* 94: 22–30

1475 Uto K (2000) Nek2B, a novel maternal form of Nek2 kinase, is essential for the assembly or maintenance
1476 of centrosomes in early Xenopus embryos. *The EMBO Journal* 19: 1816–1826

1477 Vigneron S, Sundermann L, Labbé J-C, Pintard L, Radulescu O, Castro A & Lorca T (2018) Cyclin A-cdk1-
1478 Dependent Phosphorylation of Bora Is the Triggering Factor Promoting Mitotic Entry.
1479 *Developmental Cell* 45: 637-650.e7

1480 Vik TA & Ryder JW (1997) Identification of Serine 380 as the Major Site of Autophosphorylation of
1481 Xenopus pp90rsk. *Biochemical and Biophysical Research Communications* 235: 398–402

1482 Virant-Klun I, Leicht S, Hughes C & Krijgsveld J (2016) Identification of Maturation-Specific Proteins by
1483 Single-Cell Proteomics of Human Oocytes. *Molecular & Cellular Proteomics* 15: 2616–2627

1484 Walczak CP, Leto DE, Zhang L, Riepe C, Muller RY, DaRosa PA, Ingolia NT, Elias JE & Kopito RR (2019)
1485 Ribosomal protein RPL26 is the principal target of UFMylation. *Proc Natl Acad Sci USA* 116:
1486 1299–1308

1487 Warner JR & McIntosh KB (2009) How Common Are Extraribosomal Functions of Ribosomal Proteins?
1488 *Molecular Cell* 34: 3–11

1489 Wassmann K (2022) Separase Control and Cohesin Cleavage in Oocytes: Should I Stay or Should I Go?
1490 *Cells* 11: 3399

1491 Wessel D & Flügge UI (1984) A method for the quantitative recovery of protein in dilute solution in the
1492 presence of detergents and lipids. *Anal Biochem* 138: 141–143

1493 Whitmire E, Khan B & Coué M (2002) Cdc6 synthesis regulates replication competence in Xenopus
1494 oocytes. *Nature* 419: 722–725

1495 Wilk K, Bilinski S, Dougherty MT & Kloc M (2005) Delivery of germinal granules and localized RNAs via
1496 the messenger transport organizer pathway to the vegetal cortex of Xenopus oocytes occurs
1497 through directional expansion of the mitochondrial cloud. *Int J Dev Biol* 49: 17–21

1498 Wind M, Kelm O, Nigg EA & Lehmann WD (2002) Identification of phosphorylation sites in the polo-like
1499 kinases Plx1 and Plk1 by a novel strategy based on element and electrospray high resolution
1500 mass spectrometry. *Proteomics* 2: 1516–1523

1501 Woodland HR (1974) Changes in the polysome content of developing Xenopus laevis embryos. *Dev Biol*
1502 40: 90–101

1503 Wu X-J, Thomas P & Zhu Y (2018) Pgrmc1 Knockout Impairs Oocyte Maturation in Zebrafish. *Front*
1504 *Endocrinol* 9: 560

1505 Wühr M, Freeman RM, Presler M, Horb ME, Peshkin L, Gygi SP & Kirschner MW (2014) Deep Proteomics
1506 of the Xenopus laevis Egg using an mRNA-Derived Reference Database. *Current Biology* 24:
1507 1467–1475

1508 Yamamoto TM, Cook JM, Kotter CV, Khat T, Silva KD, Ferreyros M, Holt JW, Knight JD & Charlesworth A
1509 (2013) Zar1 represses translation in Xenopus oocytes and binds to the TCS in maternal mRNAs
1510 with different characteristics than Zar2. *Biochimica et Biophysica Acta (BBA) - Gene Regulatory*
1511 *Mechanisms* 1829: 1034–1046

1512 Yanagitani K, Juszkiewicz S & Hegde RS (2017) UBE2O is a quality control factor for orphans of
1513 multiprotein complexes. *Science* 357: 472–475

1514 Yang C, Dominique GM, Champion MM & Huber PW (2022) Remnants of the Balbiani body are required
1515 for formation of RNA transport granules in Xenopus oocytes. *iScience* 25: 103878

1516 Yang M, Jin Y, Fan S, Liang X, Jia J, Tan Z, Huang T, Li Y, Ma T & Li M (2019) Inhibition of neddylation
1517 causes meiotic arrest in mouse oocyte. *Cell Cycle* 18: 1254–1267

1518 Yew N, Mellini ML, Martinez CK & Woude GFV (1992) Meiotic initiation by the mos protein in Xenopus.
1519 *Nature* 355: 649–652

1520 Zhang M, Zhang J, Yan W & Chen X (2016) p73 expression is regulated by ribosomal protein RPL26
1521 through mRNA translation and protein stability. *Oncotarget* 7: 78255–78268

1522 Zhang Z, Liu R, Zhou H, Li Q, Qu R, Wang W, Zhou Z, Yu R, Zeng Y, Mu J, *et al* (2023) PATL2 regulates
1523 mRNA homeostasis in oocytes by interacting with EIF4E and CPEB1. *Development* 150:
1524 dev201572

Zitouni S, Francia ME, Leal F, Montenegro Gouveia S, Nabais C, Duarte P, Gilberto S, Brito D, Moyer T, Kandels-Lewis S, *et al* (2016) CDK1 Prevents Unscheduled PLK4-STIL Complex Assembly in Centriole Biogenesis. *Current Biology* 26: 1127–1137

Figure 1

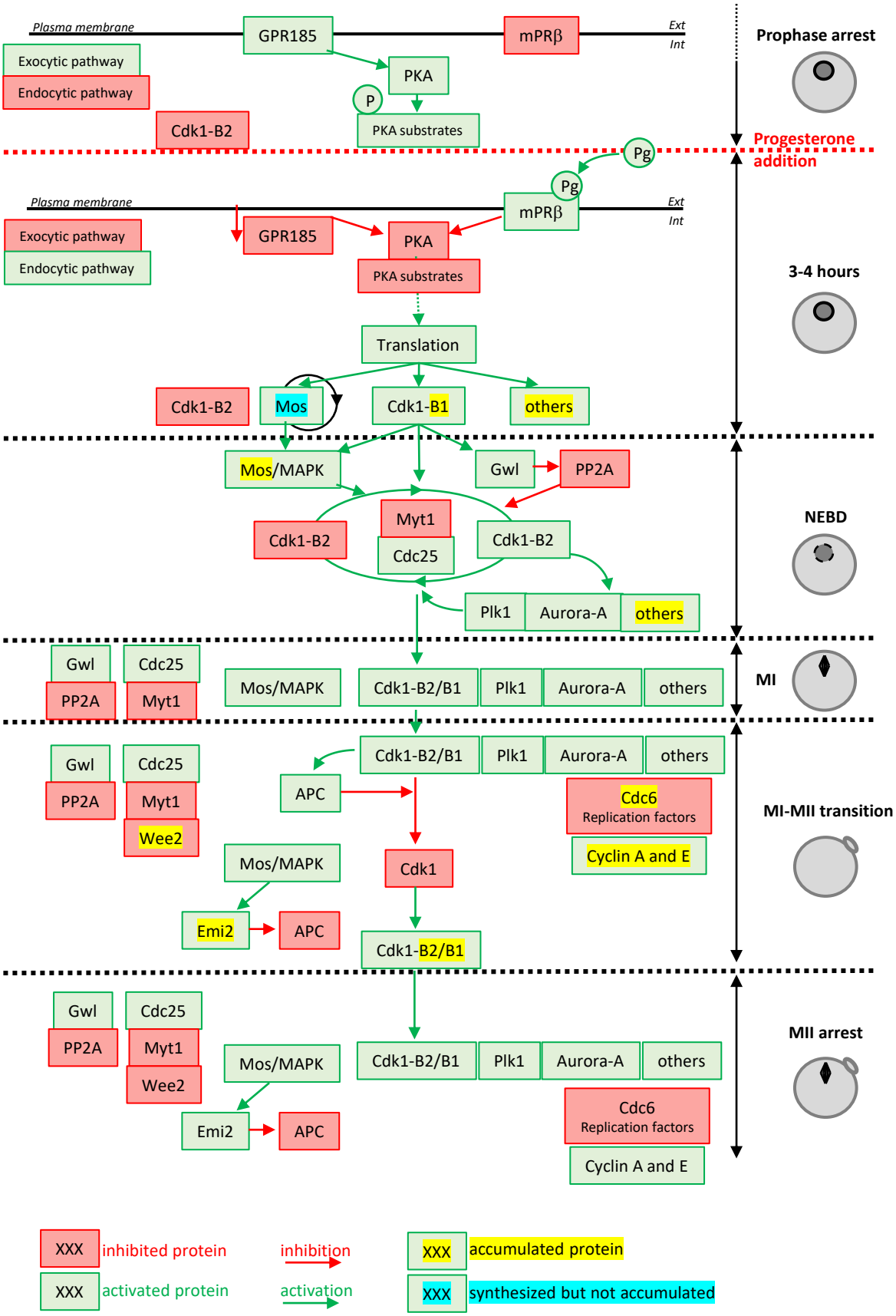
Plasma membrane
GPR185
mPRβ
Ext
Int
Exocytic pathway
Endocytic pathway
PKA
P
PKA substrates
Cdk1-B2
Prophase arrest
Progesterone addition
Pg
Pg
Plasma membrane
mPRβ
Ext
Int
Exocytic pathway
Endocytic pathway
GPR185
PKA
PKA substrates
3-4 hours
Translation
Cdk1-B2
Mos
Cdk1-B1
others
Mos/MAPK
Gwl
PP2A
Myt1
Cdk1-B2
Cdc25
Cdk1-B2
NEBD
Plk1
Aurora-A
others
Gwl
Cdc25
PP2A
Myt1
Mos/MAPK
Cdk1-B2/B1
Plk1
Aurora-A
others
MI
Cdk1-B2/B1
Plk1
Aurora-A
others
Gwl
Cdc25
PP2A
Myt1
Wee2
APC
Cdc6
Replication factors
Cyclin A and E
MI-MII transition
Mos/MAPK
Cdk1
Emi2
APC
Cdk1-B2/B1
Gwl
Cdc25
PP2A
Myt1
Wee2
Mos/MAPK
Cdk1-B2/B1
Plk1
Aurora-A
others
MII arrest
Emi2
APC
Cdc6
Replication factors
Cyclin A and E
XXX
inhibited protein
inhibition
XXX
accumulated protein
XXX
activated protein
activation
XXX
synthesized but not accumulated

Figure 1 continued

Figure 1. Molecular events coordinating *Xenopus laevis* oocyte meiotic divisions. From top to bottom: The prophase arrest is maintained by high PKA activity due to the constitutively expressed GPR185 receptor. The exocytic pathway is active while the endocytic pathway is downregulated. Cdk1-Cyclin B2 complexes are present under an inactive state due to Cdk1 phosphorylation. Progesterone activates the mPRb receptor, GPR185 is inactivated, the exocytosis and endocytosis pathways are inverted. PKA is inactivated and promotes translation and/or accumulation of new proteins, among them Mos (that does not accumulate due to its instability) and Cyclin B1 (due to its stabilization). New Cyclin B1 proteins associate with Cdk1 and form a starter amount of Cdk1 activity. This Cdk1 starter stabilizes Mos and promotes Cdk1-Cyclin B2 activation through the regulation of Myt1, Cdc25, Gwl and PP2A. The autoamplification loop is launched, whereby more Cdk1 is activated, more it activates kinases as Mos-MAPK, Aurora-A and Plk1, all of them contributing with Cdk1 to regulate Myt1 and Cdc25, hence accelerating Cdk1 activation. Phosphorylated substrates trigger NEBD and the MI spindle assembly as well as protein translation. APC is activated under the control of Cdk1 and leads to Cyclin B degradation. The Cdk1 activity decreases and allows anaphase I and expulsion of the 1st polar body. Under the Mos/MAPK control, Emi2/Erp1 inactivates APC, halting Cyclin B degradation. The re-accumulation of Cyclin B increases Cdk1 activity that triggers the formation of the MII spindle, avoiding the assembly of a nucleus and DNA replication. APC remains inhibited by Emi2/Erp1, what ensures the oocyte arrest in MII. Color code: red: inactivated proteins; green: activated proteins; red arrow: inhibition; green arrow: activation; yellow highlight: accumulated protein; blue highlight: protein synthesized but not accumulated.

Figure 2

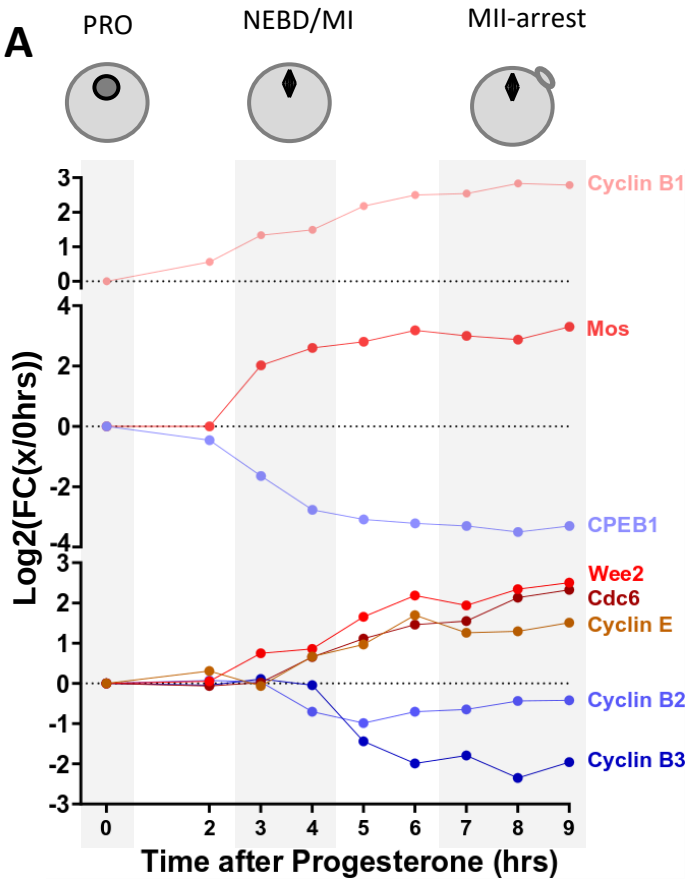
A
PRO
NEBD/MI
MII-arrest
Cyclin B1
Mos
CPEB1
Wee2
Cdc6
Cyclin E
Cyclin B2
Cyclin B3
Log2(FC(x/0hrs))
Time after Progesterone (hrs)

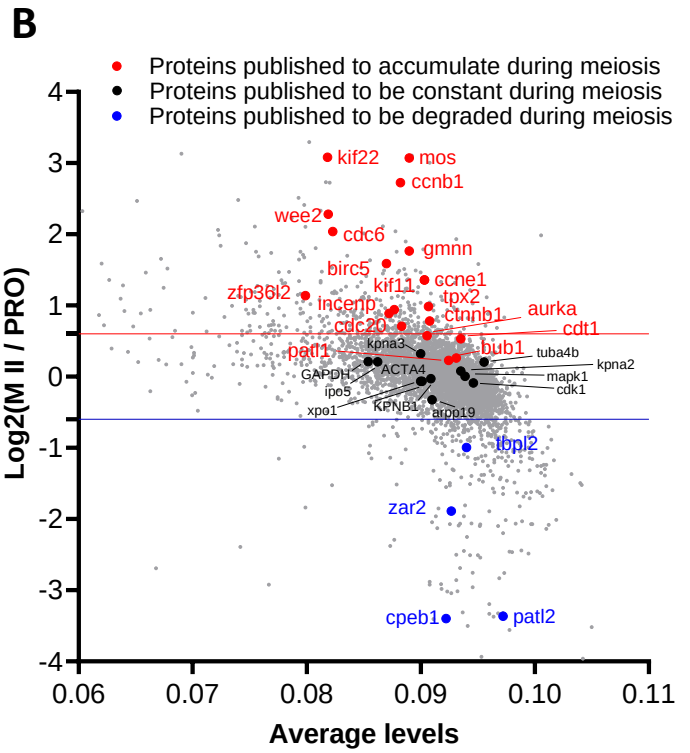
B
Proteins published to accumulate during meiosis
Proteins published to be constant during meiosis
Proteins published to be degraded during meiosis
kif22
mos
ccnb1
wee2
cdc6
gmnn
birc5
kif11
ccne1
zfp36l2
incenp
tpx2
ctnnb1
aurka
cdc20
cdt1
pad1
kpna3
bub1
tuba4b
kpna2
GAPDH
ACTA4
mapk1
cdk1
ipo5
xpo1
KPNB1
arpp19
tbpl2
zar2
cpeb1
patl2
Log2(M II / PRO)
Average levels

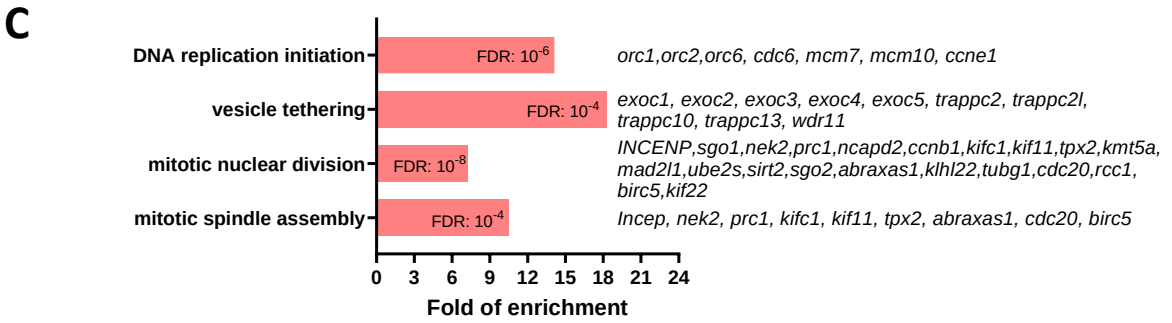
C
DNA replication initiation
FDR: 10-6
orc1,orc2,orc6, cdc6, mcm7, mcm10, ccne1
vesicle tethering
FDR: 10-4
exoc1, exoc2, exoc3, exoc4, exoc5, trappc2, trappc2l, trappc10, trappc13, wdr11
mitotic nuclear division
FDR: 10-8
INCENP,sgo1,nek2,prc1,ncapd2,ccnb1,kifc1,kif11,tpx2,kmt5a, mad2l1,ube2s,sirt2,sgo2,abraxas1,klhl22,tubg1,cdc20,rcc1, birc5,kif22
mitotic spindle assembly
FDR: 10-4
Incep, nek2, prc1, kifc1, kif11, tpx2, abraxas1, cdc20, birc5
Fold of enrichment

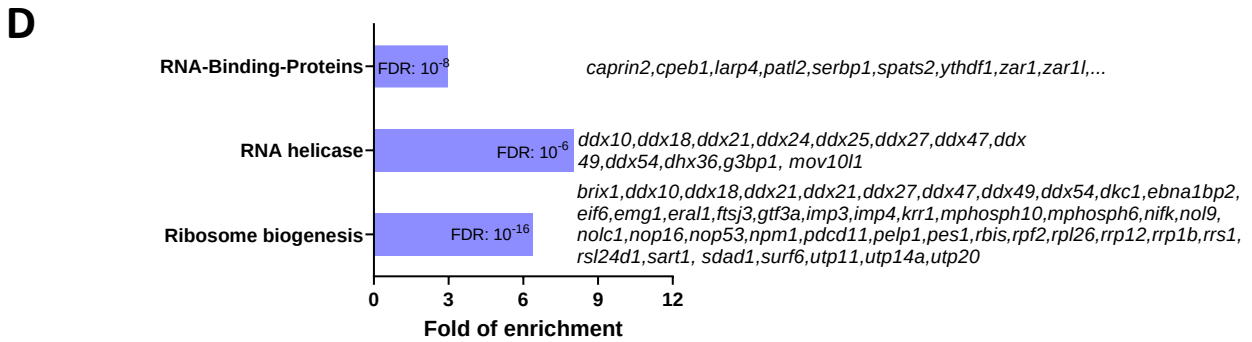
D
RNA-Binding-Proteins
FDR: 10-8
caprin2,cpeb1,larp4,patl2,serbp1,spats2,ythdf1,zar1,zar1l,...
RNA helicase
FDR: 10-6
ddx10,ddx18,ddx21,ddx24,ddx25,ddx27,ddx47,ddx 49,ddx54,dhx36,g3bp1, mov10l1
Ribosome biogenesis
FDR: 10-16
brix1,ddx10,ddx18,ddx21,ddx21,ddx27,ddx47,ddx49,ddx54,dkc1,ebna1bp2, eif6,emg1,eral1,ftsj3,gtf3a,imp3,imp4,krr1,mphosph10,mphosph6,nifk,nol9, nolc1,nop16,nop53,npm1,pdcd11,pelp1,pes1,rbis,rpf2,rpl26,rrp12,rrp1b,rrs1, rsl24d1,sart1, sdad1,surf6,utp11,utp14a,utp20
Fold of enrichment

Figure 2 continued

Figure 2. Changes in the protein levels during meiotic divisions. (**A**) The relative changes in the concentration of proteins whose accumulation/degradation has been reported to correlate with the critical stages of *Xenopus* meiotic divisions have been plotted. (**B**) Changes of protein stoichiometry during meiotic maturation. The log2 fold changes between the concentration of each protein in PRO-arrested oocytes and MII-arrested oocytes was plotted. The red line marks the 1.5-fold change used as a threshold to identify accumulating proteins. The blue line marks the 0.75-fold change used as threshold to distinguish proteins that are degraded during meiosis. Proteins, whose changes in homeostasis during meiotic divisions are documented in the literature, are marked with the following color code: red, for proteins accumulating; black, for proteins which are expressed at a stable level; and blue, for proteins that are degraded. (**C-D**) Gene ontology analysis of the biological processes enriched among the proteins found to accumulate (in red, panel **C**) or degraded (in blue, panel **D**) during meiosis. The statistical significance of the enrichment is expressed as false discovery rate (FDR). A representative subset of the proteins belonging to each group is displayed.

Figure 2-figure supplement 3

A

	PRO I		MI				MII - arrest								
Gene name	0	2	3	4	5	6	7	8	9	FC (MII/PRO)	Log2- FC (MII/PRO)	FC (MII/PRO) (Peuchen, 2017)	Log2- FC (MII/PRO) (Peuchen, 2017)	PMID	
kif22 (XKid)	0.018	0.019	0.036	0.053	0.074	0.094	0.120	0.138	0.187	8.5	3.1	not detected	not detected	12360284	
mos	0.015	0.015	0.061	0.091	0.105	0.136	0.120	0.110	0.148	8.4	3.1	0.9	-0.2	2474853	
ccnb1	0.021	0.031	0.053	0.059	0.095	0.119	0.122	0.150	0.145	6.6	2.7	not detected	not detected	10512866	
wee2	0.027	0.028	0.045	0.048	0.084	0.121	0.102	0.135	0.151	4.9	2.3	not detected	not detected	10673504	
cdc6	0.034	0.033	0.035	0.054	0.074	0.094	0.100	0.149	0.171	4.1	2.0	0.5	-1.0	12384698, 12384699,26092930	
gmnn	0.037	0.038	0.056	0.072	0.099	0.122	0.105	0.130	0.142	3.4	1.8	1.2	0.3	19656945	
birc5 (survivin)	0.044	0.047	0.053	0.056	0.085	0.101	0.113	0.145	0.139	3.0	1.6	2.2	1.1	18378691	
ccne1	0.046	0.057	0.044	0.073	0.090	0.149	0.110	0.113	0.131	2.6	1.4	not detected	not detected	11413001	
zfp36l2	0.059	0.058	0.066	0.053	0.048	0.045	0.132	0.123	0.135	2.2	1.1	not detected	not detected	18385675	
tpx2	0.057	0.061	0.071	0.085	0.098	0.107	0.109	0.115	0.115	2.0	1.0	not detected	not detected	19121998	**UP**
kif11 (Eg5)	0.058	0.061	0.073	0.077	0.091	0.100	0.103	0.110	0.119	1.9	0.9	1.7	0.8	8026619	
incenp	0.059	0.065	0.069	0.075	0.096	0.093	0.101	0.101	0.126	1.9	0.9	1.5	0.5	18378691	
ctnnb1	0.064	0.051	0.078	0.088	0.097	0.109	0.105	0.118	0.107	1.7	0.8	1.0	0.0	9876185	
cdc20	0.064	0.058	0.082	0.091	0.097	0.089	0.111	0.102	0.101	1.6	0.7	0.5	-1.1	11413001	
aurka (Eg2)	0.067	0.069	0.088	0.089	0.099	0.104	0.094	0.098	0.108	1.5	0.6	1.3	0.3	10704364	
cdt1	0.072	0.071	0.081	0.098	0.098	0.114	0.096	0.115	0.100	1.4	0.5	1.0	0.0	19656945	
bub1	0.081	0.075	0.099	0.083	0.107	0.102	0.097	0.093	0.101	1.2	0.3	not detected	not detected	11231148	
patl1	0.085	0.075	0.089	0.089	0.095	0.100	0.096	0.104	0.099	1.2	0.2	4.6	2.2	20826699	
kpna3	0.081	0.088	0.075	0.085	0.087	0.09	0.1	0.106	0.098	1.3	0.3	0.6	-0.7	26399853	
gapdh	0.079	0.0885	0.0815	0.083	0.0795	0.0825	0.0905	0.0925	0.0915	1.2	0.2	0.5	-1.03398944	26399853	
ipo5	0.082	0.0845	0.0835	0.0735	0.088	0.08	0.093	0.0965	0.095	1.2	0.2	0.5	-0.9	26399853	
tuba4b	0.079	0.106	0.082	0.132	0.092	0.096	0.078	0.08	0.115	1.2	0.2	0.4	-1.5	20531391	
kpna2	0.09	0.0875	0.096	0.101	0.092	0.09	0.096	0.088	0.101	1.1	0.1	1.1	0.1	26399853	
mapk1	0.092	0.095	0.093	0.098	0.091	0.099	0.092	0.099	0.086	1.0	0.0	0.6	-0.7	26092930	
kpnb1	0.1	0.088	0.08	0.086	0.077	0.093	0.087	0.092	0.115	1.0	0.0	0.5	-1.1	26399853	
xpo1	0.093	0.093	0.086	0.086	0.094	0.092	0.089	0.092	0.086	1.0	-0.1	0.6	-0.8	26399853	
acta4	0.089	0.101	0.086	0.099	0.09	0.09	0.085	0.081	0.089	1.0	-0.1	not detected	not detected	20826699	
cdk1	0.0965	0.092	0.1005	0.0975	0.098	0.095	0.0915	0.0935	0.087	0.9	-0.1	1.0	0.0	26092930	**CONSTANT**
arpp19	0.1015	0.085	0.1125	0.0885	0.1025	0.086	0.085	0.075	0.083	0.8	-0.3	0.6	-0.7	24525567	
zar1	0.211	0.096	0.109	0.083	0.088	0.086	0.076	0.062	0.064	0.3	-1.6	0.3	-1.8	23827238	
tbpl2	0.135	0.123	0.132	0.089	0.093	0.071	0.075	0.055	0.073	0.5	-1.0	not detected	not detected	19650908	
zar2	0.218	0.0985	0.0935	0.0845	0.0835	0.0795	0.065	0.0525	0.059	0.3	-1.9	not detected	not detected	23827238	
patl2	0.273	0.286	0.108	0.057	0.036	0.033	0.028	0.025	0.029	0.1	-3.3	0.4	-1.3	20826699	
cpeb1	0.306	0.223	0.098	0.045	0.036	0.033	0.031	0.027	0.031	0.1	-3.4	0.4	-1.2	11237472, 11927567	**DOWN**

B

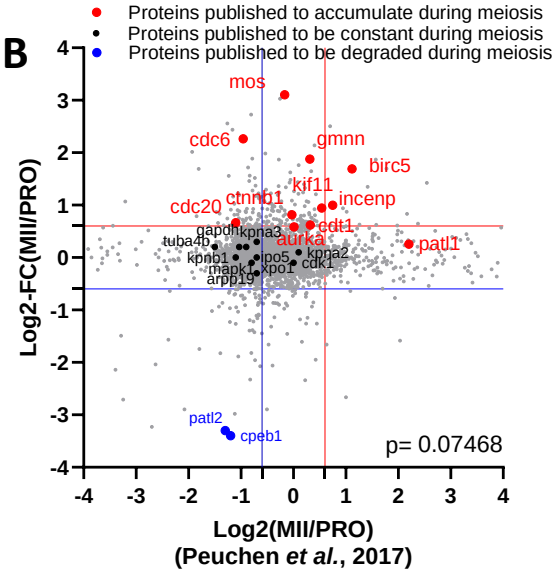

C

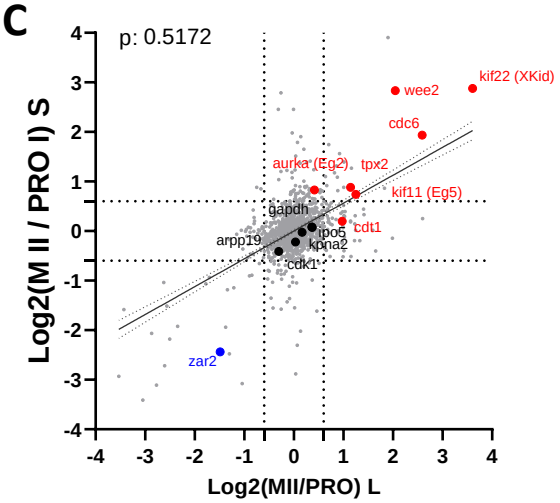

D

		S		
		UP	Constant	DOWN
L	UP	19	57	0
	Constant	62	1042	39
	DOWN	2	38	22

E

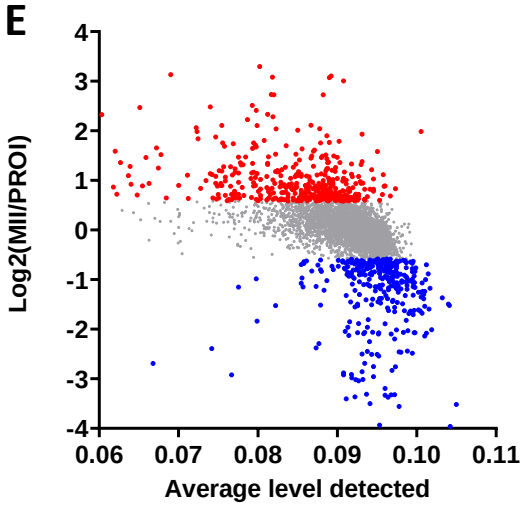

Figure 2-figure supplement 3 continued

Figure 2-figure supplement 3. Validation of the proteomic dataset. (**A**) Table summarizing proteins whose changes in protein level have been documented using Western blot. The PMID of the original publication displaying the Western blot is reported. The changes in abundance detected in our dataset are color-coded with a scale from green to red. Log2 fold changes between prophase and metaphase II from our dataset are color-coded with a scale from red to blue and compared to another previously published dataset (Peuchen *et al*, 2017). (**B**) Proteome-wide comparison of our dataset with (Peuchen *et al*, 2017). Proteins whose abundance was previously published are color-coded in red for the ones that accumulate, black for the constant, and blue for the ones that are degraded. (**C**) Changes in protein abundance between prophase and metaphase II were calculated for each protein were we could distinguish the .S and .L isoforms, and plotted. The Pearson correlation between the isoforms was calculated with Prism. (**D**) Table summarizing the comparison between .S and .L isoforms presented in panel **C**. (**E**) Correlation plot between the changes in protein abundance occurring during the prophase to metaphase II transition and the relative abundance in prophase oocytes.

Figure 2-figure supplement 4

A

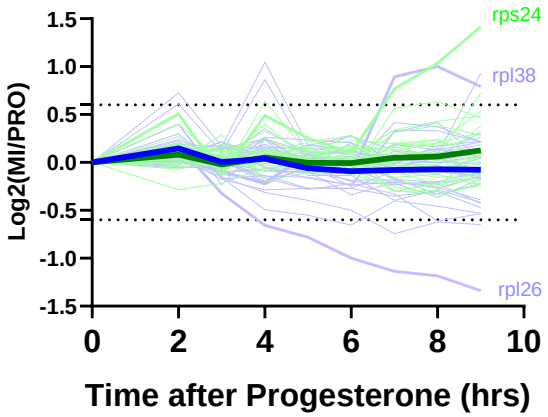

B

			n. of proteins degraded bearing the consensus	Substrates (reference)
APC	D-Box	R-x-x-L-x-x-x-x-N	56 (11%)	Ccnb 2 (PMDI: 1846030), CKAP2 (PMDI: 17339342)
	KEN	K-E-N-x-x-x-N	2 (1%)	
	ABBA	I/L/V/F-x-I/L/M/V/P-F/H/Y-x-D/E	128 (25%)	
SCF	BtrcP	D/T-SGxxS	22 (4%)	CPEB1 (PMDI: 11237472)
	FBXW7:	I/L-I/L/P-T/S-P-x-x-S/T	8 (2%)	
None of the identified degron			253 (57%)	

Figure 2-figure supplement 4. Protein degradation during meiotic maturation: ribosomal proteins, E3 ligases targets. (**A**) Changes in protein abundance of ribosomal proteins between prophase (PRO) and metaphase II (MII) are plotted. Dashed lines represent the threshold used for defining the differentially expressed proteins. (**B**) Table summarizing the different degron consensus motifs identified and the number of proteins in our dataset bearing these motifs. Examples of proteins bearing different degrons are listed along with supporting literature.

Figure 3

A

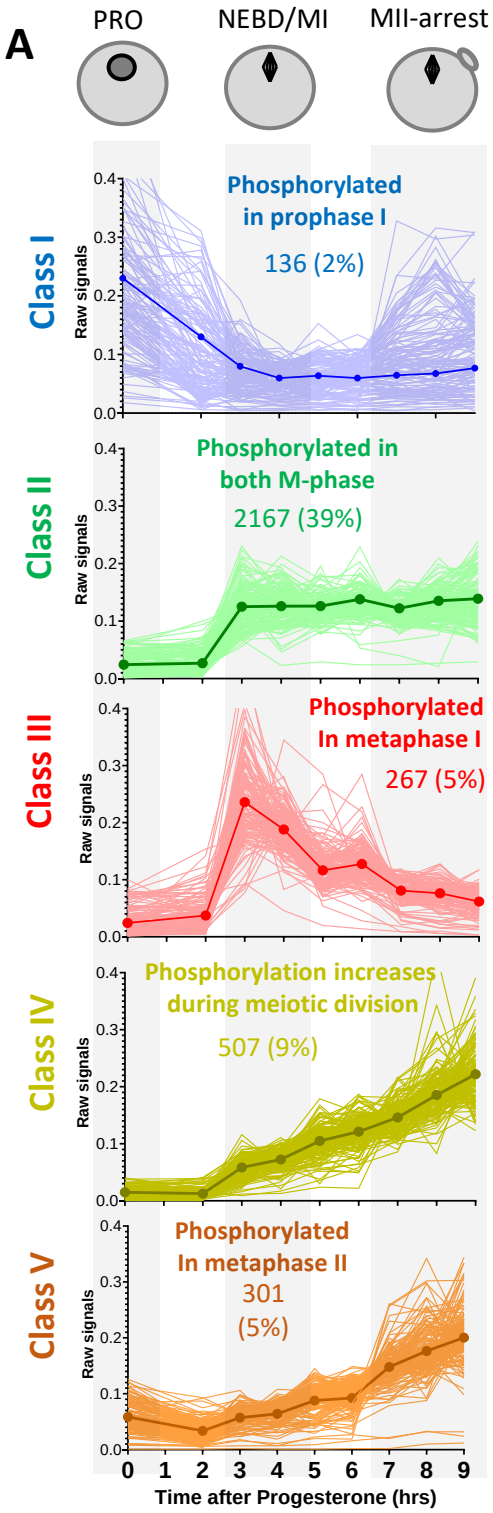

B

	gene name	description	PMID
Vessicle trafficking and membrane organization	C2CD2L	an endoplasmic reticulum protein that functions both as membrane tether to the plasma membrane and as phospholipid transporter	32693056
	MAGI1	a scaffolding protein localized at the plasma membrane	35389514
	NKTR	a membrane-anchored protein with function in protein folding	7906541
	LDLRAP1	interacts with the cytoplasmic tail of the LDL receptor and facilitates the clathrin-mediated endocytosis of LDLR and other members of this family	15728179
	PI4KB	PKA substrate that regulates Golgi reorganization during mitosis, and is involved in Golgi-to-plasma membrane trafficking	23712958
Actin cytoskeleton	WIPF2	induces reorganization of the actin filament network around the plasma membrane by cooperating with WASP/WASL88	21785420
	SPTBN1	an actin crosslinking and molecular scaffold protein that is involved in Ca2+ and calmodulin-dependent exocytosis	32601107
	ITPRID2	tethers IP3 receptors to the actin under the plasma membrane to mediate Ca2+ signalling	34301929
Translation	PATL1	RNA binding protein involved in mRNA stabilization and translation repression	20826699
	eIF4ENIF1	binds and sequesters eIF4E inhibiting protein translation initiation.	16157702
	Maskin	component of the translation repression complex nucleated by CPEB1 that is involved in mantaining translation repression in Prophase arrested oocytes.	10635326
Ubiquitn ligases	Ube2O	E2/E3 ubiquitin-protein ligase with both E2 and E3 ligase activities.	30468556
	Faf2	endoplasmic reticulum–associated protein involved in the dissolution of RNA stress granules	34739333
	Ube4b	E3-ubiquitin ligase, with unknow function.	
	DCUN1D5	catalyzes the neddylation of cullins that is required for the activation of the cullin-E3 ubiquitin ligase.	26906416

Figure 3. Changes in protein phosphorylation during meiotic divisions. (**A**) Relative phosphopeptide signals were normalized for the changes in the total level of the proteins. The changes in the phosphopeptides were measured between the three biological stages of meiotic divisions (PRO = 0hr, NEBD/MI = average of 3 and 4 hours, and MII-arrest = average of 7 to 9 hours).

Figure 3 continued

Class I (n=136 - 2%, in blue) includes proteins bearing a phosphosite whose occupancy decreases during meiosis resumption (Log2FC(MI/PRO)<-1). Class II (n=2167 - 39%, in green) contains proteins that are highly phosphorylated from MI (Log2FC(MI/PRO)>1) to MII (-1<Log2FC(MII/MI)<1). Class III (n=267 - 5%, in red) consists of proteins whose phosphorylation is specific of MI (Log2FC(MI/PRO)>1, Log2FC(MII/MI)<-1). Class IV (n=507 - 9%, yellow) is composed of proteins whose phosphorylation increases from MI (Log2FC(MI/PRO)>1) to MII, picking in MII (Log2FC(MII/MI)> 1). Class V (n=301 – 5%, orange) comprises proteins whose phosphorylation does not vary in MI (-1<Log2FC(MI/PRO)<1) but are phosphorylated only in MII (Log2FC(MII/MI)>1). The average signal of each Class was plotted with a thick and dark line. (**B**) Table summarizing the proteins bearing phosphosites belonging to Class I.

Figure 4

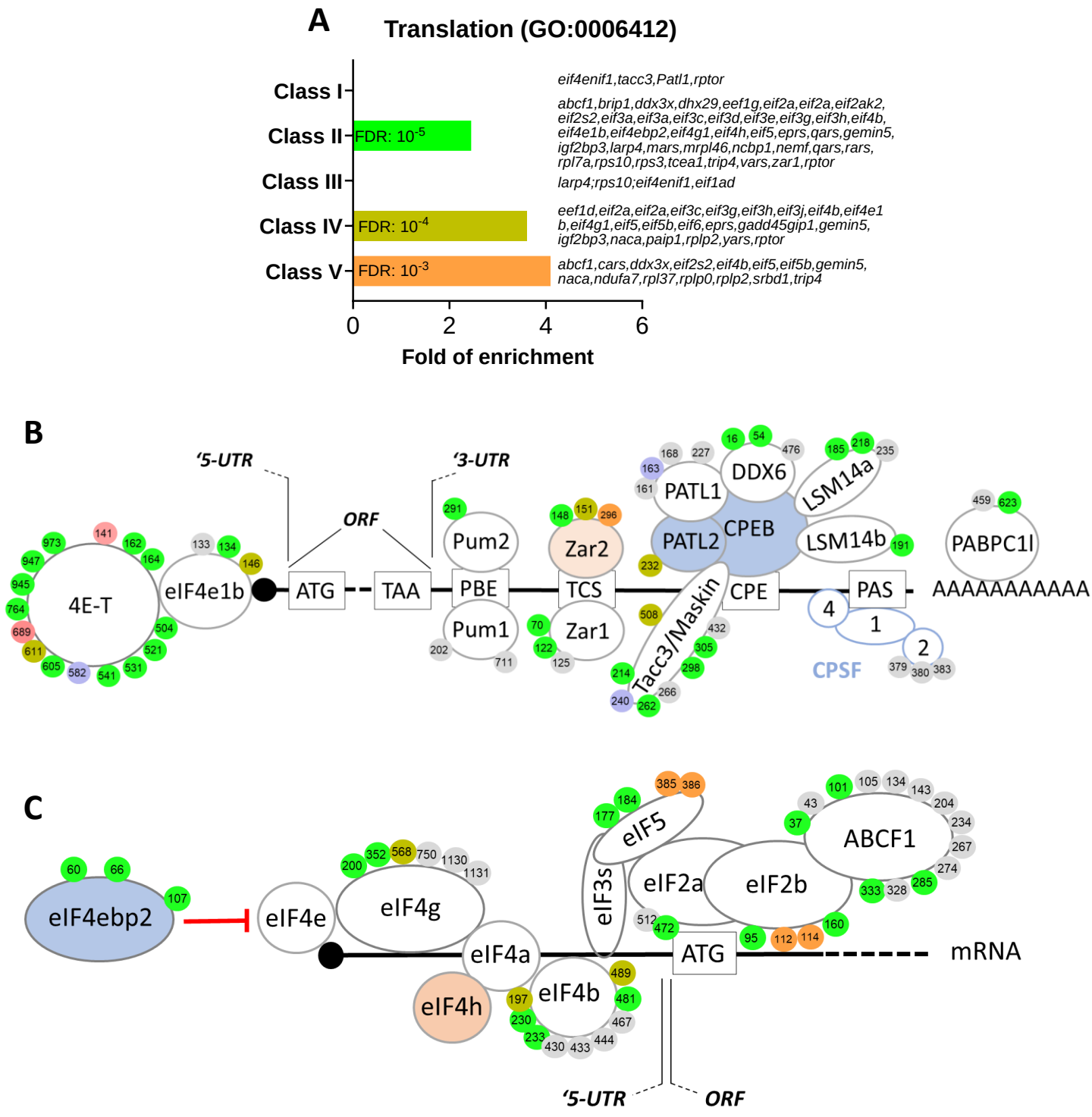

Figure 4. RNA-binding proteins and translation initiation factors are dynamically phosphorylated during meiotic divisions. (**A**) Gene ontology enrichment analysis of the biological process "translation" (GO:0006412) among the phosphopeptides found in each class defined in Fig. 3A. (**B-C**) Graphical representation of the phosphorylation dynamics of RBPs (**B**) and translation initiation factors (**C**) during meiotic divisions. Proteins are color-coded to highlight the changes in protein abundance during meiotic divisions: unchanged=white, decreased=blue, increased=light orange. The phosphorylated sites are color-coded: unchanged, grey; Class I, blue; Class II, green; Class III, red; Class IV, yellow; Class V, orange. The numbering is referred to the iso-allele which has higher number of phosphorylation sites detected.

Figure 4-figure supplement 1

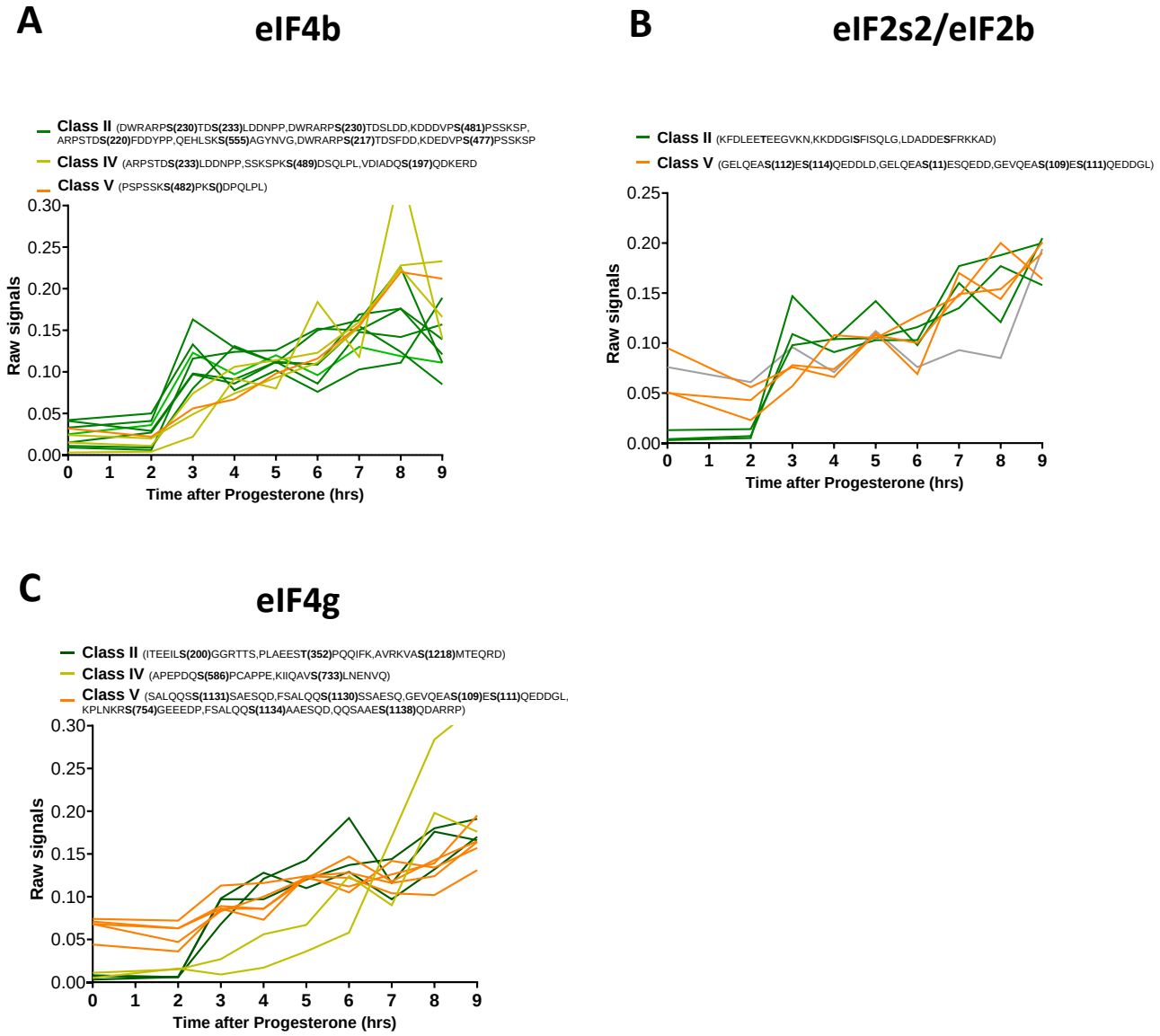

Figure 4-figure supplement 1. Phosphorylation patterns of components of the initiation translation machinery during meiotic divisions. (**A**-**C**) Levels of phosphorylation sites of eIF4b (**A**), eIF2s2/eIF2b(**B**) and eIF4g (**C**) during meiotic divisions are plotted. The phosphorylation curves are color-coded: Class II, green; Class IV, yellow, Class V, orange.

Figure 5

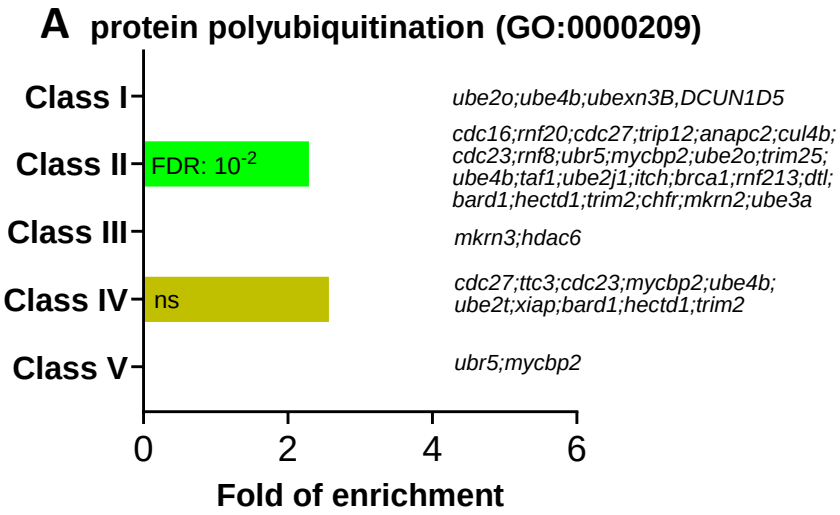

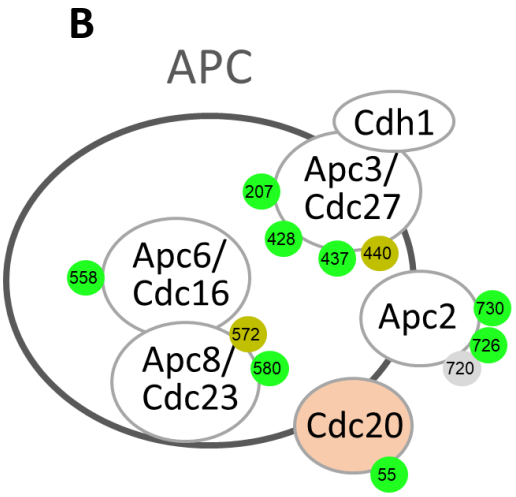

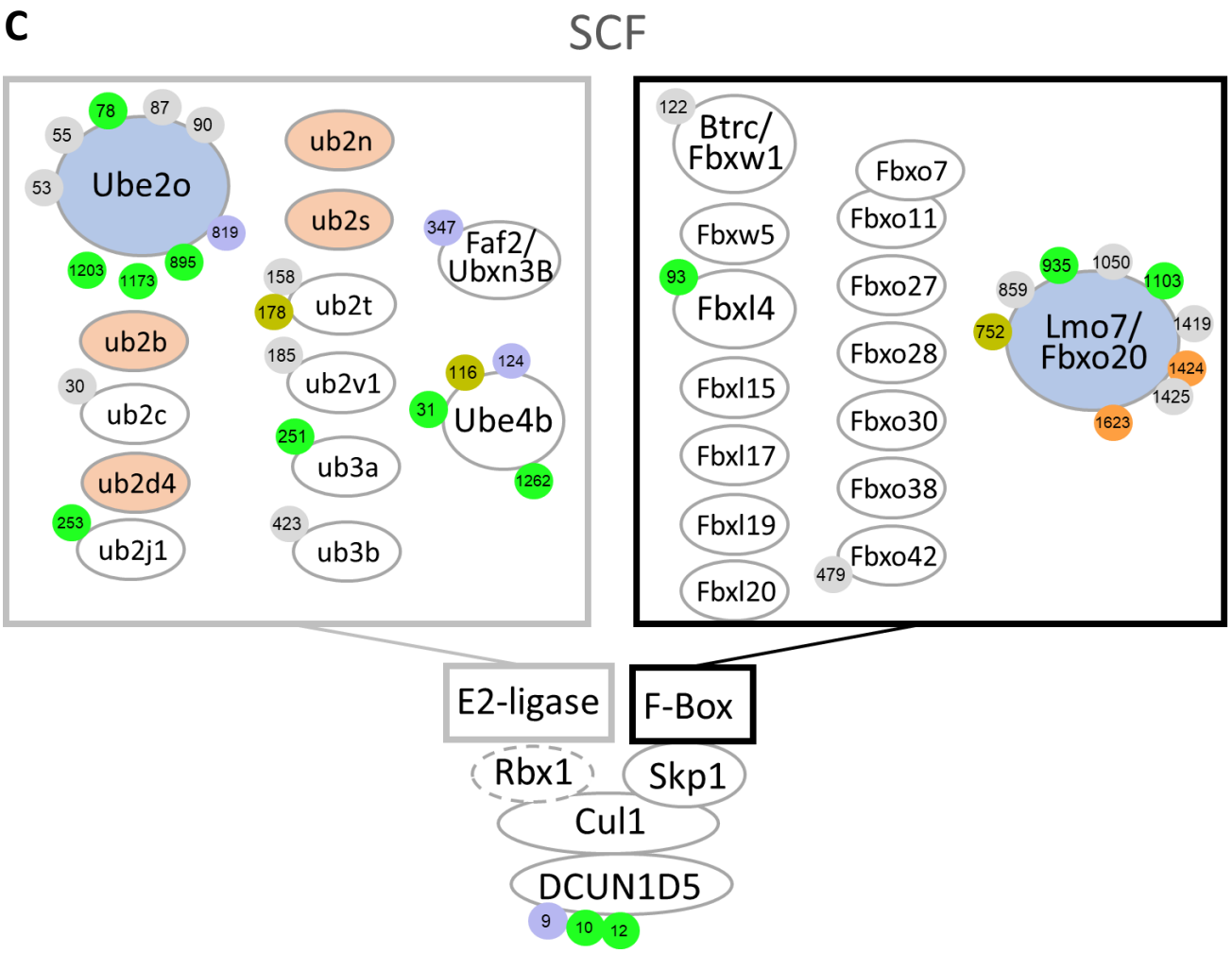

Figure 5. E2 and E3 ubiquitin ligases are highly regulated by phosphorylation. (**A**) Gene ontology enrichment analysis of the biological process "protein polyubiquitination" (GO:0000209) among the phosphopeptides found in each class defined in Fig. 3A. (**B-C**) Graphical representation of the phosphorylation dynamics of the components of two E3 ubiquitin ligases, the anaphase promoting complex (APC) (**B**) and the Skp, Cullin, F-box containing complex (SCF) (**C**) during meiotic divisions. Proteins are color-coded to highlight changes in protein abundance during meiotic divisions: unchanged=white, decreased=blue, increased=light orange. The phosphorylated sites are color-coded: unchanged, grey; Class I, blue; Class II, green; Class III, red; Class IV, yellow; Class V, orange. The numbering is referred to the iso-allele which has higher number of phosphorylation sites detected.

Figure 6

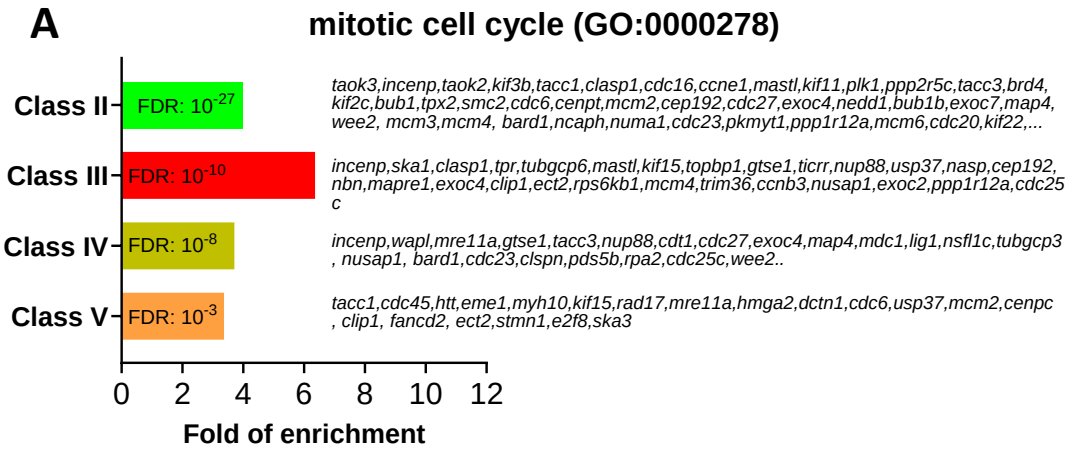
A
mitotic cell cycle (GO:0000278)
Class II
FDR: 10^-27
taok3,incenp,taok2,kif3b,tacc1,clasp1,cdc16,ccne1,mastl,kif11,plk1,ppp2r5c,tacc3,brd4, kif2c,bub1,tpx2,smc2,cdc6,cenpt,mcm2,cep192,cdc27,exoc4,nedd1,bub1b,exoc7,map4, wee2, mcm3,mcm4, bard1,ncaph,numa1,cdc23,pkmyt1,ppp1r12a,mcm6,cdc20,kif22,...
Class III
FDR: 10^-10
incenp,ska1,clasp1,tpr,tubgcp6,mastl,kif15,topbp1,gtse1,ticrr,nup88,usp37,nasp,cep192, nbn,mapre1,exoc4,clip1,ect2,rps6kb1,mcm4,trim36,ccnb3,nusap1,exoc2,ppp1r12a,cdc25 c
Class IV
FDR: 10^-8
incenp,wapl,mre11a,gtse1,tacc3,nup88,cdt1,cdc27,exoc4,map4,mdc1,lig1,nsfl1c,tubgcp3 , nusap1, bard1,cdc23,clspn,pds5b,rpa2,cdc25c,wee2..
Class V
FDR: 10^-3
tacc1,cdc45,htt,eme1,myh10,kif15,rad17,mre11a,hmga2,dctn1,cdc6,usp37,mcm2,cenpc , clip1, fancd2, ect2,stmn1,e2f8,ska3
0 2 4 6 8 10 12
Fold of enrichment

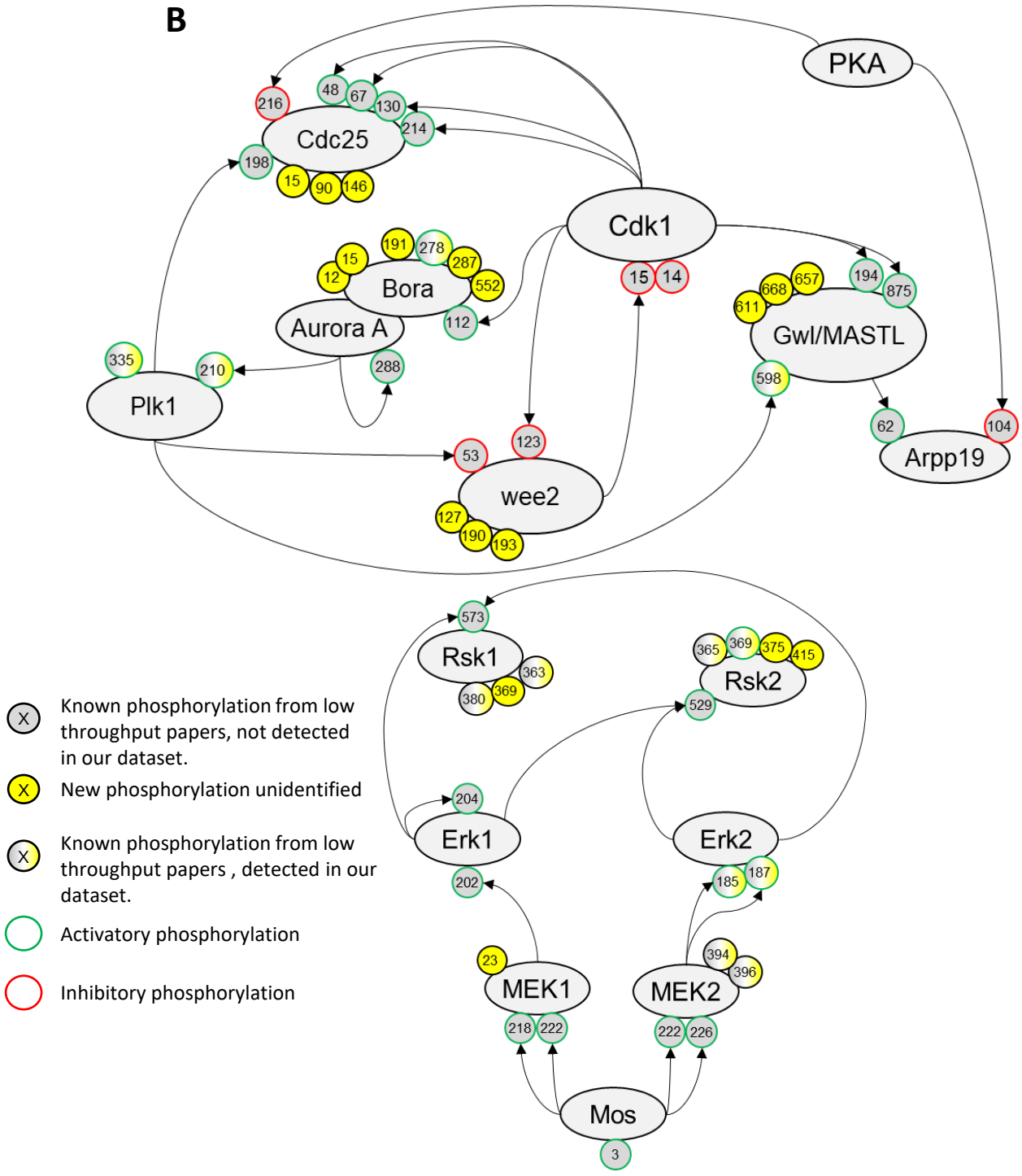
B
PKA
Cdc25
216
48
67
130
214
198
15
90
146
Cdk1
15
14
Bora
12
15
191
278
287
552
112
Aurora A
288
Plk1
335
210
Gwl/MASTL
668
657
611
194
875
598
Arpp19
62
104
wee2
53
123
127
190
193
Rsk1
573
363
380
369
Rsk2
365
369
375
415
529
Erk1
204
202
Erk2
185
187
MEK1
23
218
222
MEK2
394
396
222
226
Mos
3
Known phosphorylation from low throughput papers, not detected in our dataset.
New phosphorylation unidentified
Known phosphorylation from low throughput papers , detected in our dataset.
Activatory phosphorylation
Inhibitory phosphorylation

Figure 6 continued

Figure 6. The network of phosphorylations regulating Cdk1 and the Mos/MAPK pathway. (**A**) Gene ontology enrichment analysis of the biological process "mitotic cell cycle" (GO:0000278) among the phosphopeptides found in each class defined in Fig. 3A. (**B**) Graphical representation of the network of phosphorylations of cell cycle regulators controlling Cdk1 activation (**upper panel**) and the Mos/MAPK pathway (**lower panel**). The human nomenclature numbering has been used for the phospho-sites. The phosphosites are displayed by dots and color-coded: yellow background, new sites identified in this paper and never described elsewhere; grey background, phosphosites already documented in vertebrates by low throughput papers and not identified in this paper; grey-yellow background, phosphosites already documented in vertebrates by low throughput papers and also identified in this paper. The functional effect of the phosphorylation is indicated by the color of the dot contour line: green, activatory; red, inhibitory; black, unknown.

Figure 6-figure supplement 1

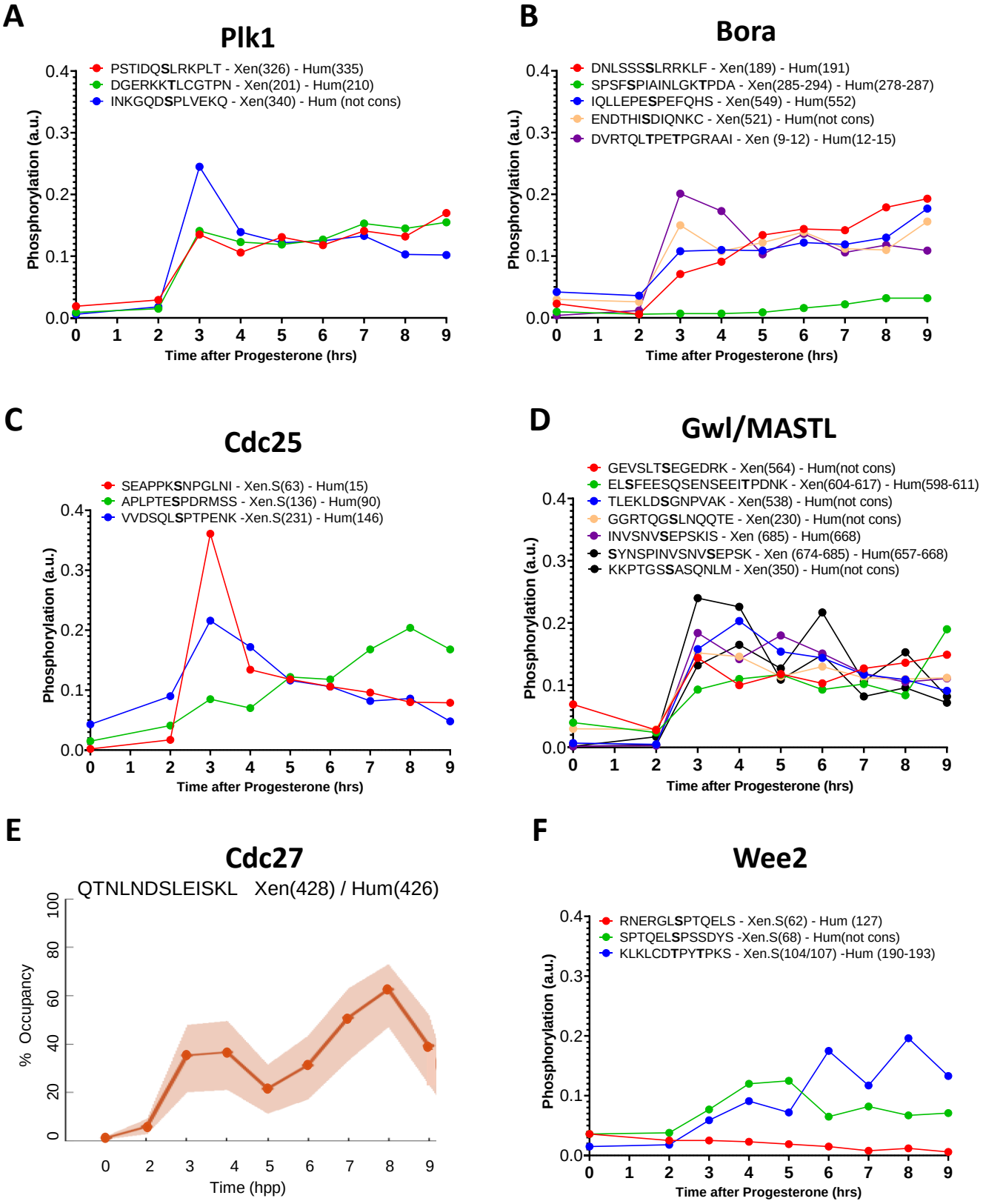

Figure 6-figure supplement 1. Phosphorylation patterns of Cdk1 regulators during meiotic divisions. (**A**-**D** and **F**) Levels of phosphorylation sites of Plk1 (**A**), Bora (**B**), Cdc25 (**C**), Gwl/MASTL (**D**) and Wee2 (**F**) during meiotic divisions are plotted. The peptide sequences are reported with the phosphorylation sites marked in bold. The number of the residue phosphorylated is reported between breakers according to the *Xenopus* and human nomenclature. (**E**) The phosphorylation occupancy for S428 of Cdc27 is plotted with its confidence intervals.

Figure 6-figure supplement 2

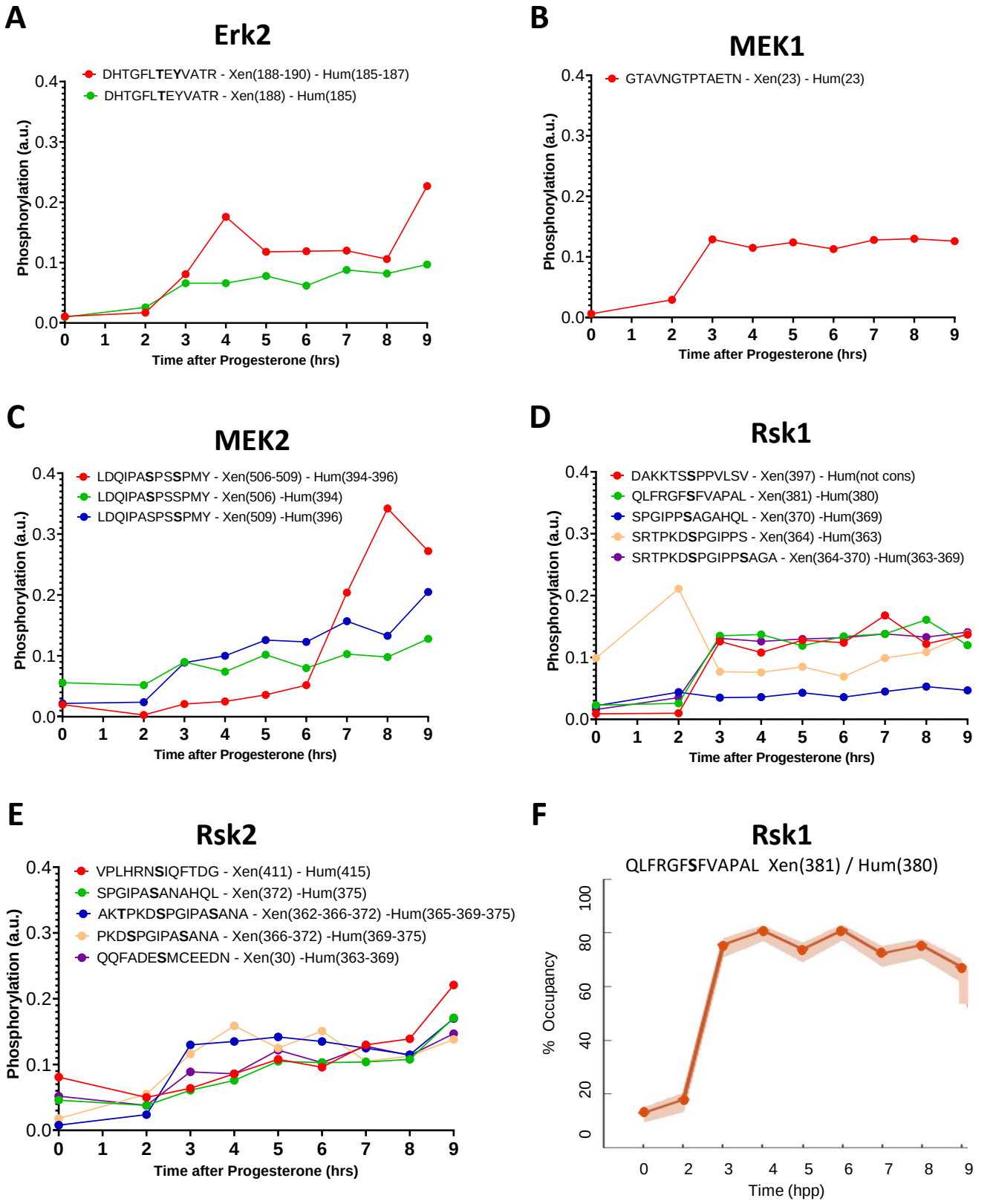

Figure 6-figure supplement 2. Phosphorylation patterns of the mos/MAPK pathway during meiotic divisions. (**A**-**E**) Levels of phosphorylation sites of Erk1 (**A**), Bora (**B**), MEK1 (**C**), MEK2 (**D**) and Rsk2 (**E**) during meiotic divisions are plotted. The peptide sequences are reported with the phosphorylation sites marked in bold. The number of the residue phosphorylated is reported between breakers according to the *Xenopus* and human nomenclature. (**F**) The phosphorylation occupancy for S381 of Rsk1 is plotted with its confidence intervals.

Figure 7

A Nucleoporins concentration (nM)

	PRO	MII
NUP107	157	161
NUP133	166	172
NUP153	117	144
NUP155	186	191
NUP160	134	140
NUP188	120	124
NUP205	360	383
NUP210	97	119
NUP214	150	131
NUP35	327	308
NUP37	309	317
NUP43	218	237
NUP50	712	725
NUP54	160	166
NUP58	385	388
NUP62	440	440
NUP85	134	145
NUP88	110	110
NUP93	665	693
NUP98	476	442

B Nuclear pore organization (GO:0006999)

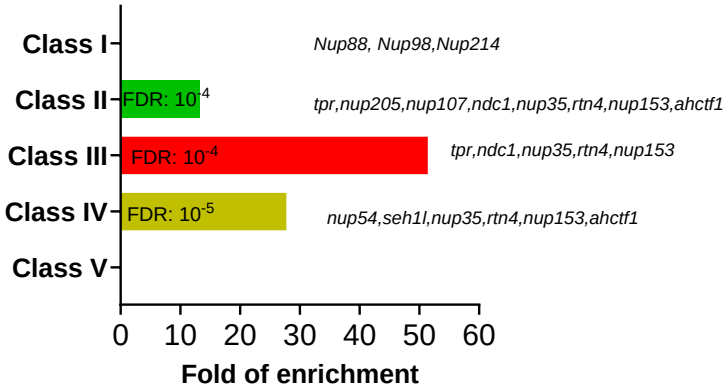

C Nup35/Nup53

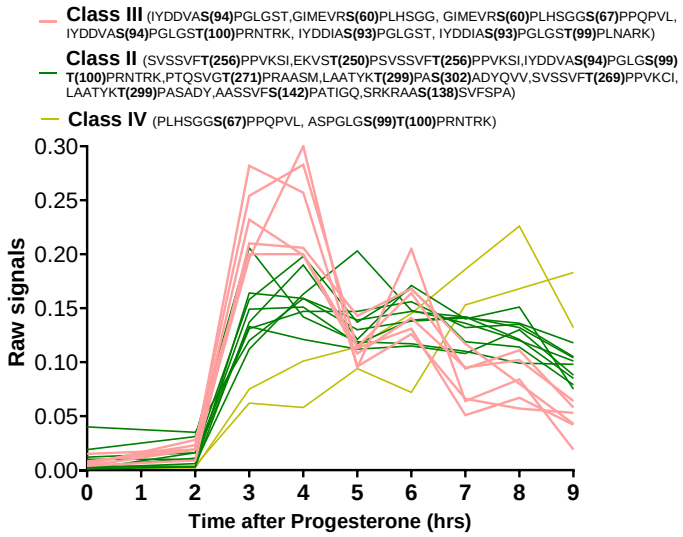

D Nup35/Nup53

GVMEMRSPLFSGG Xen(59) / Hum(59)

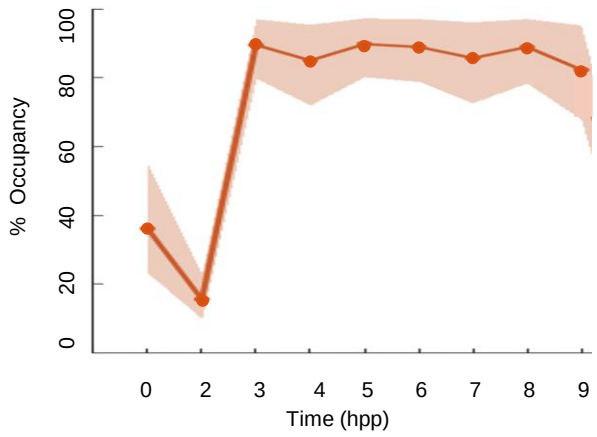

Figure 7. The phosphorylation pattern of nuclear pore components during meiotic divisions. (**A**) Absolute concentration (nM) of nucleoporins in prophase (PRO) and metaphase II (MII) oocytes. (**B**) Gene ontology enrichment analysis of the biological process "nuclear pore organization" (GO:0006999) among the phosphopeptides found in each class defined in Fig. 3A. (**C**) Phosphorylation patterns of Nup35/Nup53. The phosphorylation curves are color-coded: Class II, green; Class III, red; Class IV, yellow. (**D**) High precision phospho-occupancy calculation of S59 phosphorylation pattern of Nup35/Nup53.

Figure 8

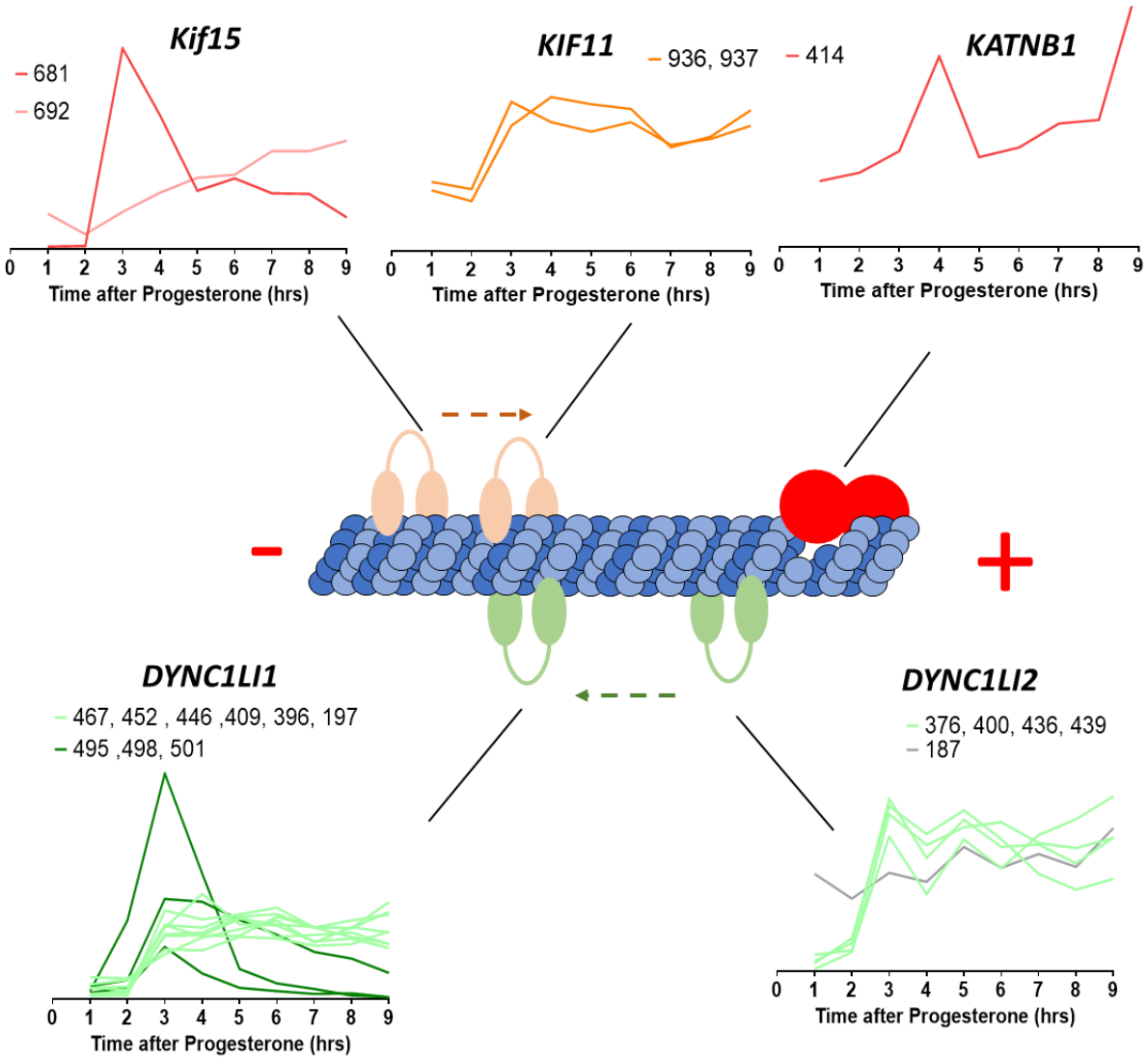

Figure 8. Microtubule-interacting proteins phosphorylation during meiotic divisions. Graphic representation of the phosphorylation dynamics of kinesins (Kif15, Kif11), dyneins (DYNC1LI1, DYNC1LI2) and katanin (KATNB1) during meiotic divisions. The sites of the phosphorylation detected are marked above each panel.

Figure 8-figure supplement 1

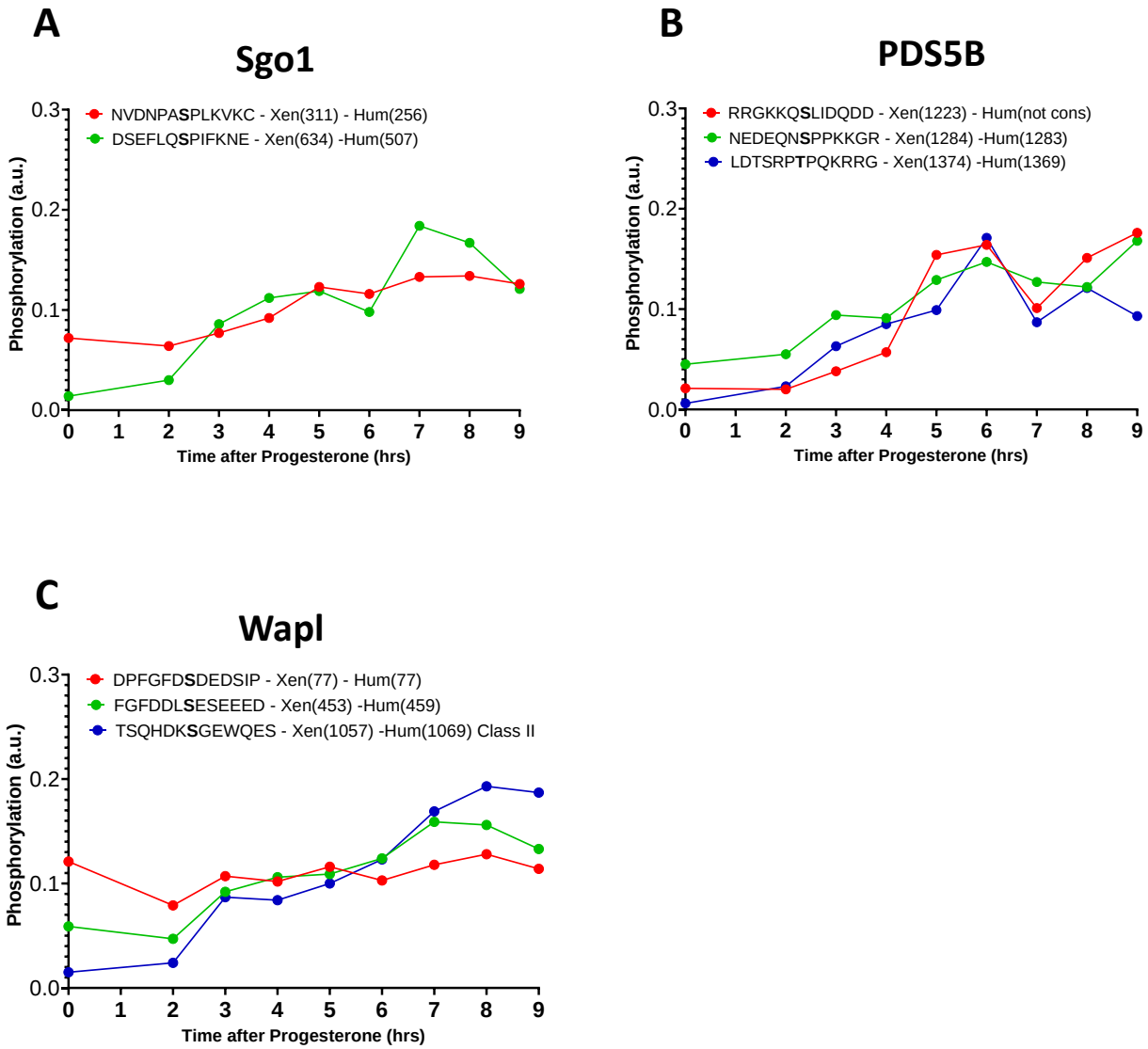

Figure 8-figure supplement 1. Phosphorylation patterns of cohesins during meiotic divisions. (**A**-**C**) The levels of phosphorylation sites of Sgo1 (**A**), PDS5B (**B**) and Wapl (**C**) during meiotic divisions are plotted. The peptide sequences are reported with the phosphorylation sites marked in bold. The position of the residue phosphorylated is reported in breakets according to the *Xenopus* and human nomenclature.

Table 1

		Proteome										(Whur,2014)	(Session,2016)
	Gene name	0	2	3	4	5	6	7	8	9	Log2 FC (MII/PRO)	Estimated concentration in MII-arrested oocytes (nM)	Count per Million (CPM) in PRO I
Proximal part	SAS-6	0.11	0.09	0.10	0.10	0.09	0.09	0.09	0.09	0.08	-0.3	36	20
	CENPJ	0.07	0.09	0.09	0.10	0.10	0.11	0.09	0.10	0.09	0.4	9	56
	Cep135	not detected										5	1
Central core	POC1B	0.05	0.05	0.07	0.08	0.09	0.14	0.11	0.10	0.11	1.2	7	96
	POC5	0.05	0.06	0.07	0.08	0.09	0.10	0.10	0.11	0.12	1.1	39	100
	CETN1	0.08	0.08	0.11	0.09	0.09	0.09	0.10	0.09	0.10	0.2	not detected	3
	SFI1	not detected										3	7
	POC1A	not detected										20	54
	CETN2	not detected										82	not detected
	WDR90	not detected										5	25
	FAM161A	not detected										not detected	34
Distal appendages	SCLT1	0.10	0.09	0.10	0.11	0.10	0.10	0.08	0.08	0.08	-0.4	13	2
	FBF1	0.11	0.12	0.11	0.12	0.11	0.11	0.08	0.07	0.06	-0.7	not detected	17
	CEP83	not detected										not detected	7
	CEP89	not detected										not detected	1
Sub-distal appendages	FBF1	0.11	0.12	0.11	0.12	0.11	0.11	0.08	0.07	0.06	-0.7	not detected	17
	CEP164	0.10	0.08	0.11	0.09	0.12	0.09	0.08	0.06	0.08	-0.4	1	not detected
	NIN	0.11	0.09	0.11	0.07	0.08	0.11	0.10	0.08	0.10	-0.2	4	27
	TUBE1	0.10	0.09	0.10	0.10	0.10	0.11	0.09	0.09	0.09	-0.1	7	8
	TUBD1	0.08	0.08	0.08	0.09	0.09	0.11	0.09	0.09	0.10	0.1	13	28
	ODF2	not detected										7	8
	CEP128	not detected										3	17
	CNTRL	not detected										6	26
	CEP170	not detected										4	3
	TCHP	not detected										2	16
	CCDC68	not detected										not detected	3
	tubz1	not detected										not detected	10
	CCDC120	not detected										not detected	not detected
Centriole duplication	CCP110	0.06	0.07	0.06	0.08	0.08	0.09	0.10	0.12	0.12	0.9	7	20
	CEP152	0.07	0.07	0.10	0.10	0.10	0.12	0.10	0.11	0.09	0.6	7	161
	CEP192	0.08	0.08	0.08	0.08	0.09	0.09	0.10	0.11	0.10	0.5	21	24
	STIL	0.08	0.08	0.07	0.08	0.10	0.11	0.10	0.11	0.12	0.5	14	100
	CEP63	0.07	0.06	0.11	0.11	0.13	0.12	0.10	0.09	0.09	0.5	4	33
	CEP76	0.07	0.07	0.07	0.08	0.09	0.14	0.10	0.07	0.12	0.5	12	57
	RTTN	0.09	0.09	0.09	0.10	0.10	0.11	0.09	0.09	0.08	0.0	18	14
	CEP97	0.10	0.10	0.10	0.10	0.09	0.10	0.10	0.09	0.09	-0.1	15	1
	SAS-6	0.11	0.09	0.10	0.10	0.09	0.09	0.09	0.09	0.08	-0.3	36	42
	Plk4	not detected										not detected	not detected
PCM	KIF22	0.02	0.02	0.04	0.05	0.07	0.09	0.12	0.14	0.19	3.1	33	464
	SSX2IP	0.03	0.03	0.05	0.07	0.09	0.11	0.11	0.13	0.16	2.1	20	10
	TUBG1	0.04	0.04	0.04	0.04	0.04	0.04	0.12	0.12	0.11	1.5	166	101
	tpx2	0.06	0.06	0.07	0.08	0.10	0.11	0.11	0.12	0.11	1.0	43	516
	kif11	0.06	0.06	0.07	0.08	0.09	0.10	0.10	0.11	0.12	0.9	44	185
	dync1li1	0.06	0.0735	0.0605	0.0675	0.062	0.0605	0.104	0.1185	0.087	0.8	169	38
	dync2h1	0.067	0.057	0.073	0.074	0.092	0.098	0.104	0.105	0.128	0.7	35	3
	prc1	0.06	0.07	0.08	0.09	0.10	0.12	0.09	0.10	0.10	0.7	32	13
	CEP152	0.07	0.07	0.10	0.10	0.10	0.12	0.10	0.11	0.09	0.6	7	33
	kif4a	0.08	0.07	0.08	0.09	0.09	0.09	0.10	0.10	0.10	0.4	100	120
	TUBGCP4	0.08	0.08	0.08	0.09	0.10	0.08	0.10	0.10	0.10	0.2	14	20
	nedd1	0.08	0.08	0.09	0.08	0.09	0.08	0.10	0.10	0.09	0.2	30	12
	dync2i1	0.0875	0.076	0.0915	0.088	0.0965	0.0975	0.0925	0.0935	0.101	0.1	not detected	11
	CKAP5	0.09	0.09	0.09	0.09	0.09	0.10	0.09	0.10	0.09	0.1	67	102
	dynll2	0.086	0.111	0.077	0.102	0.09	0.08	0.086	0.085	0.104	0.1	411	60
	dync2i2	0.089	0.081	0.1	0.099	0.106	0.098	0.09	0.087	0.095	0.0	not detected	35
	TUBGCP3	0.09	0.08	0.09	0.09	0.10	0.10	0.09	0.10	0.09	0.0	33	10
	KATNB1	0.09	0.09	0.10	0.10	0.10	0.10	0.09	0.09	0.09	0.0	20	108
	dynlt1	0.086	0.1	0.114	0.09	0.09	0.07	0.083	0.085	0.093	0.0	138	49
	dync1i2	0.091	0.104	0.104	0.073	0.081	0.106	0.091	0.089	0.092	0.0	232	48
	PCNT	0.09	0.09	0.09	0.10	0.10	0.10	0.09	0.09	0.09	0.0	16	23
	NPM2	0.08	0.10	0.08	0.12	0.08	0.08	0.07	0.07	0.09	0.0	1181	116
	dync2li1	0.086	0.074	0.084	0.086	0.089	0.091	0.082	0.081	0.091	0.0	43	4
	CLASP1	0.09	0.08	0.09	0.10	0.10	0.10	0.09	0.09	0.08	-0.1	15	48
	TUBGCP2	0.09	0.09	0.10	0.10	0.10	0.09	0.09	0.09	0.09	-0.1	59	22
	dync1li2	0.097	0.089	0.099	0.104	0.094	0.099	0.091	0.094	0.086	-0.1	26	27
	dynll1	0.099	0.101	0.094	0.096	0.092	0.105	0.089	0.093	0.089	-0.1	51	130
	NEK9	0.09	0.10	0.10	0.10	0.10	0.10	0.09	0.08	0.08	-0.2	45	27
	TACC3	0.10	0.10	0.10	0.10	0.10	0.10	0.09	0.09	0.08	-0.2	115	117
	TUBGCP6	0.10	0.09	0.11	0.10	0.10	0.10	0.08	0.08	0.08	-0.3	8	14
	NPM3	0.11	0.09	0.12	0.11	0.10	0.10	0.09	0.09	0.08	-0.3	150	70
	KATNA1	0.10	0.10	0.10	0.09	0.10	0.09	0.09	0.08	0.08	-0.3	63	30
	NPM1	0.12	0.09	0.12	0.10	0.09	0.09	0.08	0.08	0.08	-0.6	308	102
	TUBGCP5	not detected										24	not detected
	KATNAL1	not detected										5	not detected
	KATNAL2	not detected										not detected	22

Table 1 continued

Table 1. Centrosomal components during meiotic divisions. Expression patterns of the components of the centrioles and the pericentriolar material. The changes in protein abundance are color-coded: unchanged=white, decreased=blue, increased=light orange. The estimation of the protein and mRNA concentrations was derived by published datasets and color-coded on a white-green scale for protein concentrations and on a white-yellow scale for mRNA concentrations.

Table 1-table supplement 1

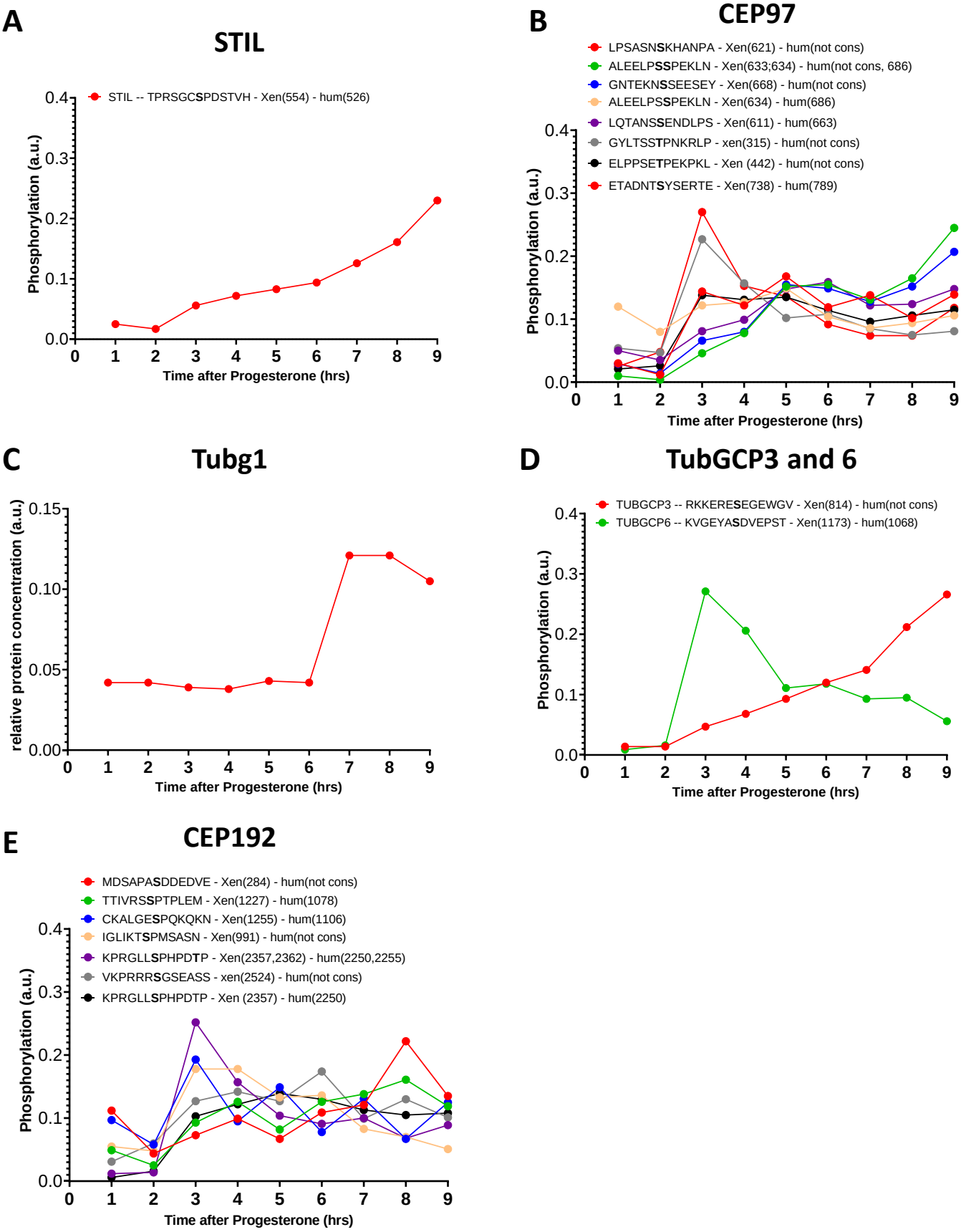

Table 1-table supplement 1. Phosphorylation patterns of centrosomal proteins during meiotic divisions. **(A-E)** The levels of phosphorylation sites of STIL (**A**), CEP97 (**B**), Tubg1 (**C**), TubGCP3 and 6 (**D**), CEP192 (**E**) during meiotic divisions are plotted. The peptide sequences are reported with the phosphorylation sites marked in bold. The number of the residue phosphorylated is reported between breakers according to the *Xenopus* and human nomenclature.

Appendix 1

Estimating the absolute abundance of proteins

Following previously published methods (Wühr *et al*, 2014; Peshkin *et al*, 2015), the absolute protein concentration was estimated here based on ion current (denoted I) prorated to the isobarically labeled fractions. The respective sample fractions were estimated using our published Bayesian approach (Peshkin *et al*, 2019), which integrates peptide signal and peptide-level measurement agreement into a maximum likelihood estimate of the true protein ratio and the associated confidence interval (BACIQ). Specifically, we want to construct the following relation applicable to all measured proteins:

$$log(C_S^P) = A_P\, log(Q_S^P) + B_p,\ Q_S^P = \frac{1}{N_P^T} \cdot F_S^P \cdot I$$

where:

Q_S^P is the isobarically labeled fractions of the total I ion current;

C_S^P is the absolute abundance (in Moles) of the protein p at a stage *s;*

N_P^T is the theoretical number of (unique) peptides obtained by "*in-silico* digestion" script (available in the supplementary materials) using the following parameters: miss_cleav=2, min_len=7, max_len=57, enz='[KR]' and FASTA file of the considered protein sequences;

F_S^P is the fraction of the total signal observed in the isobaric peptide signal quantitation channels corresponding to the sample from stage S;

I is the total ion current reported using only unique peptides as obtained from *cq_area_sum* column of export from the MS platform;

A_P and B_P are the linear regression parameters.

Using the calibration protein data, we can fit (using two-way regression to avoid any bias towards one of the variables) a linear function (1) in log/log space and extrapolate from it by estimating the regression parameters A_P and B_P universal for all proteins. To calibrate the protein measurements, we used previously published(Peshkin *et al*, 2015) concentrations C_S^P for 5960 proteins in *Xenopus laevis* egg. The parameters A_P and B_P are obtained using symmetrical linear regression analysis (in log-log space; Fig.1) between C_{egg}^P (concentration in the egg stage post-fertilization) and Q_S^P (isobarically labeled fractions of the total I ion current). Further, we only used in the regression analysis proteins with highly confident mapping between proteins in both data sets by sequence homology. The highly confident mapping - reciprocal best hit (RBH) by sequence homology is defined by HMMER3 pipeline (Savova *et al*, 2017) with the perfect E-values both ways) matches of proteins between data published in (Peshkin *et al*, 2015) and proteins in the current study. This filter leaves 617 proteins used in regression analysis as shown in Fig. 1 for one of three biological repeats (Clutch A).

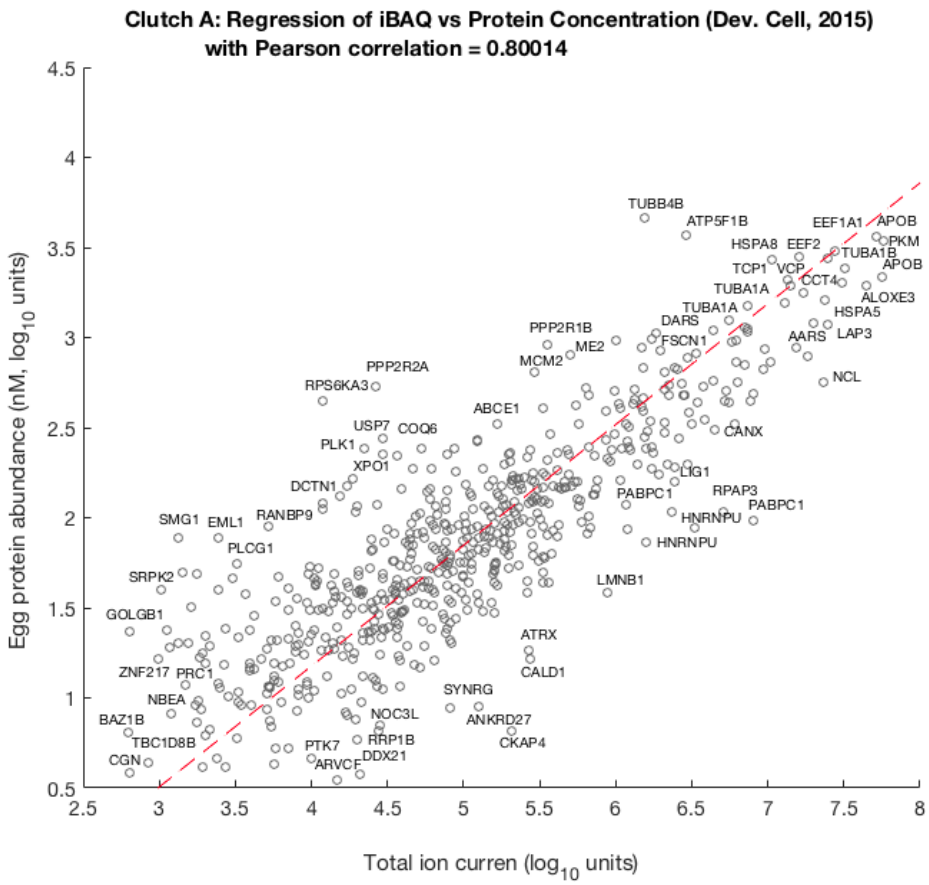

Methods Figure 1. *Scatter plot of per-channel pro-rated ion current* Q_S^P *(isobarically labeled fractions of the total* I *ion current) adjusted by theoretical number of tryptic peptides against egg protein abundance as previously published by* (Peshkin *et al*, 2015). *Pearson correlation between these quantities is ca. 0.8 the best linear fit leads to the following relation:* $log(C_S^P) = 0.67 * log(Q_S^P) - 1.5$

Using the fitting parameters, we converted mass spectrometry measurements into absolute abundance for all proteins detected in the experiments for three biological repeats (Clutch A, B and C). To additionally validate the identification and estimated concentrations of proteins in this study, we performed the comparison with previously published data by (Wühr *et al*, 2014) matching proteins via respective human gene symbol as assigned via reciprocal HMMER3 run. Fig. 2 shows Venn diagram illustrating that vast majority of proteins we identified (5063 or 86%) were also detected and confirmed in previously published data, while there are 800 novel proteins. Our current study was done for quantitative comparison across multiple timepoints and thus, being a labeled mass spectrometry experiment, could not be as deep as the unlabeled single sample unlabeled mass spectrometry study by (Wühr *et al*, 2014).

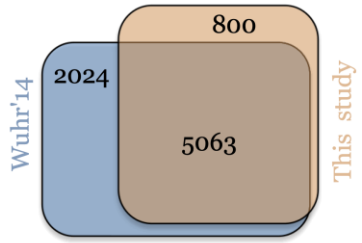

Methods Figure 2. *Venn diagram comparing proteins identified in this study to previously published by* (Wühr *et al*, 2014)*. This study has 800 unique proteins versus 2024 unique proteins in the data by* (Wühr *et al*, 2014)*. There are 5063 proteins in common.*

The 5063 proteins common between our data and (Wühr *et al*, 2014) are used to make comparison of proteins concentrations as shown in Fig. 3. Pearson's correlation between previously published protein concentrations and obtained oocyte proteins in this study is 0.81. The maximum deviation of the extrapolated value from previously estimated value is ca. 3 nM. The differences between studies might result from the biological variation between frogs, difference in gene symbol assignment between studies or differences in the sample preparation.

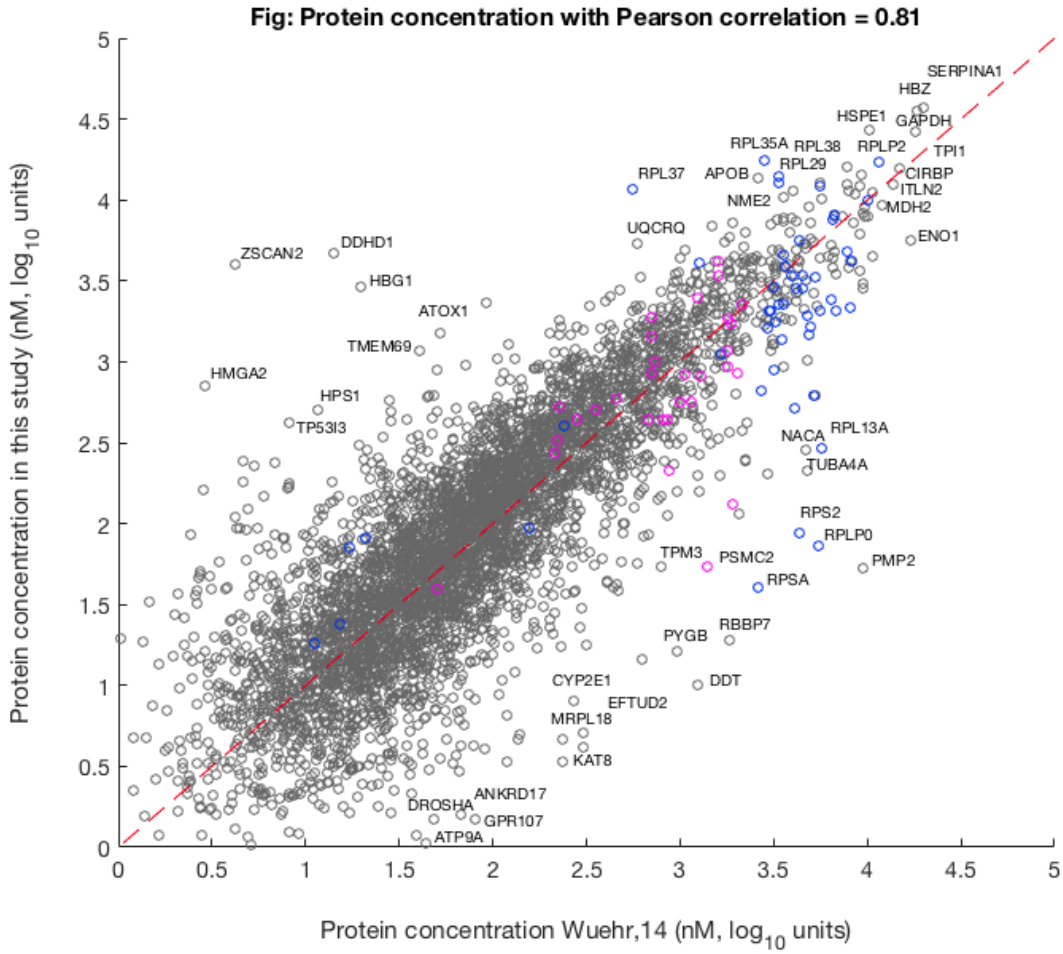

Methods Figure 3. *Comparison of average concentration (i.e., mean value of 3 different oocyte samples) with egg data published previously by* (Wühr *et al*, 2014)*. The magenta points show the location of proteasome units and blue points show the ribosomal proteins.*

Identification and exclusion of follicular cells proteins

Oocytes are surrounded in ovary by an envelope of follicular cells, blood vessels and connective tissue. To study the dynamics of protein expression in oocytes after progesterone stimulation, we physically removed the follicular matter with forceps. This process is imperfect, leaving some amount of follicular matter attached to the oocytes. To control for admixture of the follicular layers, the removed follicular material was separately collected and profiled as one of the samples in mass spectrometry. The average relative protein abundance in oocyte was compared to follicular protein expression as shown in Fig. 4 across a total of 7062 proteins.

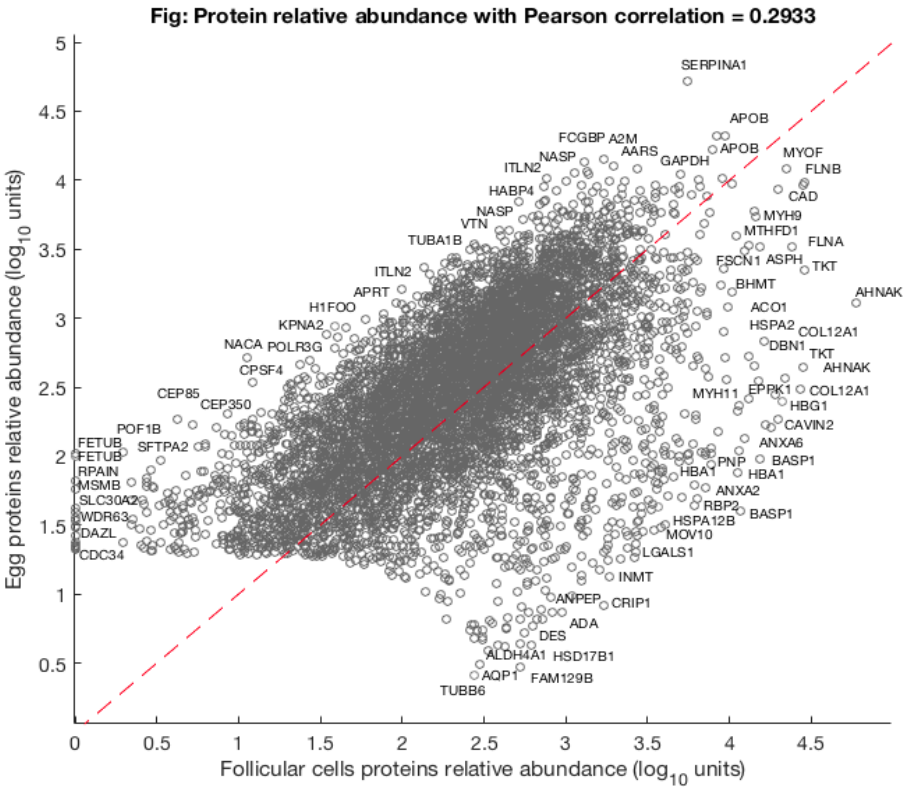

Methods Figure 4. *A scatter plot of a relative protein abundance in oocyte against abundance in follicular tissue. The low abundant proteins are naturally masked in the follicular sample as they are contrasted to 10 oocyte samples, thus severely underrepresented in a pooled sample.*

Fig. 4 shows oocyte specific genes FETUB and H1FOO as well as the follicular cells specific proteins HBG1 and TUBB6. The cut off for selecting "exclusively follicular proteins" was somewhat arbitrarily selected at 0.6 orders difference in log-log space or roughly 4-fold enrichment in the follicle taking into account that oocyte material is impure and itself contains substantial follicular residuals. These over-expressed 648 follicular proteins were removed from the oocyte protein analysis since the dynamics of these proteins reflects the artifactual fluctuation in presence of the remaining follicular cells in oocyte samples.

Occupancy Calculation

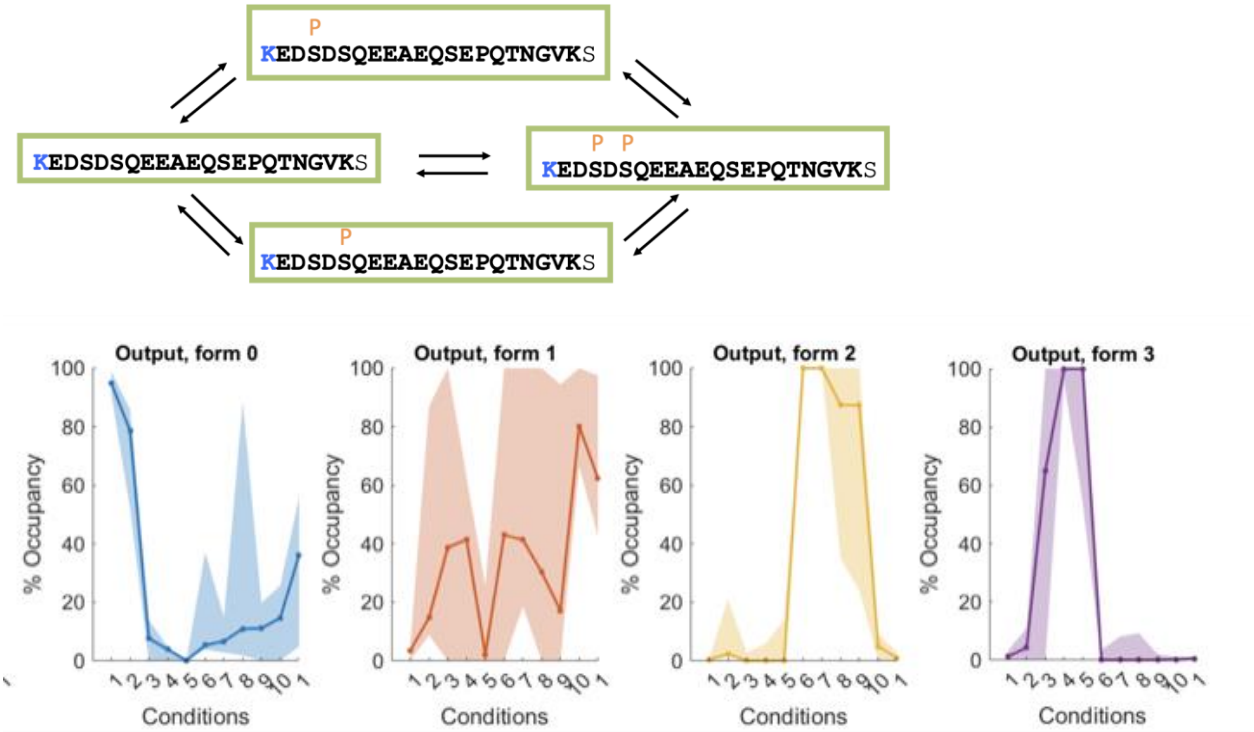

Methods Figure 5. An illustration of occupancy calculation for a single peptide where four phospho-forms are measured: the de-phosphorylated, singly phosphorylated on a serine in one of two alternative positions, and doubly phosphorylated on both serines. All interconversions **(A)** across four forms are allowed by our calculation. The resulting stoichiometry and respective confidence intervals **(B)** estimated for each form following (Presler *et al*, 2017) and BACIQ (Peshkin *et al*, 2019). Points 1-9 are the timepoints post progesterone stimulation, the two rightmost points are protease-treated samples.

References

Peshkin L, Gupta M, Ryazanova L & Wühr M (2019) Bayesian Confidence Intervals for Multiplexed Proteomics Integrate Ion-statistics with Peptide Quantification Concordance*[S]. *Molecular & Cellular Proteomics* 18: 2108–2120

Peshkin L, Wühr M, Pearl E, Haas W, Freeman RM, Gerhart JC, Klein AM, Horb M, Gygi SP & Kirschner MW (2015) On the Relationship of Protein and mRNA Dynamics in Vertebrate Embryonic Development. *Developmental Cell* 35: 383–394

Presler M, Van Itallie E, Klein AM, Kunz R, Coughlin ML, Peshkin L, Gygi SP, Wühr M & Kirschner MW (2017) Proteomics of phosphorylation and protein dynamics during fertilization and meiotic exit in the *Xenopus* egg. *Proc Natl Acad Sci USA* 114: E10838–E10847

Savova V, Pearl EJ, Boke E, Nag A, Adzhubei I, Horb ME & Peshkin L (2017) Transcriptomic insights into genetic diversity of protein-coding genes in X. laevis. *Developmental Biology* 424: 181–188

Wühr M, Freeman RM, Presler M, Horb ME, Peshkin L, Gygi SP & Kirschner MW (2014) Deep Proteomics of the Xenopus laevis Egg using an mRNA-Derived Reference Database. *Current Biology* 24: 1467–1475

Appendix 2

A

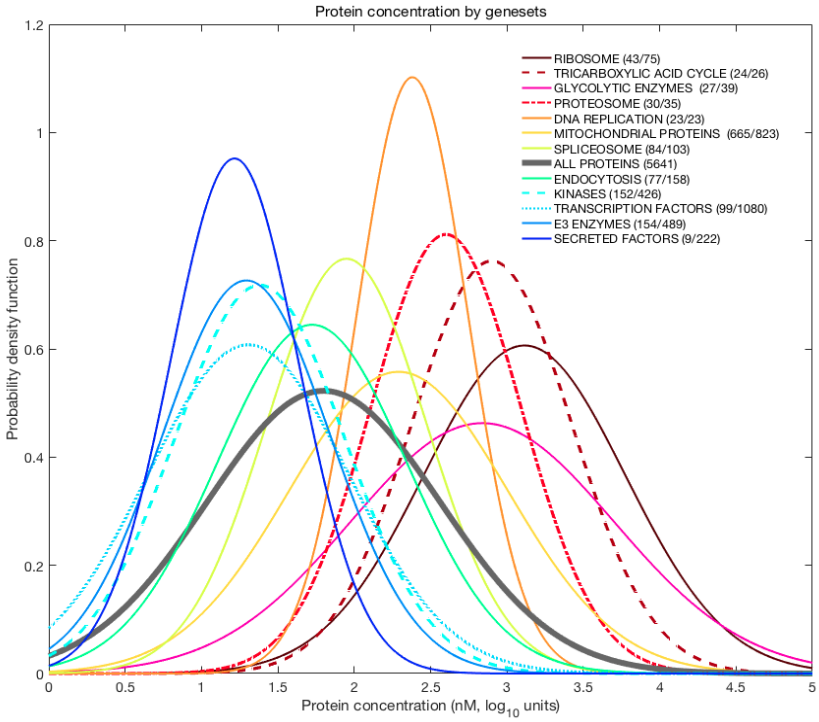

B

Group	Mean (nM, log10 units)	Standard Deviation (nM, log10 units)
Ribosome	3.115	0.658
Tricarboxylic Acid Cycle	2.9	0.523
Glycolytic Enzymes	2.838	0.862
Oxidative Phosphorylation	2.684	0.573
Fatty Acid Metabolism	2.663	0.57
Pentose Phosphate Pathway	2.643	0.674
Proteosome	2.601	0.492
DNA Replication	2.38	0.362
Mitochondrial Proteins	2.29	0.715
Xenobiotic Metabolism	2.242	0.785
Peroxisome	2.177	0.69
RNA Degradation	2.102	0.667
Lysosome	2.037	0.646
Spliceosome	1.95	0.52
Ligands	1.866	0.978
All Proteins	1.799	0.764
RNA Polymerase	1.787	0.485
Endocytosis	1.724	0.619
Extra Cellular Matrix	1.719	1.09
Phosphatases	1.628	0.738
Cell Cycle	1.624	0.581
Receptors	1.596	0.745
Chromatin	1.588	0.681
Mitotic Spindle	1.574	0.739
Collagens	1.441	0.497
Kinome	1.381	0.556
Transcription Factors	1.306	0.657
E3 Enzymes	1.293	0.549
Secreted Factors	1.215	0.419

Appendix 2. Distribution of absolute protein abundance in the oocyte by functional set. (**A**) Each set is approximated by a Gaussian using respective mean and standard deviation. The number of detected proteins and total proteins in each category is marked in the legend. (**B**) Parameters of Gaussian distributions (mean and standard deviation) for different groups.

Appendix 3

A

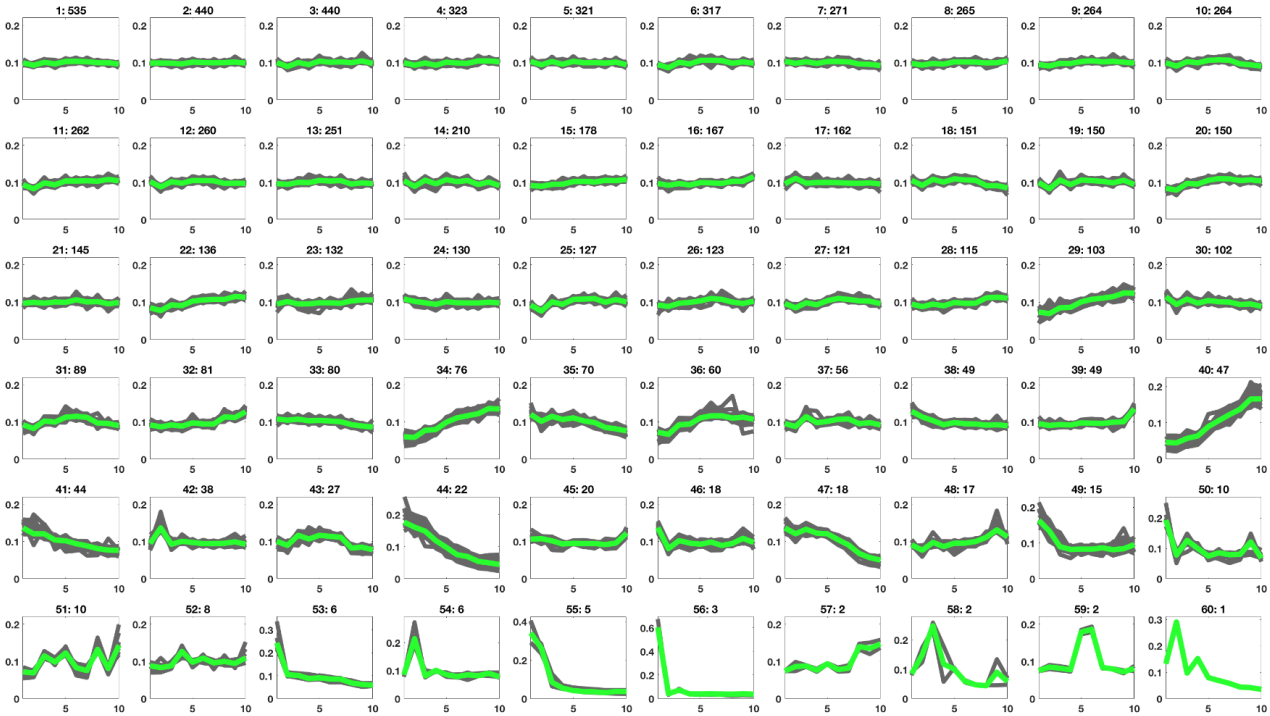

B

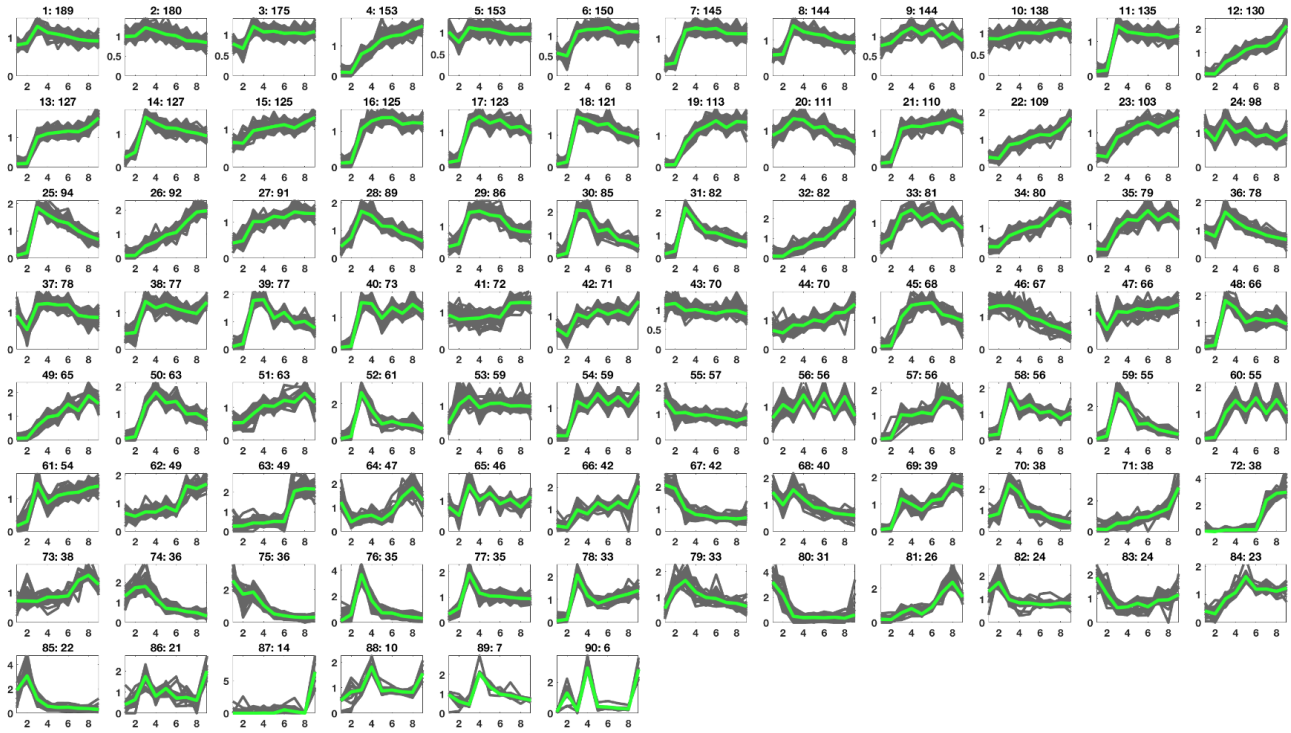

Appendix 3 continued

Appendix 3. Clusters of dynamics of oocyte protein expression and phosphorylation in response to progesterone. Key clusters of the protein expression (**A**) and phospho-site dynamics **(B)** after progesterone stimulation of an oocyte as obtained by a K-means clustering based on cosine similarity distance. The clusters are arranged in the order of cardinality, starting with the most populated ones. Each subplot is labeled by the cluster ID and the number of proteins in that cluster.

Methods.

The relative protein abundance data across subsequent hourly timepoints post-progesterone stimulation was clustered using K-means clustering algorithm with cosine similarity distance. The number of clusters was selected to ensure proteins in each cluster are closely concordant and under-clustered for visualization purpose, resulting in 60 and 90 clusters for protein and phosphopeptides respectively. The code to perform this clustering procedure is available upon request and was run using MATLAB (version R2022b). The K-means clustering algorithm converges to local minima only, therefore, we performed multiple clustering realization to identify the most biologically plausible clusters, as shown in panels A-B. Resulting clusters are ordered by cardinality, most populated clusters first.